STOCHASTIC MODELING OF COOPERATIVE WIRELESS MULTI-HOP NETWORKS

A Dissertation
Presented to
The Academic Faculty

by

Syed Ali Hassan

In Partial Fulfillment
of the Requirements for the Degree
Doctor of Philosophy in the
School of Electrical and Computer Engineering

Georgia Institute of Technology
December 2011

STOCHASTIC MODELING OF COOPERATIVE WIRELESS MULTI-HOP NETWORKS

Approved by:

Professor Mary Ann Ingram, Advisor
School of Electrical and Computer Engineering
Georgia Institute of Technology

Professor Erik Verriest
School of Electrical and Computer Engineering
Georgia Institute of Technology

Professor Ye (Geoffrey) Li
School of Electrical and Computer Engineering
Georgia Institute of Technology

Professor Liang Peng
School of Mathematics
Georgia Institute of Technology

Professor Xiaoli Ma
School of Electrical and Computer Engineering
Georgia Institute of Technology

Date Approved: October 2011

DEDICATION

To my Parents.

ACKNOWLEDGEMENTS

I would like to gratefully and sincerely thank Dr. Mary Ann Ingram for her guidance, understanding, patience, and most importantly, her friendship during my graduate studies at Georgia Tech. Her infectious enthusiasm and unlimited zeal have been major driving forces throughout my graduate years. More importantly, she demonstrated her faith in my ability to rise to the occasion and do the necessary work and has always been a strong advocate for me. Thank you Dr. Ingram for being such a nice adviser.

My special thanks go to the members of my thesis committee, Dr. Ye (Geoffrey) Li, Dr. Xiaoli Ma, and Dr. Liang Peng for their terrific support during this tenure. I also express my appreciation to Dr. Erik Verriest for being on my dissertation committee. Their enlightening suggestions have greatly improved my research and the quality of this dissertation. I appreciate the faith and funding of the National University of Sciences and Technology (NUST) Pakistan, National Science Foundation (NSF), School of Electrical and Computer Engineering (ECE) at Georgia Tech, and Higher Education Commission (HEC) Pakistan, in giving me the opportunity to pursue my doctoral research in an uninterrupted manner.

I thank my awesome friends and colleagues (former/present) at the Smart Antenna Research Lab and Georgia Tech, Alper Akanser, Murtaza Askari, Yong Jun Chang, Jin Woo Jung, Haejoon Jung, Muhammad Omer Jamal, Azhar Hasan, Syed Minhaj Hassan, Dr. Aravind Kailas, Xiangwei Zhou, and Dr. Gao Zhen for the support they have lent me over all these years. Further, I thank all my friends outside Georgia Tech including Bushra Chaudry, Ali Imran and so many others for always being there for me. My time at Georgia Tech was made enjoyable in large part due to the many

friends that became a part of my life. I am grateful for time spent with roommates and friends, especially Syed Hussain Raza and Sajid Saleem, for my backpacking buddies and our memorable trips into the mountains, lakes, beaches, deserts and visits to so many restaurants.

My very special thanks to the persons whom I owe everything I am today, my parents. Their unwavering faith and confidence in my abilities and in me is what has shaped me to be the person I am today. Thank you for everything. I would also like to thank my brother and sisters and their families for their love and support. Finally, I would like to take the opportunity to thank all my teachers and staff at Georgia Tech.

TABLE OF CONTENTS

LIST OF TABLES

LIST OF FIGURES

ABBREVIATIONS

AWGN	$\triangleq$	Additive White Gaussian Noise
BER	$\triangleq$	Bit-Error Rate
CDF	$\triangleq$	Cumulative Distribution Function
CFO	$\triangleq$	Carrier Frequency Offset
CRB	$\triangleq$	Cramer Rao Bound
CT	$\triangleq$	Cooperative Transmission
DF	$\triangleq$	Decode and Forward
EDS	$\triangleq$	Estimation using Data Statistics
FDA	$\triangleq$	Fully Data Aided
MIMO	$\triangleq$	Multiple-Input Multiple-Output
MM	$\triangleq$	Method of Moments
ML	$\triangleq$	Maximum Likelihood
MSE	$\triangleq$	Mean Square Error
NCFSK	$\triangleq$	Non Coherent Frequency Shift Keying
NDA	$\triangleq$	Non Data Aided
NMSE	$\triangleq$	Normalized Mean-Square Error
OLA	$\triangleq$	Opportunistic Large Array
PDA	$\triangleq$	Partially Data Aided
PDF	$\triangleq$	Probability Density Function
QoS	$\triangleq$	Quality of Service
SISO	$\triangleq$	Single-Input Single-Output
SNR	$\triangleq$	Signal-to-Noise Ratio

SUMMARY

Multi-hop wireless transmission, where radios forward the message of other radios, is becoming popular both in cellular as well as sensor networks. This research is concerned with the statistical modeling of multi-hop wireless networks that do cooperative transmission (CT). CT is a physical layer wireless communication scheme in which spatially separated wireless nodes collaborate to form a virtual array antenna for the purpose of increased reliability. The dissertation has two major parts. The first part addresses a special form of CT known as the Opportunistic Large Array (OLA). The second part addresses the signal-to-noise ratio (SNR) estimation for the purpose of recruiting nodes for CT.

In an OLA transmission, the nodes from one level transmit the message signal concurrently without any coordination with each other, thereby producing transmit diversity. The receiving layer of nodes receives the message signal and repeats the process using the decode-and-forward cooperative protocol. The key contribution of this research is to model the transmissions that hop from one layer of nodes to another under the effects of channel variations, carrier frequency offsets, and path loss. It has been shown for a one-dimensional network that the successive transmission process can be modeled as a quasi-stationary Markov chain in discrete time. By studying various properties of the Markov chain, the system parameters, for instance, the transmit power of relays and distance between them can be optimized. This optimization is used to improve the performance of the system in terms of maximum throughput, range extensions, and minimum delays while delivering the data to the destination node using the multi-hop wireless communication system.

A major problem for network sustainability, especially in battery-assisted networks, is that the batteries are drained pretty quickly during the operation of the network. However, in dense sensor networks, this problem can be alleviated by using

a subset of nodes which take part in CT, thereby saving the network energy. SNR is an important parameter in determining which nodes to participate in CT. The more distant nodes from the source having least SNR are most suitable to transmit the message to next level. However, practical real-time SNR estimators are required to do this job. Therefore, another key contribution of this research is the design of optimal SNR estimators for synchronized as well as non-synchronized receivers, which can work with both the symbol-by-symbol Rayleigh fading channels as well as slow flat fading channels in a wireless medium.

CHAPTER I

INTRODUCTION

Wireless multi-hop transmission, both in cellular as well as sensor networks, has attracted many researchers for solving the key issues of signal propagation under fading environments. For large coverage areas, wireless multi-hop transmission, has the advantage of reduced cost of deployment, compared to the networks that have a base station or access point within one hop of every user. A conventional multi-hop network employs a path or route, which is an arrangement of point-to-point links, over which the signal propagates from the source to the destination. However, in a multi-hop route through a wireless network, each link is generally subject to receiver thermal noise and multi-path effects, causing non-negligible probability of link failure. The end-to-end probability of *success* in delivering the packet, from the source to the destination, is the product of all the link probabilities of success, and therefore the end-to-end probability of success is much lower than the link probability of success when there are many hops. A multi-hop transmission or a broadcast on a line network faces similar issues. Link layer functions, such as retransmission, may attempt to save the packet, at the cost of significant extra energy and delay. Cooperative transmission (CT) has been proposed as a means to improve link reliability or provide range extension, by having multiple radios transmit the same message to a receiver through uncorrelated fading channels.

This dissertation addresses two issues in CT networks. The first issue is the statistical modeling of a special form of cooperative diversity known as the Opportunistic Large Array (OLA). In an OLA transmission, the nodes from one level transmit the message signal concurrently without any coordination with each other, thereby

producing transmit diversity. The receiving nodes receive the message signal and repeat the process using the decode-and-forward (DF) cooperative protocol. Because only a minimal amount of inter-node coordination is needed, OLAs are particularly well suited for mobile networks, such as large groups of people with smart phones or swarms of robots. The key contribution of this research is to model the transmissions that hop from one layer of nodes to another under the effects of channel variations and path loss. We model a special case of the DF OLA network, where the nodes are uniformly spaced along a line. This topology can be considered a precursor to a strip-shaped network or a uni-cast cooperative route for the finite density case. Typical examples include structural health monitoring and sensors employed in hallways of buildings in a linear fashion. The topology would also be consistent with a *plastic communication cable*, in which small wireless relays are embedded along a cable made of a non-conducting material. Such "*plastic wires*" might find applications in areas of high electric fields.

For the purpose of modeling, we assume that the distance between the source and the destination is long enough that the transmission reaches a kind of steady state. Specifically, we assume that the conditional probability that the kth node in a level decodes, given that the previous level had at least one node transmitting, is the same for each level. This allows us to apply the well-established theory of quasi-stationary discrete time Markov chains with an absorbing state. The absorbing state is defined to be when all the nodes in one hop cannot decode the message, and the transmissions stop propagating. Once we have the quasi-stationary distribution, we can determine network performance, such as packet delivery ratio and latency over a given distance as a function of system parameters such as transmit power, inter-node distance and path loss exponent.

The successful transmission of message signal over a linear network poses some challenges that are present if the nodes along the link or route are equally spaced.

However, if the nodes are not equally spaced, e.g., because of mobility or random placement, there is an additional probability of very weak links, or a network partition, where a gap is so large that no single-input-single-output (SISO) link can bridge the gap. Another contribution of this research is that it analyzes a line network that employs OLA network and considers a kind of quantized random deployment along a line. In particular, we study the case where the potential node locations are equally spaced, but the presence or absence of a node in each location follows a Bernoulli process.

The second issue addressed in this dissertation is the estimation of signal-to-noise ratio. Estimates of signal-to-noise ratio (SNR) are used in many wireless receiver functions, including signal detection, power control algorithms and turbo decoding etc. Although SNR is an important parameter in studying performance analysis of different communication systems, it can also be used in determining which nodes to participate in the CT. The more distant nodes from the source having least SNR are most suitable to transmit the message to the next level. However, practical real-time SNR estimators are required to evaluate system performance. Furthermore, if the radios are energy constrained, e.g., if they are in a sensor network, constant envelope modulation and non-coherent demodulation are desirable to reduce circuit consumption of energy. FSK enables efficient power amplification in the transmitter and a simple receiver design that employs envelope detection. Therefore, another key contribution of this research is the design of optimal SNR estimators that can work with both the symbol-by-symbol Rayleigh fading channels as well as slow flat fading channels in a wireless medium. Failure to synchronize with the carrier frequency often results in erroneous estimates of SNR. Thus, in this dissertation, we estimate the SNR of a non-coherent FSK receiver in the presence of a carrier frequency offset (CFO), treating the CFO as a nuisance parameter. The CFO estimation problem is quite tedious to solve because of its highly non-linear nature, hence analytical

methods cannot be directly applied to solve the problem at hand. Therefore, we derive a maximum likelihood estimator for the SNR that uses a moment-based CFO estimator. We also derive the Cramer-Rao lower bound (CRB) for the SNR estimator. We provide two types of SNR estimators: a data-aided (DA) estimator that uses the pilot symbols and a non-data aided (NDA) estimator that does blind estimation on the received symbols.

CHAPTER II

ORIGIN AND HISTORY OF THE PROBLEM

2.1 Modeling Cooperative Wireless Networks

Cooperative relaying methods have attracted a lot of interest in the past few years. Cooperative transmission (CT) is an attractive technique in achieving higher system performance in terms of capacity and diversity gains in wireless systems. It has been proposed as a means to improve link reliability or provide range extension, by having multiple radios transmit the same message to a receiver through uncorrelated fading channels. Exploiting the broadcast nature of wireless networks, the relay nodes help the transmission of data through different channels, resulting in considerable improvement in system performance.

A conventional multi-hop cooperative communication system employs a relay node in addition to the source and destination [1], [2]. The Figure 1a represents a pair of terminals S and D who wants to communicate with each other. If there is a wireless link between them, then the top curve in Figure 1b represents the outage probability as a function of signal-to-noise ratio (SNR) [2]. An outage occurs if the received signal by D drops below a certain specified SNR threshold. However, if a relay $R1$ is employed to assist the source in sending the message to the destination, the middle curve in Figure 1b represents an SNR advantage of approximately 13dB as compared to the direct transmission. Using another relay node R2 further improves the system performance with an SNR advantage of 19dB. Therefore, CT improves the connectivity of network by providing diversity gain.

Two approaches are commonly used in cooperative relaying scenarios. The first is known as amplify-and-forward transmission (AF), where the relay amplifies the

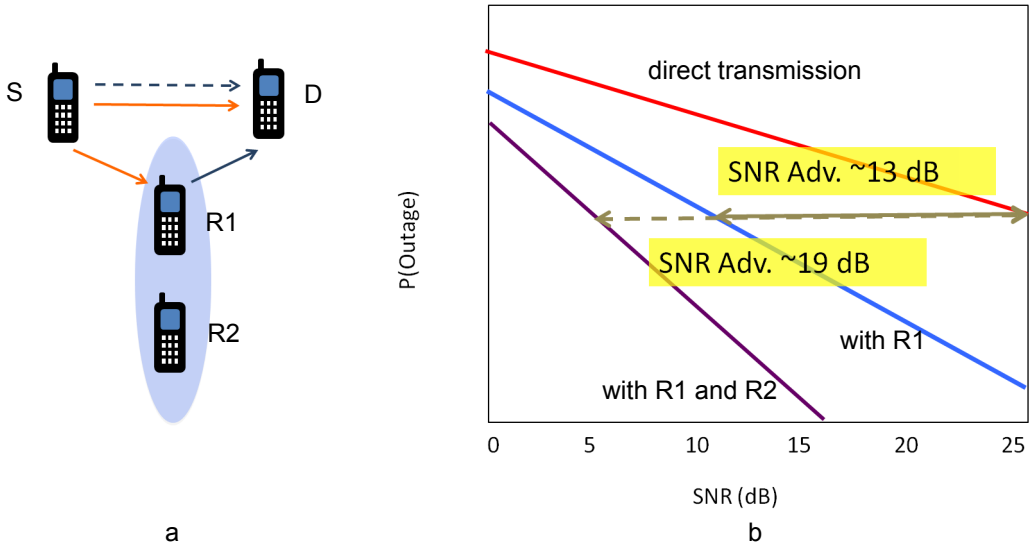

Figure 1: a: Cooperative and direct transmission topologies, b: Probability of outage vs SNR for various topologies

received signal and forwards it to the destination. The second approach is decode-and-forward transmission (DF) where the relay decodes the incoming signal first and then re-encodes and broadcasts it [2]. A lot of work has been done on systems having a single cooperative node operating as relay. Some researchers focus on the receiver design to mitigate the effects of inter-symbol interference (ISI) and reducing the bit-error rate (BER) of transmission [3], while others focus on channel capacity and outage behaviors [4]. Another approach is the use of multiple relays in which more than one relay station help the source in transmission of data. The technique commonly known as relay selection in described in [5] and [6]. More recently, a multiple relay approach with feedback is proposed in [7]. These schemes show considerable system performance and have great potential to be used in many wireless applications especially in cellular networks.

One promising, very fast, and energy efficient multi-hop CT technique is the Opportunistic Large Array (OLA), which is suitable for networks consisting of a large number of nodes or sensors having communication capabilities conveying information in a networked manner to the destination [8]–[21]. This type of multi-hop network

known as ad-hoc wireless sensor network (WSN) has also attracted considerable research in the past several years. In an OLA transmission, the source sends the message signal in the first time slot. Exploiting the broadcast nature of wireless networks, a group of relays, in the vicinity of the source, decodes the message and those nodes become part of the first level OLA. This process continues until the message signal reaches the destination node. Because inter-node coordination is not needed, OLAs are particularly well suited for mobile networks, such as large groups of people with smart phones. For example, an OLA broadcast may complement or supplant base station or access point transmissions, harnessing the other radios in a network to increase the reliability and speed of a broadcast. A set of nodes being separated in space, each having a single antenna, collectively form a 'virtual-multiple-input-multiple-output (MIMO) system,' thereby offering the benefits of diversity protection from multi-path fading and spectrum efficiency.

There are many uncertainties that influence exactly which radios participate in an OLA. Path loss effects, multi-path fading, shadowing, imperfect signal-to-noise ratio (SNR) calculation, effects of finite density of nodes in an area, optimal power allocation for the relays, timing and carrier synchronization issues are among those uncertainties that affect the propagation of signals in an OLA transmission. Currently, there is no way to model general OLA transmissions short of brute force Monte Carlo simulation, and this has been a barrier to the fundamental analysis of this transmission technique. Most of the previous theoretical works in cooperative transmission deal with the single [1], [2] or dual relay system [24]–[27]. The authors in [8] studied large dense networks, using the *continuum* assumption. Under this assumption, the number of nodes goes to infinity while the power per unit area is kept fixed. This assumption is not appropriate for low-density networks. The continuum model was also used in [20] and [28], where the authors studied broadcasting and uni-casting protocols with the path loss as the only channel impairment. Most finite

density studies have used simulations, as in [23]. These papers derived conditions under which broadcasting over an infinite disk or strip is guaranteed. In contrast, we obtain closed-form theoretical results without the continuum assumption, by deploying a simple one-dimensional network where the nodes are uniformly spaced on a grid. By applying the quasi-stationary Markov chain analysis, we show that there is no condition guaranteeing infinite propagation of OLAs. There is only a probability of successfully delivering a packet over a given distance. Although our analysis focuses on the delivery of only a single packet, in many applications, numerous packets, composing for example a video file, could be injected into such a cooperative route, one every few time slots, similarly to how they are injected in a non-cooperative route.

2.2 SNR Estimation

Signal-to-noise ratio (SNR) is an important parameter to be estimated in a wireless communication network. The estimates of SNR can be used in choosing one of the relaying protocols (AF or DF) to enhance the overall system performance in terms of achieving higher capacity and reducing the rate-loss. Wireless sensor nodes have severe constraints in terms of their limited battery-reserve, computational power, and storage capacity. These constraints correspondingly impact the kind of operations that can be supported by the network and limit the reliability, survivability, and lifetime of such networks. SNR estimation is a way for a receiver to determine if it is near the edge of the decoding range of its source, and therefore, in a preferred location to participate in a cooperative transmission [20]. Furthermore, if the radios are energy constrained, e.g., if they are in a sensor network, constant envelope modulation and non-coherent demodulation are desirable to reduce circuit consumption of energy. It is, therefore, required to estimate the SNR for communication systems employing non-coherent modulation schemes such as frequency shift keying (FSK). Several authors have attacked the problem of estimating SNR for binary phase shift keying (BPSK)

and FSK. For example, [38] compares a variety of techniques for SNR estimation in additive white Gaussian noise (AWGN) for M-PSK signals. Many approaches also include the channel effects such as multi-path fading and address the issues of SNR estimation for fading channels for BPSK, e.g., in [39]–[42]. FSK enables efficient power amplification in the transmitter and a simple receiver design that employs envelope detection [46]. In [48], the authors have estimated the average SNR for non-coherent binary FSK (NCBFSK) receiver, assuming a Rayleigh fading channel and unit noise power spectral density. However, in implementations, noise power must also be estimated. Also the approach in [48] cannot be generalized to M-FSK SNR estimation.

In many wireless indoor applications and fixed wireless networks, the channel frequency response does not change rapidly. Thus a block of data undergoes a constant non-random fade. Estimation of SNR in such a case is of prime interest for various receiver functions. Assumption of a slow fading channel can be converted to a fast fading channel by assuming sufficient channel interleaving or by frequency hopping. But these techniques may not be suitable for some applications, e.g., wireless sensor networks, where the sensor nodes should be as simple as possible; devising such algorithms in these applications tends to increase the transmitter complexity. Thus a practical way of estimating SNR in slow fading environments is desirable.

The subject of the current research is to overcome the challenges of SNR estimation for non-coherent MFSK systems in both symbol-by-symbol Rayleigh fading channels and in slow flat fading channels.

CHAPTER III

STOCHASTIC MODELING OF DETERMINISTIC LINE NETWORKS

This chapter describes the framework used to analyze and model the cooperative transmissions network in a line network. The placement of the nodes is deterministic and takes into account the effects of channel impairments and finite density of the relays. The rest of the chapter is organized as follows. In the next section, we define the network parameters and propose a model of the network via discrete time Markov chains (DTMC) and obtain a quasi-stationary distribution of this chain in Section 3.2. In Section 3.3, we derive the transition probability matrix for the proposed model and we propose an iterative algorithm for optimizing the membership function in Section 3.4. We will then validate the analytical results with those of numerical simulations in Section 3.5.

3.1 System Description for the Cooperative Network

In this section, we describe our model for the signal-to-noise ratio (SNR) in each receiver, and state our other assumptions. Consider a line of nodes where adjacent nodes are a distance d apart from one another, as shown in Figure 2. We assume that the nodes transmit synchronously in OLAs or levels, and that a *hop* occurs when nodes in one level transmit a message and at least one node is able to decode the message for the first time. Correct decoding is assumed when a node's received SNR at the output of the diversity-combiner, from the previous level only, is greater than or equal to a modulation-dependent threshold, τ. Exactly one time slot later, all the nodes that just decoded the message relay the message. Thus, this type of cooperative

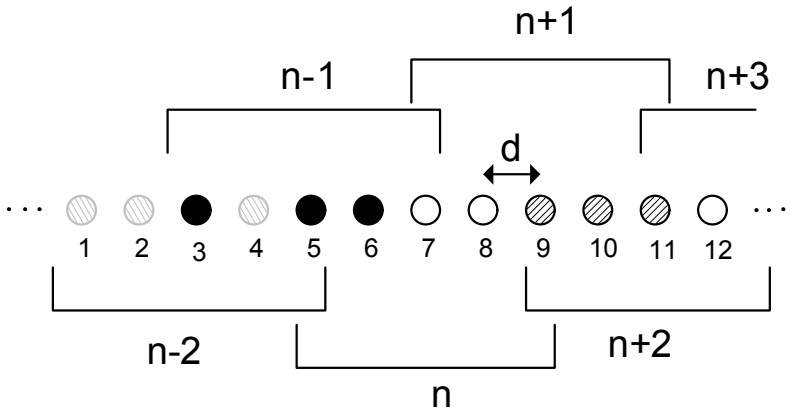

Figure 2: A sample outcome of the transmission system with the overlapping windows; $M = 5$ and $h_d = 2$

transmission is similar to selection relaying in [2]. Once a node has relayed a message, it will not relay that message again. Let $p_n(m)$ be the *membership* probability that the mth node transmits in the nth level, given that at least one node transmitted in the $(n-1)$th level. Also let M be at least the width of the region of support of $p_n(m)$. In other words, there exists some M_0 such that $p_n(m) \geq 0$ for $M_0 \leq m \leq M_0 + M - 1$ and $p_n(m) = 0$ otherwise. As we will show later, the quasi-stationary property implies that there exists a hop distance, h_d, such that $p_{n-1}(m - h_d) = p_n(m)$. Hence h_d can be considered as a shift to the window of size M. A sample outcome of the transmissions is shown in Figure 2 where the window size, M, is 5 and hop distance or the shift in window, h_d, is 2. The nodes 1, 2, and 4 are able to decode the message and become part of level $n-2$. These nodes will relay the message in the next time slot and only the nodes in level $n-1$ may decode that message. Since node 4 has already participated in level $n-2$, so it cannot be part of any other level including $n-1$. Thus the candidate nodes are 3, 5, 6, and 7, out of which nodes 3, 5, and 6 become DF nodes in level $n-1$ and this process continues.

We assume that all the nodes transmit with the same transmit power P_t. A node receives superimposed copies of the message signal from the nodes that decoded the message correctly in the previous level, over orthogonal fading channels using equal

gain combining (EGC). Let us define $\mathbb{N}_n = \{1, 2, ..., k_n\}$, where k_n is the cardinality of the set $\mathbb{N}_n$ such that $\sup_n k_n = M$, to be the set of indices of those nodes that decoded the signal perfectly at the time instant (or hop) n. For example, from Figure 2, $\mathbb{N}_n = \{3, 4\}$ and $\mathbb{N}_{n+1} = \{3, 4, 5\}$. The received power at the jth node at the next time instant $n + 1$ is given by

$$P_{r_j}(n+1) = \frac{P_t}{d^\beta} \sum_{m \in \mathbb{N}_n} \frac{\mu_{mj}}{|h_d - m + j|^\beta}, \tag{1}$$

where the summation is over the nodes that decoded correctly in the previous level. The flat fading Rayleigh channel gain from node m in the previous level to node j in the current level is denoted by $\mu_{mj} \in \mu$; the elements of μ are independently and identically distributed (i.i.d.) and are drawn from an exponential distribution with the parameter σ_μ^2=1; β is the path loss exponent with a usual range of 2-4. Consequently, the received SNR at the jth node is given as $\gamma_j = P_{r_j}/\sigma_j^2$, where σ^2 is the variance of the noise in the receiver. Throughout the thesis, we will use the notation $P_{r_j}(n)$ as the power received at the jth node at the nth time instant. We assume perfect timing and frequency recovery at each receiver, and we also assume that there is sufficient transmit synchronization between the nodes of a level, such that all the nodes in a level transmit to the next level at the same time [22]. In other words, the transmissions only occur at discrete instants of time $n, n + 1, ...$ such that the hop number and the time instants can be defined by just one index n. By the overlapping nature of the windows, we have the following proposition.

Proposition 1 *Given M and h_d, a node at a position x can become part of several levels n, such that $\forall x > M - h_d$*

$$\left\lceil \frac{x - M}{h_d} \right\rceil + 1 \leq n \leq \left\lfloor \frac{x - 1}{h_d} \right\rfloor + 1. \tag{2}$$

Proof: Without the loss of generality, we can assume that the first node in the network is located at $x = 1$ and is a part of level $n = 1$. From the given geometry,

the starting location of nth window is given by $(n-1)h_d + 1$, while the end location as $(n-1)h_d + M$. A node at any position x in this window, lies in between these locations, i.e.

$$(n-1)h_d + 1 \leq x \leq (n-1)h_d + M. \tag{3}$$

The above inequality can be broken into two, such that

$$(n-1)h_d \leq x - 1 \qquad \text{and} \qquad x - M \leq (n-1)h_d.$$

This implies, $x - M \leq (n-1)h_d \leq x - 1$. From the necessary condition derived in (3), we get (2). ■

Corollary 1 *$\forall x \leq M - h_d$, we have $n = 1, ..., \left\lceil \frac{x}{h_d} \right\rceil$.*

One goal of this study is to find the hop distance as a function of the values of system parameters such as relay transmit power and inter-node distance. However, because of the discrete nature of the hop distance, solving the problem is this manner is quite tedious. Hence in this study, we follow the inverse approach, i.e., for a given hop distance, we will find the system parameters that generate this hop distance. We find the parameters that give the most compact OLAs.

3.2 Modeling by Markov Chain

At a certain time n, a node from the nth level will take part in the next transmission, if it has decoded the data perfectly at the current time, or it will not take part, if it did not decode correctly or it has already decoded the data in one of the previous levels. The decisions of all the nodes in the nth level can be represented as $X(n) = [\mathbb{I}_1(n), \mathbb{I}_2(n), ..., \mathbb{I}_M(n)]$, where $\mathbb{I}_j(n)$ is the ternary indicator random variable for the jth node at the nth time instant given as

$$\mathbb{I}_j(n) = \begin{cases} 0 & \text{node } j \text{ does not decode} \\ 1 & \text{node } j \text{ decodes} \\ 2 & \text{node } j \text{ has decoded at some earlier time} \end{cases} \tag{4}$$

Thus each node is represented by either 0, 1 or 2 depending upon the successful decoding of the received data. For example, from Figure 2, we have $\mathbb{I}_1(n) = \mathbb{I}_2(n) = 2$, $\mathbb{I}_3(n) = \mathbb{I}_4(n) = 1$ and $\mathbb{I}_5(n) = 0$. We observe that the outcomes of $X(n)$ are ternary M-tuples, each outcome constituting a state, and there are 3^M number of states, which are enumerated in decimal form $\left\{0, 1, ..., 3^M - 1\right\}$. Let i_n be the outcome at time n. For example, $i_n = [22110]$ in ternary, and $i_n = 228$ in decimal in Figure 2. Then we may write

$$\begin{aligned} \mathbb{P}\left\{X(n) = i_n | X(n-1) = i_{n-1}, ..., X(1) = i_1\right\} = \\ \mathbb{P}\left\{X(n) = i_n | X(n-1) = i_{n-1}\right\}, \end{aligned} \tag{5}$$

where $\mathbb{P}$ indicates the probability measure. Equation (5) implies that $X(n)$ is a discrete-time finite-state Markov Process. Assuming the statistics of the channel are same for all the hops in the network, the Markov chain can be regarded as a homogeneous one.

It can be further noticed that at any point in time, there is a probability that the Markov chain can go into an absorbing state, thus terminating the transmission. That can be a state when all the nodes at a particular hop cannot decode the message perfectly and thus Markov chain will be in the 0 state (decimal). It can be further noticed, that any possible combination of 0 and 2 will also make the state an absorbing state. Since we are enumerating the states using ternary words, the total number of states appears to be 3^M. But the following claim shows that the number of transient states in the Markov chain are less than 3^M.

Claim 1 *Given M and h_d, the possible number of states that can be reached during transitions is $\hat{N} = 3^{M-h_d} \times 2^{h_d}$, including 2^{M-h_d} number of absorbing states.*

Proof: Please see the Appendix A.

Hence we consider the Markov chain, X, on a state space $A \cup S$, where A is the

set of absorbing states, and we have

$$\lim_{n\to\infty} \mathbb{P}\{X(n) \in A\} \nearrow 1 \quad \text{a.s.} \tag{6}$$

On the other hand, the states in S (where the cardinality of S is $|S| = \hat{N} - 2^{M-h_d}$) make an irreducible state space, i.e., there is always a non-zero probability to go from any transient state to another transient state. We will define two matrices to describe the Markov Chain. The first, $\tilde{\mathbf{P}}$, is the full transition probability matrix for all the states in the set $A \cup S$. Each row in $\tilde{\mathbf{P}}$ sums to one. The second matrix, $\mathbf{P}$, is the sub-matrix of $\tilde{\mathbf{P}}$ that is formed by striking each column and row that involves transitions to and from the absorbing states in A. Therefore, $\mathbf{P}$ is the matrix corresponding to the states in S. It can be noticed that the transition probability matrix $\mathbf{P}$ on the state space S is not right stochastic, i.e., the row entries of $\mathbf{P}$ do not sum to 1 because of the *killing probabilities* given as

$$\kappa_i = 1 - \sum_{j\in S} \mathbf{P}_{ij}, \quad i \in S. \tag{7}$$

Since $\mathbf{P}$ is a square irreducible nonnegative matrix, then by the Perron-Frobenius theorem [32], there exists a unique maximum eigenvalue, ρ, such that the eigenvector associated with ρ is unique and has strictly positive entries. For the proof, please refer to [32] and [35]. Since $\mathbf{P}$ is not right stochastic, $\rho < 1$. Also since all states in S are transient and not strictly self-communicating, $\rho > 0$ [30]. Overall our assumptions imply that

$$0 < \rho < 1. \tag{8}$$

From the theory of Markov chains [35], we know that a distribution $\mathbf{u} = (u_i, i \in S)$ is called ρ-invariant distribution if $\mathbf{u}$ is the left eigenvector of the transition matrix $\mathbf{P}$ corresponding to the eigenvalue ρ, i.e.

$$\mathbf{uP} = \rho\mathbf{u}. \tag{9}$$

We are now interested in the limiting behavior of this Markov chain as time proceeds. Since $\forall n,\ \mathbb{P}\{X(n) \in A\} > 0$, eventual killing is certain. But we are interested in finding the distribution of the transient states, before the killing occurs. The so-called limiting distribution is called the quasi-stationary distribution of the Markov chain, which is independent of the initial conditions of the process. From [29] and [30], this unique distribution is given by the ρ-invariant distribution for the one step transition probability matrix of the Markov chain on S. We can find the quasi-stationary distribution by getting the *maximum* eigenvector, $\hat{\mathbf{u}}$ of $\mathbf{P}$, then defining $\mathbf{u} = \hat{\mathbf{u}}/\sum_{i=1}^{\hat{N}} \hat{\mathbf{u}}_i$ as a normalized version of $\hat{\mathbf{u}}$ that sums to one.

Thus we can define the unconditional probability of being in state j at time n as

$$\mathbb{P}\{X(n) = j\} = \rho^n u_j, \quad j \in S, \quad n \geq 0. \tag{10}$$

We also let $T = \inf\{n \geq 0 : X(n) \in A\}$ denote the end of the survival time, i.e., the time at which killing occurs. It follows then,

$$\mathbb{P}\{T > n + m | T > n\} = \rho^m, \tag{11}$$

while the quasi-stationary distribution of the Markov chain is given as

$$\lim_{n\to\infty} \mathbb{P}\{X(n) = j | T > n\} = u_j, \quad j \in S. \tag{12}$$

We also note that the membership probability can be expressed as

$$p_n(m) = \sum_{j\in\theta} u_j, \tag{13}$$

where $\theta = \{X(n) \in S : \mathbb{I}_m(n) = 1\}$.

3.3 Formulation of the Transition Probability Matrix

In this section, we will find the state transition matrix $\mathbf{P}$ for our model, the eigenvector of which will give us the quasi-stationary distribution. Let i and j denote a pair of states of the system such that $i, j \in S$, where each i and j are the decimal equivalents

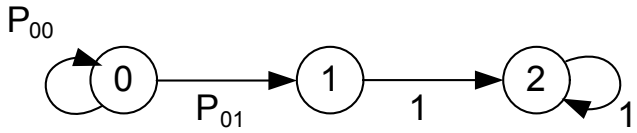

Figure 3: State transition diagram of a node

of the ternary words formed by the set of indicator random variables. Now for each node m, the probability of being able to decode at time n given that it failed to decode in the previous level is given as

$$\mathbb{P}\left\{\mathbb{I}_m(n) = 1 | \mathbb{I}_{h_d+m}(n-1) = 0\right\} = \mathbb{P}\left\{\gamma_m(n) > \tau\right\}. \tag{14}$$

Similarly, the probability of outage or the probability of $\mathbb{I}_m(n) = 0$ is given as $1 - \mathbb{P}\left\{\gamma_m(n) > \tau\right\}$ where

$$\mathbb{P}\left\{\gamma_m(n) > \tau\right\} = \int_{\tau}^{\infty} p_{\gamma_m}(y)dy. \tag{15}$$

$p_{\gamma_m}(y)$ is the probability density function (PDF) of the received SNR at the mth node. From (4), we note that a node can have three possible states, where the initial state of a node is always 0. A node can make the transitions shown in Figure 3. Hence each individual node is a state machine, and $\mathbb{I}_m(n)$ is a non-homogeneous Markov chain itself; the probabilities of transition for a single node are non-zero only at certain times. P_{01} from Figure 3, i.e., the conditional probability of success of the mth node in the nth level, is given as

$$P_{01} = \mathbb{P}\left\{\gamma_m(n) > \tau | \mathbb{I}_{h_d+m}(n-1) = 0; X(n-1) \in S\right\}. \tag{16}$$

Hence the probability of perfect decoding is based on the PDF of the received power which can be obtained as follows.

Lemma 1 *If $h_d = M$, the conditional PDF of the received power, conditioned on which nodes transmit, is hypoexponential.*

Proof: It can be seen that the power at a certain node is the sum of the finite powers from the previous level nodes, each of which is exponentially distributed.

Thus for K independently distributed exponential random variables with respective parameters λ_k, where $k = 1, 2, ..., K$, the resulting distribution of the sum of these random variables is known as hypoexponential distribution [31] which is given as

$$p_Y(y) = \sum_{k=1}^{K} C_k \lambda_k \exp(-\lambda_k y), \tag{17}$$

where

$$C_k = \prod_{\zeta \neq k} \frac{\lambda_\zeta}{\lambda_\zeta - \lambda_k}. \tag{18}$$

Although $\int_0^\infty p_Y(y)dy = 1$, it should not be thought that C_k are probabilities, because some of them will be negative. ■

For $1 \leq h_d < M$, we consider the following lemma.

Lemma 2 *For two independent exponential random variables with parameters λ and $\lambda + \epsilon$, the complementary CDF (tail probability) of their sum approaches that of a Gamma distribution, $\Gamma(2, \lambda)$, as $\epsilon \to 0$.*

Proof: The CCDF of sums of two independent exponential random variables is given as

$$F_x(x) = \sum_{k=1}^{2} C_k \exp(-\lambda_k x); \tag{19}$$

where $C_1 = \frac{-\lambda}{\epsilon}$ and $C_2 = \frac{\lambda}{\epsilon} + 1$. Thus the CCDF is given as

$$F_x(x) = \exp(-\lambda x)\lambda \left[-\frac{\exp(-\epsilon x)}{\epsilon} + \frac{1}{\epsilon} \right] + \exp(-\lambda x). \tag{20}$$

Taking $\lim_{\epsilon \to 0}$ and using L'Hospital's rule, we get

$$F_x(x) = \exp((-\lambda x))(1 + \lambda x) \tag{21}$$

which is the CCDF of $\Gamma(2, \lambda)$. ■

With the help of these lemmas, let's consider the following theorem.

Theorem 1 *The received power at any node in the network, conditioned on a certain pattern of nodes transmitting in the previous level, is always hypoexponentially distributed.*

Proof: If $h_d = M$, the resulting distribution is hypoexponential from Lemma 1. For $h_d < M - 1$, a node will receive powers from adjacent nodes that are either hypoexponentially distributed (if their respective parameters are different) or they are received as pairs of Gamma distributed variables. Thus the power received will be sum of exponential random variables such that there will be (groups of) two variables having same parameters and rest having distinct parameters. But using Lemma 2, the power received at any node is hypoexponential. ■

Let us define a set which consists of all those nodes that decoded the data perfectly in the previous hop as $\mathbb{N}_{n-1} = \{m_i : \mathbb{I}_{m_i}(n-1) = 1\} \ \ \forall i = 1, 2, ...M$, then from Theorem 1, P_{01} from (16) is given as

$$P_{01} = \sum_{k \in \mathbb{N}_{n-1}} C_k \exp\left(-\lambda_k^{(m)} \tau\right), \tag{22}$$

where $\lambda_k^{(m)}$ is given as

$$\lambda_k^{(m)} = \frac{d^\beta \left|h_d - k + m\right|^\beta \sigma^2}{P_t}. \tag{23}$$

To determine the possible destination states in a transition from level $n-1$ to level n, it is helpful to distinguish between two mutually exclusive sets of nodes in the nth level: 1) the nodes that were also in the M-node window of the $(n-1)$th level, i.e., nodes that are in the h_d overlap region of the two consecutive windows, and 2) the remaining $M - hd$ nodes that are not in the overlap region. We denote these two sets of nodes as $\mathbb{N}_{OL}^{(n)}$ and $\overline{\mathbb{N}}_{OL}^{(n)}$, respectively, where OL stands for *overlap*.

Suppose node k in $\mathbb{N}_{OL}^{(n)}$ decoded in the previous $(n-1)$th level; this would be indicated by $\mathbb{I}_{h_d+k}(n-1) = 1$. This node will not decode again, and therefore $\mathbb{I}_k(n) = 2$. Similarly, if that node decoded prior to the $(n-1)$th level, then $\mathbb{I}_{h_d+k}(n-1) = 2$. In this case also, we must have $\mathbb{I}_k(n) = 2$. Alternatively, if the node has not previously decoded, then $\mathbb{I}_{h_d+k}(n-1) = 0$, and $\mathbb{I}_k(n)$ can equal 0 or 1, depending on the previous state and the channel outcomes; $\mathbb{I}_k(n) = 2$ is not possible. If the node k is in the $\overline{\mathbb{N}}_{OL}^{(n)}$, then there is no previous level index for this node, and, again we can have

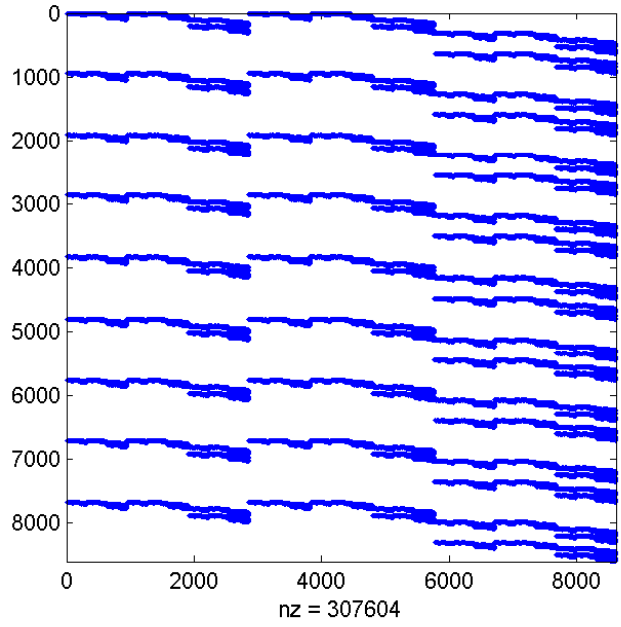

Figure 4: Sparse structure of the transition probability matrix with $M = 9$ and $h_d = 2$

$\mathbb{I}_k(n) \in \{0, 1\}$ depending on the previous state and channel outcomes, but we may not have $\mathbb{I}_k(n) = 2$.

Let a superscript on the indicator functions show the value of the indicator given the ith state. For example, if $i = \{22110\}$, then $\mathbb{I}_5^{(i)}(n) = 0$. Therefore, considering the above discussion, one-step transition probability going from the state i in level $n-1$ to state j in level n is always 0 when either of the following conditions is true:

Condition I: $\mathbb{I}_k^{(j)}(n) \in \{0, 1\}$ and $\mathbb{I}_{h_d+k}^{(i)}(n-1) \in \{1, 2\}$,

Condition II: $\mathbb{I}_k^{(j)}(n) = 2$ and $\mathbb{I}_{h_d+k}^{(i)}(n-1) = 0$.

Thus the one step transition probability for going from state i to state j is 0 if condition I or II holds; otherwise it is given as

$$P_{ij} = \prod_{k \in \mathbb{N}_n^{(j)}} \left(\sum_{m \in \mathbb{N}_{n-1}^{(i)}} C_m \exp\left(-\lambda_m^{(k)} \tau\right) \right) \bullet \prod_{k \in \overline{\mathbb{N}}_n^{(j)}} \left(1 - \sum_{m \in \mathbb{N}_{n-1}^{(i)}} C_m \exp\left(-\lambda_m^{(k)} \tau\right) \right) \tag{24}$$

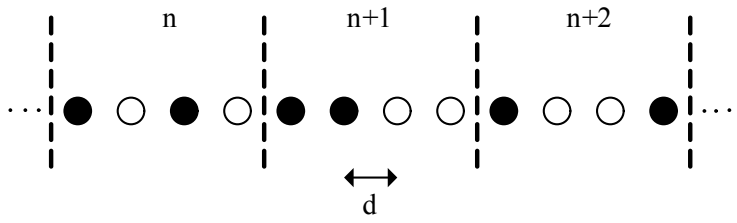

Figure 5: Arrangement of nodes on a grid with non-overlapping windows; $M = 4$ and $h_d = 4$

where $\mathbb{N}_n^{(j)}$ and $\overline{\mathbb{N}}_n^{(j)}$ are the indices of those nodes which are 1 and 0, respectively, in state j at level n. Thus it can be seen that the transition probability matrix will contain a large number of zeros. The smaller the hop distance, the larger are the number of zeros in the matrix. Thus the resulting matrix is highly sparse which helps in evaluating the Perron-Frobenius eigenvalue quickly. A sample sparse structure of this matrix that results from $M = 9$ and $h_d = 2$ is shown in Figure 4. It can be seen that there are more than 95% of zeros in the matrix. Another interesting observation is that the matrix entries start to repeat after 2/3 of the matrix. This is because there is no difference in calculating transmissions if the first node in the window is 0 or 2. Thus the calculations are further reduced by a factor of 1/3.

3.3.1 A Special Case: Non-Overlapping Windows

A special case of the transmission system is that when the hop distance becomes equal to the window size. Thus in this process, we constrain the clusters to be contained in a pre-specified non-overlapping sets of nodes. Each cluster or OLA is still opportunistic in the sense that only the nodes in the set that can decode will be part of the OLA. An example of the cluster to cluster transmission is given in Figure 5, where the correctly decoding nodes are shown as filled black circles. Since no overlap is involved, at a certain time n, each node from the nth level will take part in the next transmission, if it has decoded the data perfectly, or it will not take part, if it did not decode correctly. The decisions of all the nodes in a level can be represented as *binary* indicator random variables, $\mathbb{I}_j(n)$, taking value 1 for successful

decoding and 0 for a failure decoding. Hence the considered Markov chain, X, is defined on a state space $0 \cup S$, where S is a finite transient irreducible state space, $S = \{1, 2, ..., 2^M - 1\}$, and 0 being the absorbing state. The resulting sub-stochastic transition probability matrix $\mathbf{P}$ is a $(2^M - 1) \times (2^M - 1)$ corresponding to the states in S. For M nodes in a level, let us define the index sets corresponding to the ith state as

$$\mathbb{N}_n^{(i)} = \{1, 2, ..., k_n\} \text{ and } \overline{\mathbb{N}}_n^{(i)} = \{1, 2, ..., M\} \setminus \mathbb{N}_n^{(i)},$$

to be the sets of those nodes which are 1 and 0, respectively, in state i. Then the one step transition probability for going from state i to j is the same as given in (24), where the distribution of received power at a single node is hypoexponential from Lemma 1 and $\lambda_k^{(m)}$ is given as

$$\lambda_k^{(m)} = \frac{d^\beta (M - k + m)^\beta \sigma^2}{P_t}. \tag{25}$$

It should be noticed that in this case, there are no conditions that would lead to zero probability of transition from state i to state j and hence the matrix is not sparse.

3.4 Iterative Approach

In previous sections, we showed how to compute the quasi-stationary distribution and the membership probabilities for a given specification of system parameters, such as transmit power, path loss exponent, inter-node distance, hop distance, and for the one artificial constraint, the window width. Therefore, an infinite variety of possible solutions exist, depending on the choices of these parameters. In this section, we eliminate the artificial constraint and show how the design space dimension can be further reduced through parameter normalization and by optimizing the shape of the membership probability function.

M is an *artificial* constraint because there is no real physical need for it, however, it strongly impacts the size of the state space and therefore the computational complexity of finding the quasi-stationary distribution. Therefore, we would like for

M to be as small as possible without significantly impacting the system performance results. The transmissions from nodes at the trailing edge of a large window will have only a small contribution to the formation of the next OLA, because of disparate path loss (especially in a line-shaped network), and therefore, their contribution can be neglected. This suggests that an energy efficient solution will be a uni-modal membership probability function with a narrow region of support, and therefore a small M can support it. We note that the number of nodes that relay in each hop determines the diversity order in this finite density scenario, so the most narrow membership function (a Kronecker delta) is not desirable. A final consideration is that for the broadcast application, ideally, we want every node to decode the message, and so, under our assumption that every node that decodes for the first time also relays, we have that for a hop distance of h_d, we want at least h_d nodes to relay in each hop.

Based on all of these considerations, we decided to choose the solution that yields a membership probability function that most closely resembles a square pulse of unit height that is h_d nodes wide, and takes the value of zero everywhere else on a window that is M nodes wide. This can be interpreted as corresponding to the most compact (i.e., shortest length) OLA. We find M by increasing it until the one-hop success probability (i.e., the Perron-Frobenius eigenvalue) ceases to change significantly.

To further decrease the design space dimension, we observe that the transition matrix in (24) depends on the product $\lambda_m^{(k)}\tau$, from which we can extract the normalized parameter

$$\Upsilon = \frac{\gamma_0}{\tau} = \frac{P_t}{d^\beta \sigma^2}\frac{1}{\tau}, \tag{26}$$

which can be interpreted as the SNR margin from a single transmitting node a distance d away. However, Υ is not the only independent parameter, because β and h_d also separately impact the value of $\lambda_m^{(k)}\tau$, in (23) through the factor $|h_d - k + m|^\beta$.

We now formally describe our optimization procedure. We define our ideal membership probability function as

$$\hat{q}(k) = u(k-a) - u(k-(a+h_d-1)) \quad k \geq 1, \tag{27}$$

where u is the unit step function and $a = \left\lfloor \frac{M-h_d}{2} \right\rfloor + 1$. We can express the membership probabilities for a given level in vector form as $\mathbf{q} = \{p_{m_1}, p_{m_2}, ..., p_{m_M}\}$, where the values of $p_{m_k}(n)$ can be found using either (13) or as

$$\begin{aligned} p_{m_k}(n) &= \mathbb{P}\left\{\mathbb{I}_{m_k}(n) = 1\right\} \\ &= \sum_{j=1}^{\hat{N}} \mathbb{P}\left\{\mathbb{I}_{m_k} = 1 | X(n) = j\right\} \mathbb{P}\left\{X(n) = j\right\} \\ &\forall k = \{1, 2, ..., M\} \text{ and } j \in S. \end{aligned} \tag{28}$$

Then the problem of finding the best Υ can be formulated as

$$\min_{\Upsilon > 0} \ \Xi = \frac{1}{M} \left\| \mathbf{q} - \hat{\mathbf{q}} \right\|^2. \tag{29}$$

The iterative algorithm is this case is given as follows.

1. Given h_d, initialize the algorithm with a window size of $M = 2h_d$.
2. Compute the Perron-Frobenius eigenvalue, $\rho(M)$, over a range of SNR margins.
3. Increment the window size by one, and compute $\rho(M+1)$ using Step 2.
4. If $|\rho(M+1) - \rho(M)| < \epsilon$, for some small $\epsilon > 0$, M is the desired window size and the convergence is achieved. Otherwise go to Step 3.

By using the iterative technique, we are able to find the optimal window size M over a range of SNR margins. To choose the SNR margin that gives a close approximation to (27), minimize (29) over the SNR margin range to get the best value of SNR margin where we achieve the minimization. This value of Υ is the one that yields a given h_d with maximum probability.

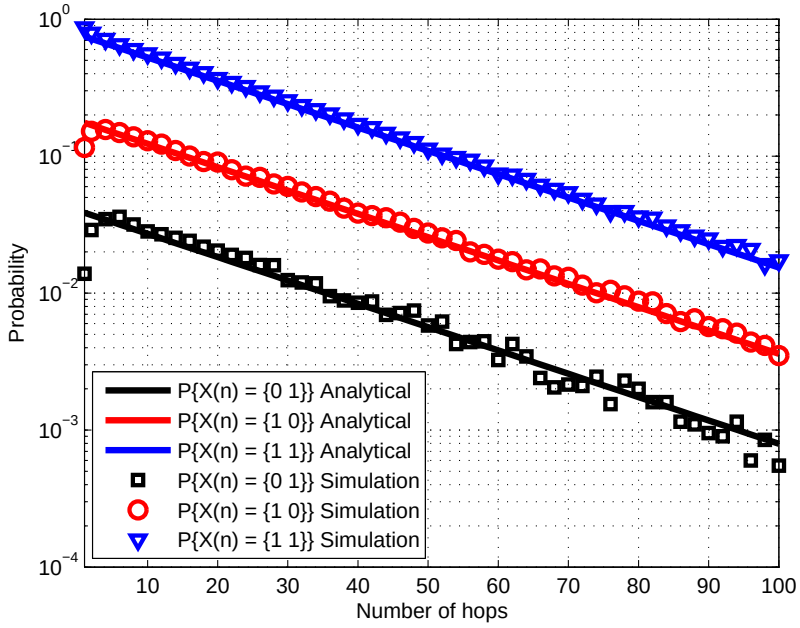

Figure 6: Distribution of the states for $M = 2$ and $h_d = 2$ for non-overlapping windows

3.5 Results and System Performance

In this section, we compare the analytical results with those of numerical simulations for different sets of parameters and we investigate system performance as a function of certain parameters. For the purpose of the simulations, we calculate the received power at each node based on the previous state (assuming an initial distribution of nodes at the first hop), which is used to set the indicator functions as either 0,1 or 2 depending upon the threshold criterion. These indicator functions will form the current state and the process continues. We finally obtain the distribution of the chain by simulating over 20,000 trials. The Perron-Frobenius eigenvalue of $\mathbf{P}$ has been found using [33].

Figure 6 shows the state probabilities of the Markov chain as a function of hop n, when both the window size and the hop distance are assumed to be two, i.e., $M = h_d = 2$. The SNR margin is 12dB with a path loss exponent of 2. Thus, it can be seen that the analytical results are quite close to that of the simulations. It can be further

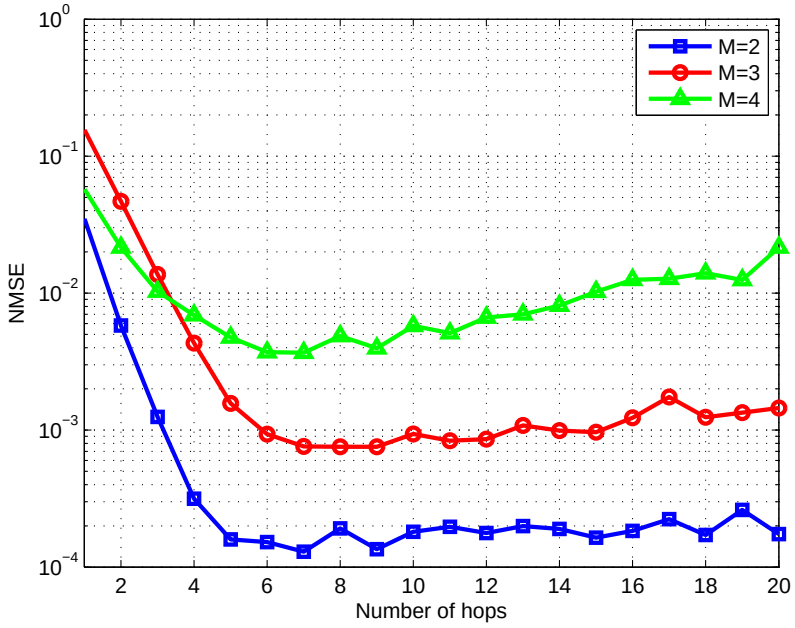

Figure 7: NMSE between the quasi-stationary distributions from analysis and simulations

noticed that as we increase the hop number, the probability of being in a transient state decreases, which asserts the relationship as described in (6). Figure 7 shows the normalized mean squared error (NMSE) between the quasi-stationary distribution assuming different values of non overlapping window, M, where the NMSE is defined as

$$NMSE = \frac{1}{2^M - 1} \frac{\|\mathbf{u} - \hat{\mathbf{u}}\|_2^2}{< \mathbf{u} >^2}, \tag{30}$$

where $\hat{\mathbf{u}}$ is the quasi-stationary distribution obtained from simulation, $||.||_2^2$ is the squared Euclidean norm and $< . >$ is the mean value of the vector. The figure shows that as we increase the hop number, we approach the quasi-stationary distribution quite fast. As we increase M, the NMSE starts to increase and these deviations in the numerical and analytical results can be attributed as the precision errors while calculating the eigenvalues of larger matrices.

Figure 8 depicts the trend of eigenvalues as we increase the SNR margin for

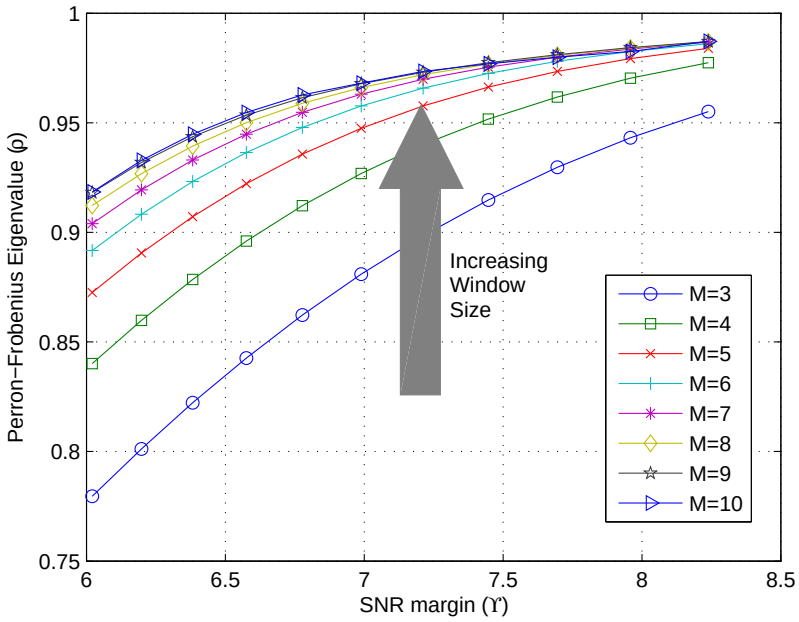

Figure 8: Behavior of Perron-Frobenius Eigenvalues as M increase for a hop distance of 2 and $\beta = 2$

different window sizes and a hop distance of 2. The behavior is quite obvious that increasing SNR margin increases the probability of survival of the transmissions. It can be further noticed that for a given value of SNR margin, the curves start to converge as we increase the window size, thereby indicating that after a specific window size, even if we increase M, there is no change in the transmissions outcome which agrees with the iterative algorithm that we discussed in Section 3.4.

Figure 9 shows the error surfaces for the overlapping window case, generated by (29) for a hop distance of 2 and different window sizes. It can be seen that the error surface is convex that contains a minimum for a particular value of SNR margin, Υ. It can be further noticed, that as we increase the window size the difference between the errors becomes smaller in the same vicinity of Υ. Thus, for a window size of 10 and a hop distance of 2, we can select the SNR margin of around 6dB to give us desired membership probability function. Figure 10 shows the numerical simulation result for conditional membership probabilities of the nodes to different levels, where

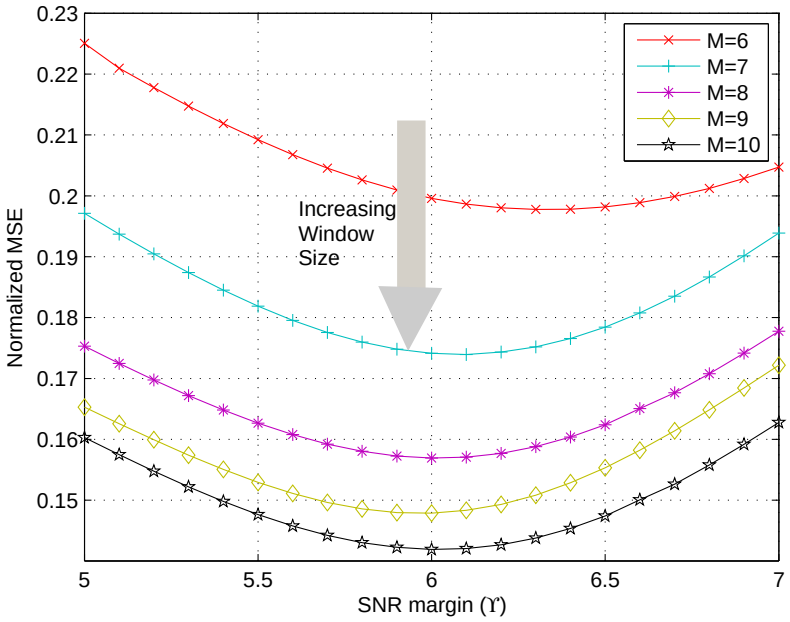

Figure 9: Error curves for different window sizes for a hop distance of 2 and $\beta = 2$

the values Υ and M are taken from the iterative algorithm. It can be seen that the distance between the peaks of any two membership functions is always 2. Thus a window size of 10 seems reasonable to get a hop distance of 2 with an SNR margin of approximately 6dB. The sub-figure in the right top corner shows the analytical membership function obtained from (28) by using the quasi-stationary distribution.

Figure 11 shows the effect of increasing the path loss exponent on the Perron eigenvalue for a hop distance of 3. It can be noticed that for the same value of success probability, we require more SNR margin. The convergence of the iterative algorithm can also be seen in this figure. Also it can be noticed that for higher path loss exponent, the curves converge fast as compared to smaller path loss exponent. This effect can be attributed to the fact that if path loss exponent is higher, adding a new node to window will not increase the success probability as the transmissions are weaker to reach there. The converse holds true for a small path loss exponent.

From the deployment perspective of the network, it is sometimes desirable to determine the values of certain parameters like transmit power of relays or distance

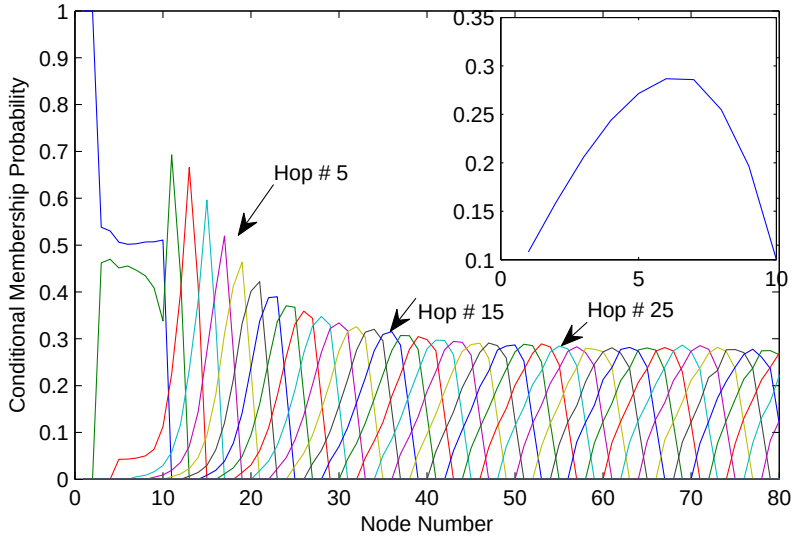

Figure 10: Conditional membership probabilities of the nodes for $h_d = 2$ for a window size of 10 and $\Upsilon = 6dB$. The sub-figure shows the analytical membership function

between them to obtain a certain quality of service (QoS), η. In other words, we are interested in finding the probability of delivering the message at a certain distance without having entered the absorbing state, and we desire this probability to be at least η where $\eta \sim 1$ ideally. Thus (11) gives us a nice upper bound on the value of m (the number of hops) one can go with a given η, i.e. $\rho^m \geq \eta$, which gives

$$m \leq \frac{\ln \eta}{\ln \rho}. \tag{31}$$

Thus if the destination is far off, we require more hops, which will require a larger value of ρ. Now ρ is a nonlinear function of the SNR margin, Υ, where a large SNR margin corresponds to a large node degree, whereas an SNR margin of 1 implies a node degree of exactly two in this line-network. Figure 12 shows the relationship between required SNR margin to reach the destination node at a particular normalized distance for different values of hop distance. The normalized distance, which is the true distance divided by d, is defined as the product of h_d and the number of hops (made to reach the destination).We have taken three values of the quality of service, η to show our result. We observe that the performance of all the cooperative cases

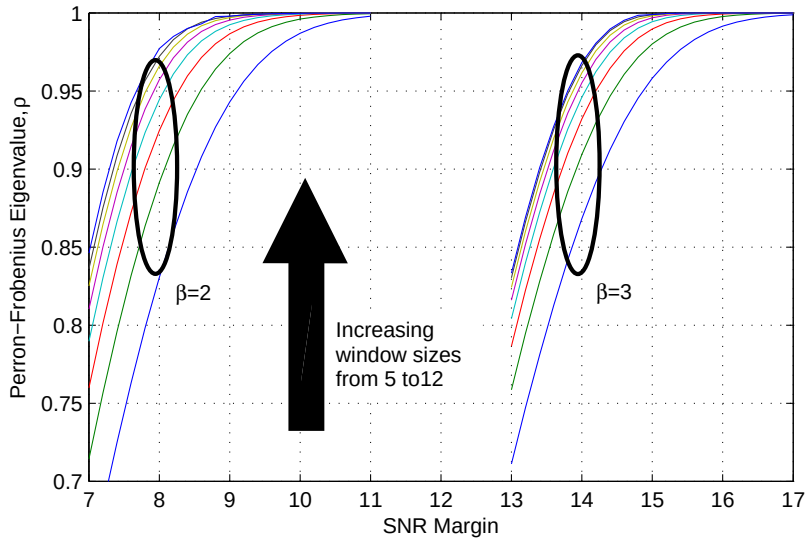

Figure 11: Effects of path loss exponent on the convergence of eigenvalues for a hop distance of 3

exceeds that of non-cooperative case for a particular value of SNR margin, in terms of the normalized distance. It can be further noticed that the transmissions with cooperative case can reach a particular point in two ways, i.e., keeping both the hop distance and SNR margin small or having a higher hop distance with a higher SNR margin, where the latter has lower latency, i.e., fewer hops, and higher QoS, η. The results are also plotted for a higher path loss exponent, i.e., $\beta = 3$. However, from Figure 11 we know that a high SNR margin is required to get the same value of success probability. Thus we observe that if we increase the path loss exponent and also the SNR margin, we get results that are close to the case of small path loss exponent with small SNR margin. The non-cooperative results show that we can reach a small distance with a considerably small success probability when we use the same SNR margin for the high path loss exponent.

Figure 12 also supports our expectation that fixing the transmit power, while lowering the data rate, will increase the range that can be obtained for a given packet delivery ratio (PDR). Lowering the data rate implies lowering the decoding threshold, which implies from (26) a higher SNR margin. Figure 12 shows that for $\beta = 2$,

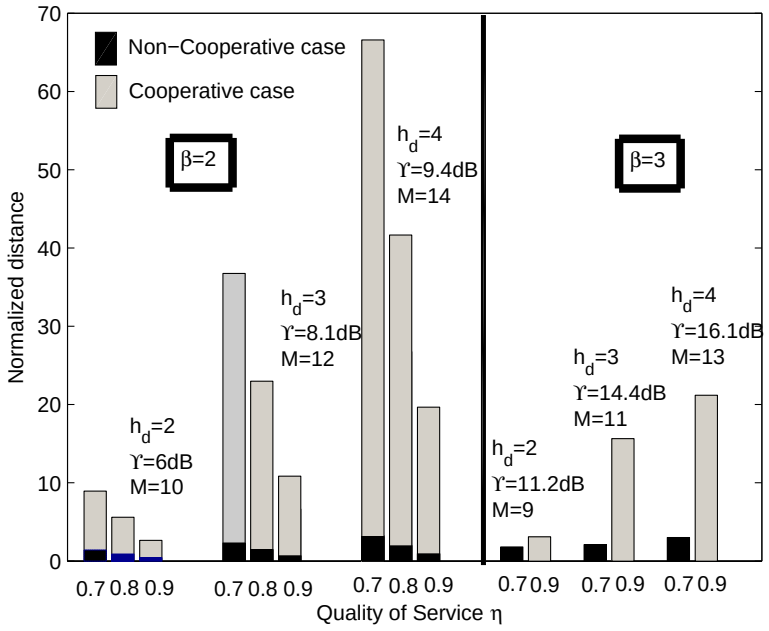

Figure 12: Normalized distance for various cooperative vs. non-cooperative cases

lowering the decoding threshold by 3.4dB (i.e., increasing Υ from 6 to 9.4) increases the distances by nearly a factor of 7 for a PDR of 90% ($\eta = 0.9$).

From the broadcast perspective, another important parameter is to find the fraction of nodes that have decoded in the network. If we assume that the Markov chain is in the quasi-stationary state, and has not entered the absorbing state over a linear network of interest, then the fraction of decoded nodes in the network is the same as the fraction of the nodes in any one hop. From Figure 10, we can see that we do not exactly get a rectangular membership function, which implies that not all the nodes in the network may have decoded the data. Let N_d be a random variable that denotes the number of forwarding nodes such that n_{d_j} are the realizations of this variable where $j = 1, 2, ...|S|$. Hence the average number of the nodes that have decoded the data is given as

$$\mathbb{E}(N_d) = \sum_{j=1}^{|S|} n_{d_j} u_j \tag{32}$$

where n_{d_j} is the number of DF nodes in the jth state and u_j is the quasi-stationary

probability of that state. Hence for the cases that are described in Figure 12, the results are summarized in Table I. It can be seen that as we increase the hop distance (and the SNR margin consequently), we get more nodes that are able to decode in a given hop.

Table 1: Fraction of DF nodes for various hop distances

Hop distance, h_d	2	3	4
% of nodes decoded, $\beta = 2$	92.30	94.67	97.02
% of nodes decoded, $\beta = 3$	93.54	95.98	98.21

3.6 Performance of Co-Located Groups of Nodes

In this section, we consider another topology for the deployment of nodes in a one-dimensional network. The first deployment scenario considers nodes, equally spaced on a line as described in Section 3.3.1 and Figure 5, while the second topology has groups of co-located nodes, such that the groups are equally spaced on the line, and such that the two networks have equal average density. We call the former topology as equi-distant topology. To some applications, the equi-distant node topology, as in the top part of Figure 13, might be attractive, owing to the distributed nature of sensors that can monitor a large area at many different locations, e.g., in structural health monitoring of a bridge. However, the cooperating nodes in this topology will necessarily have disparate path loss, leading possibly to a lower effective diversity. Therefore, we consider allowing each set of cooperating nodes to be in a co-located group (still separated slightly to have uncorrelated fading channels) as shown in the bottom of Figure 13. To compare the two topologies, we restrict the collections of candidates for cooperation in a given hop to have the same number of nodes and have the same centroid, as shown in Figure 13. Therefore, the only difference between the two topologies is that the cooperating nodes in equi-distant topology have disparate path losses, while cooperating nodes in the co-located groups topology do not. Our results will show that the co-located groups topology always perform better, but

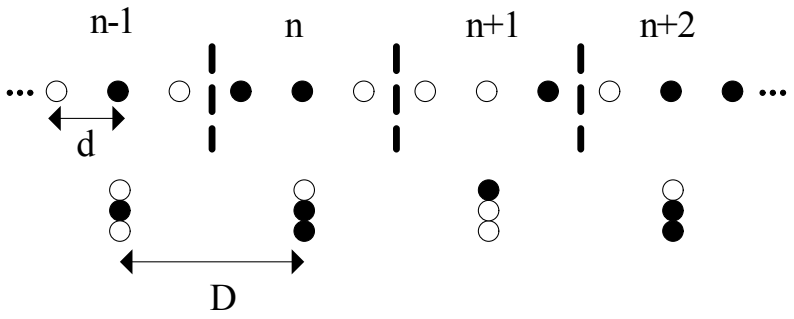

Figure 13: Equi-distant and co-located topologies in line network

the magnitude of improvement depends on the system and channel parameters. We consider the same modeling approach as in Section 3.3.1, where the state of each node is characterized by a binary indicator function such that for jth node at time n, $\mathbb{I}_j(n) = 1$ represents successful decoding and $\mathbb{I}_j(n) = 0$ represents a failure in decoding. Hence the transition probability is given by (24) with $\lambda_k^{(m)}$ as defined in (25). For the other topology, we consider the following sub-section.

3.6.1 Transition Matrix for Co-Located Groups Topology

In this case, the received power at a certain node in a group is the sum of the finite powers from the previous-level nodes, where the power received from each transmitting node is exponentially distributed with the same parameter $\tilde{\lambda} = D^{\beta}\sigma_k^2/P_t$. Since all the nodes are co-located, and there are no disparate path losses that affect the parameter of the exponential distribution, the PDF of the received power at the kth node in a cluster is Gamma distribution [31] given as

$$p_{\gamma_k}(y) = \frac{1}{(\mathcal{K}_n - 1)!}\tilde{\lambda}^{\mathcal{K}_n} y^{(\mathcal{K}_n - 1)} \exp\Big(-\tilde{\lambda} y\Big). \tag{33}$$

Evaluating (15) to get the conditional success of the kth node, we have

$$\mathbb{P}\left\{\gamma_k(n) > \tau\right\} = \frac{1}{(\mathcal{K}_n - 1)!}\Gamma(\mathcal{K}_n, \tilde{\lambda}\tau), \tag{34}$$

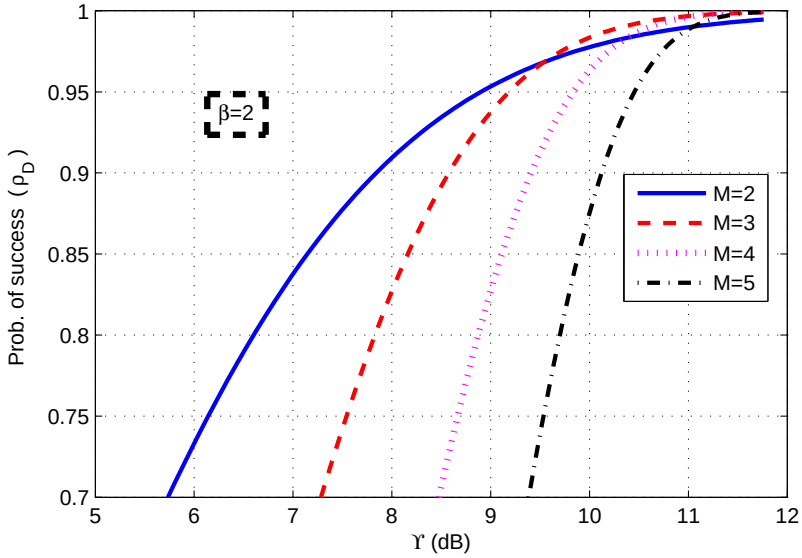

Figure 14: Behavior of eigenvalues in the co-located topology.

where $\Gamma(\mathcal{K}_n, \tilde{\lambda}\tau)$ is the upper incomplete Gamma function. We define $\Phi(k) := \mathbb{P}\{\gamma_k(n) > \tau\}$, then after some manipulation, (34) becomes

$$\Phi^{(k)} = \exp\left(-\tilde{\lambda}\tau\right) \sum_{p=0}^{\mathcal{K}_n - 1} \frac{-\tilde{\lambda}\tau}{p!}. \tag{35}$$

Then the one step transition probability for going from State i to j is given as

$$\mathbb{P}_{ij} = \prod_{k \in \mathbb{N}_{n+1}^{(j)}} \left(\Phi^{(k)}\right) \prod_{k \in \overline{\mathbb{N}}_{n+1}^{(j)}} \left(1 - \Phi^{(k)}\right). \tag{36}$$

3.6.2 Results and Performance Analysis

In this section, we show the relative performance of the two topologies in terms of the one-step success probability of making a successful hop, which indicates that at least one node in the forward level has decoded the message successfully. As in prebvious analysis, to reduce the design space, we let $\Upsilon = \frac{P_t}{\tau\sigma^2}$ as the normalized SNR with respect to the threshold τ and call this the SNR margin. Note that in the simulation results, we have used $d = 1$, which implies that the Υ, in the equi-distant topology, can be thought of as SNR margin from a single transmitter d distance away. We

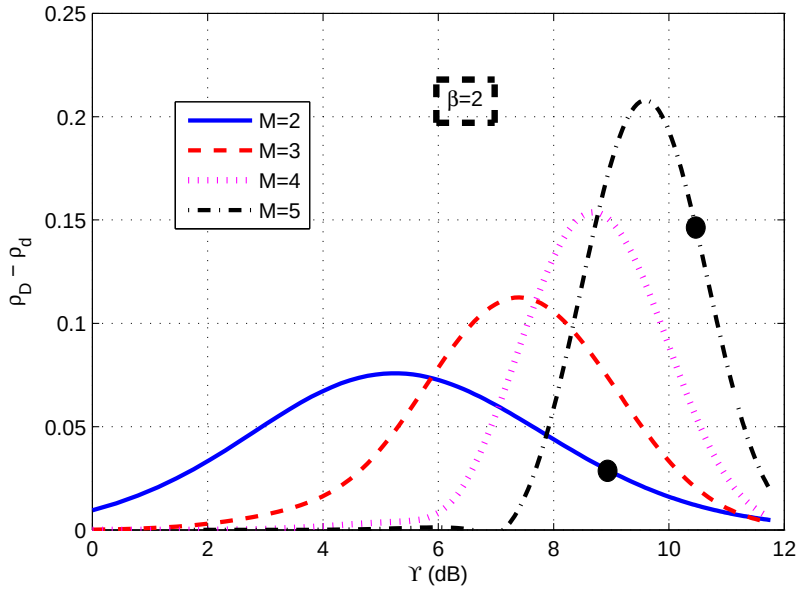

Figure 15: Eigenvalue differences between two topologies; $\beta = 2$.

denote the one step success probability for equi-distant topology as ρ_d and for co-located groups topology as ρ_D. Figure 14 shows the behavior of ρ_D as a function of Υ for a path loss exponent of 2. It can be observed that for a specific cluster size, the success probability increases monotonically with the increase in SNR margin. It can be further noticed that if we increase the cluster size, an additional SNR margin is required to get the same success probability than a smaller sized cluster. This is because by increasing the cluster size, the inter-group distance also increases, which requires more SNR margin to get the same quality of service.

Figure 15 shows the difference between the success probabilities of co-located and equi-distant topologies for the path loss exponent of 2. We observe that the difference increases as we increase M. However, this difference dominates at some specific SNR margin values. For instance, if we require 95% success probability for $M = 2$ in a co-located case, then from Figure 14, we require $\Upsilon = 8.9dB$. However, from Figure 15, we notice that at this SNR margin, the equi-distant topology also performs almost the same since $\rho_D - \rho_d \approx 0.027$ as indicated by the black circle. For the same packet

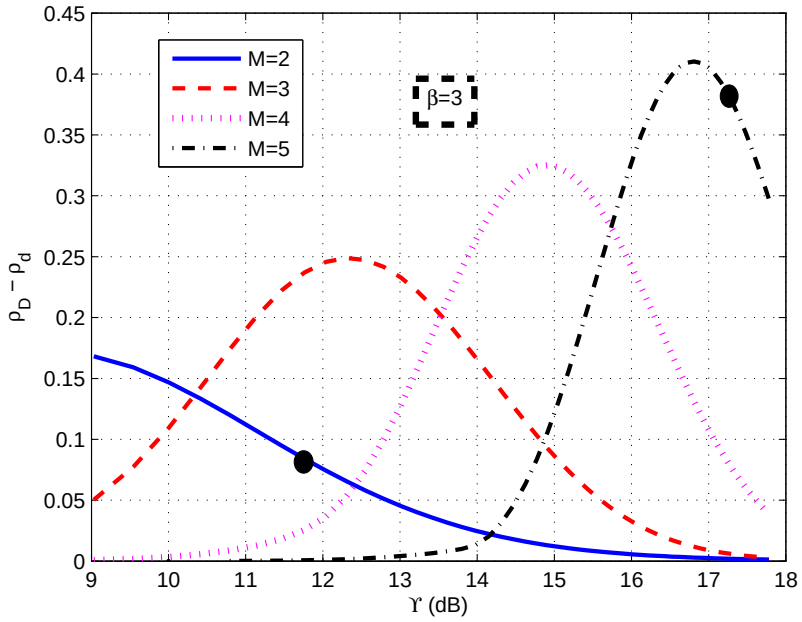

Figure 16: Eigenvalue differences between two topologies; $\beta = 3$.

delievery ratio for $M = 5$, the co-located case requires $\Upsilon = 10.45dB$, however the difference in success probabilities for the two cases is more significant at 0.1485 at this SNR margin value. At very high SNR margin, e.g., 12dB, the performance of both the topologies is again the same, because the path loss effects are diminished with high transmit power and partition constraint. An interesting observation is seen by increasing the path loss exponent. Figure 16 shows $\rho_D - \rho_d$ for $\beta = 3$ where the black circles show the 95% success probability for the co-located topology. We observe a larger difference between the two toplogies, especially for the rightmost dot, which says that for $M = 5$, the co-located case has 0.95 probability of success, while the equally spaced case has only 0.57 probability of success. We attribute this difference to the large differences in path loss among the (up to) 5 equally spaced transmitters.

CHAPTER IV

STOCHASTIC MODELING FOR RANDOM PLACEMENT OF NODES

In this chapter, we extend the approach described in the previous chapter to the case in which the nodes are randomly deployed over a line, according to a Bernoulli process. As in Chapter 3, the channel model includes path loss with an arbitrary exponent, and independent Rayleigh fading. The increased number of states, due to the Bernoulli deployment, necessitated a formulation in terms of Kronecker products, which greatly simplifies the analysis and the number of computations required to compute the transition matrix. The new formulation allows us to quantify the SNR penalty for random placement of nodes, relative to the regular placement case, for various granularities of placement possibilities. In contrast to deterministic deployment, the analytical results reveal non-unity upper bounds for the probabilities of one-OLA-hop success, because of the possibility of too few or no nodes in a local area.

The rest of the chapter is organized as follows. In the next section, we define the network parameters and propose a model of the network. In Section 4.2, we derive the transition probability matrix for the proposed model and give its compact representation. The results and system performance are given in Section 4.3.

4.1 System Model

As shown in Figure 17, our deployment model is to place nodes according to a Bernoulli process on equally spaced candidate locations, such that at most one node can be placed at a location. In other words, for every candidate location, a Bernoulli

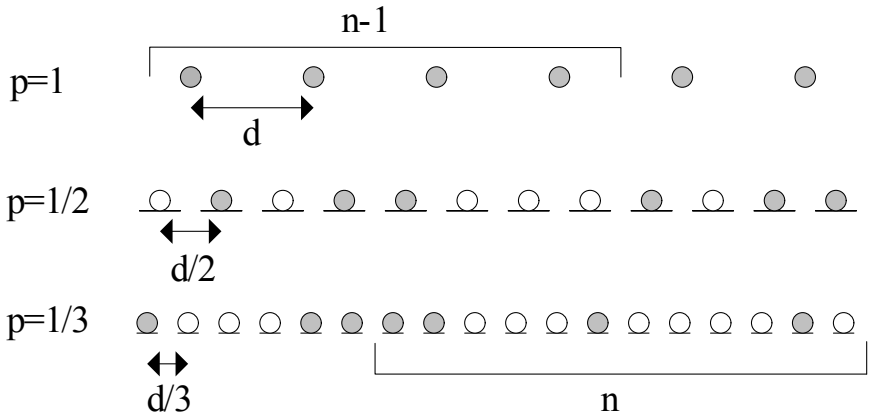

Figure 17: Deterministic and random placement of nodes

random variable $\mathcal{B}$ has the outcome $\mathcal{B} = 1$ with probability p if a node is present, and $\mathcal{B} = 0$ with probability $1 - p$, if the node is not present. If p is a very small number, this Bernoulli deployment can be considered to be an approximation to a Poisson point process (PPP). We wish to compare line networks with the same average density of nodes, but with different degrees of randomness and spatial granularity. In Fig. 17, the $p = 1$ case shows a deterministic deployment of nodes with a fixed density. We assume that the node locations are integer multiples of d, where d is the inter-node distance on the one-dimensional grid. The subsequent plots in Figure 17 show examples of possible Bernoulli deployments with $p = 1/2$ and $p = 1/3$, respectively. The filled-in circles indicate the existence of a node while the hollow circles show the absence of a node. Thus, p can be regarded as the *granularity parameter* and as $p \to 0$, the resulting deployment follows a PPP.

At a certain hop number n, a node, if present at a slot, will take part in the next transmission, if it has decoded the data perfectly for the first time, or it will not take part, if it did not decode correctly or it has already decoded the data in one of the previous levels. The states of all the slots in the nth level can be represented as $\mathcal{X}(n) = [\mathbb{I}_1(n), \mathbb{I}_2(n), ..., \mathbb{I}_M(n)]$, where $\mathbb{I}_j(n)$ is the ternary indicator random variable

for the jth slot at the nth time instant given as

$$\mathbb{I}_j(n) = \begin{cases} 0 & \text{slot } j \text{ has a node, which has not decoded} \\ 1 & \text{slot } j \text{ has a node, which has decoded} \\ 2 & \text{slot } j \text{ has no node or has a node that has decoded at an earlier time} \end{cases} \tag{37}$$

Thus, each slot in a level is represented by either 0, 1 or 2 depending upon node presence and successful decoding of the received data. Hence we consider the Markov chain, $\mathcal{X}$, on a state space $\mathcal{A} \cup \mathcal{S}$, where $\mathcal{S}$ is a set of transient states and $\mathcal{A}$ is the set of absorbing states as in the previous chapter. The quasi-stationary distribution of this chain is also described by the Equations $(11 - 12)$.

4.2 The Transition Probability Matrix

For finding the state transition matrix for our model, we split our analysis into two subsections. The first subsection deals with finding the one-step transition probability of transiting from one state to another. In the next subsection, we formulate the ways in which the matrix could be obtained without explicitly calculating each transition and hence the algorithm is made less computationally complex.

4.2.1 Formation of the One-Step Transition Probability

Let i and j denote a pair of states of the system such that $i, j \in \mathcal{S}$, where each i and j are the decimal equivalents of the ternary words formed by the set of indicator random variables. To determine the possible destination states in a transition from level $n-1$ to level n, it is helpful to distinguish between two mutually exclusive sets of nodes in the nth level: 1) the nodes that were also in the M-slot window of the $(n-1)$th level, i.e., nodes that are in the $M - h_d$ overlap region of the two consecutive windows, and 2) the remaining h_d nodes that are not in the overlap region. We denote these two sets of nodes as $\mathbb{N}_{OL}^{(n)}$ and $\overline{\mathbb{N}}_{OL}^{(n)}$, respectively, where OL stands for *overlap*.

Suppose node k in $\mathbb{N}_{OL}^{(n)}$ decoded in the previous $(n-1)$th level; this would be

indicated by $\mathbb{I}_{h_d+k}(n-1)=1$. This node will not decode again, and therefore $\mathbb{I}_k(n)=2$. Similarly, if that node decoded prior to the $(n-1)$th level, or if there were no node in the kth slot of $(n-1)$th level, then $\mathbb{I}_{h_d+k}(n-1)=2$. In this case also, we must have $\mathbb{I}_k(n)=2$. Alternatively, if the node is present and has not previously decoded, then $\mathbb{I}_{h_d+k}(n-1)=0$, and $\mathbb{I}_k(n)$ can equal 0 or 1, depending on the previous state and the channel outcomes; $\mathbb{I}_k(n)=2$ is not possible. If the location k is in the $\overline{\mathbb{N}}_{OL}^{(n)}$, then there is no previous level index for this node, and, we can have $\mathbb{I}_k(n)\in\{0,1,2\}$ depending on the node presence, previous state and channel outcomes. Hence from this discussion and (37), we note that a slot can have three possible states. Hence each individual slot is a state machine, and $\mathbb{I}_k(n)$ is generally a non-homogeneous Markov chain itself; the probabilities of transition for a single node are non-zero only at certain times. This slot Markov chain is the same as depicted in Figure 3.

Let a superscript on an indicator function shows the state associated with that indicator function. For example, if $i=\{22110\}$, then $\mathbb{I}_5^{(i)}(n)=0$.Therefore, considering the above discussion, the one-step transition probability going from the state i in level $n-1$ to state j in level n is always 0, $\forall k=\{0,1,2,...,M\}$, when either of the following conditions is true

$$\textit{Condition I}: \quad \mathbb{I}_k^{(j)}(n)\in\{0,1\} \text{ and } \mathbb{I}_{h_d+k}^{(i)}(n-1)\in\{1,2\}\,, \tag{38}$$

$$\textit{Condition II}: \quad \mathbb{I}_k^{(j)}(n)=2 \text{ and } \mathbb{I}_{h_d+k}^{(i)}(n-1)=0. \tag{39}$$

In the following, we assume that the previous state is a transient state, i.e., $\mathcal{X}(n-1)\in\mathcal{S}$. For each node $k\in\mathbb{N}_{OL}^{(n)}$, the probability of being able to decode at time n given that the node exists but failed to decode in the previous level (P_{01} from Figure 3) is given as

$$\begin{aligned}\mathbb{P}\left\{\mathbb{I}_k^{(j)}(n)=1 \mid \mathbb{I}_{h_d+k}^{(j)}(n-1)=0,\mathcal{X}(n-1)\right\}=\\ \mathbb{P}\left\{\gamma_k(n)>\tau \mid \mathbb{I}_{h_d+k}^{(j)}(n-1)=0,\mathcal{X}(n-1)\right\}.\end{aligned} \tag{40}$$

If $k\in\overline{\mathbb{N}}_{OL}^{(n)}$, and $\mathcal{V}_{\overline{OL}}$ is the cardinality of set $\overline{\mathbb{N}}_{OL}^{(n)}$, then we define a sequence of

Bernoulli random variables $\mathcal{B}_(n)$ such that $\mathcal{B}_(n) = \left\{\mathcal{B}_1(n), \mathcal{B}_2(n), ..., \mathcal{B}_{\mathcal{V}_{\overline{OL}}}(n)\right\}$, and also denote the event $\left\{\mathbb{I}^{(j)}_{h_d+k}(n-1) = 0, \mathcal{X}(n-1), \mathcal{B}_k(n) = 1\right\}$ as ξ, then

$$\mathbb{P}\left\{\mathbb{I}^{(j)}_{k}(n) = 1 \mid \mathbb{I}^{(j)}_{h_d+k}(n-1) = 0, \mathcal{X}(n-1)\right\} = \mathbb{P}\left\{\gamma_k(n) > \tau \mid \xi\right\} \mathbb{P}\left\{\mathcal{B}_k(n) = 1\right\}, \tag{41}$$

and

$$\mathbb{P}\left\{\mathbb{I}^{(j)}_{k}(n) = 2, \mathcal{B}_k(n) = 0\right\} = \mathbb{P}\left\{\mathcal{B}_k(n) = 0\right\}. \tag{42}$$

Also

$$\mathbb{P}\left\{\gamma_k(n) > \tau | \xi\right\} = \int_{\tau}^{\infty} p_{\gamma_k|\xi}(y) dy. \tag{43}$$

$p_{\gamma_k|\xi}(y)$ is the conditional probability density function (PDF) of the received SNR at the kth node, conditioned on state $\mathcal{X}(n-1)$ and the node existing but not having decoded yet, and is given by the hypoexponential distribution [31]. For the formulation of one step transition probability from state i to state j, define

$\mathbb{N}^{(j)}_{\theta_{OL}} = \left\{k : k \in \mathbb{N}^{(n)}_{OL}, \mathbb{I}^{(j)}_{k}(n) = \theta\right\}, \ \theta \in \{0, 1\},$

$\mathbb{N}^{(j)}_{\theta_{\overline{OL}}} = \left\{k : k \in \overline{\mathbb{N}}^{(n)}_{OL}, \mathbb{I}^{(j)}_{k}(n) = \theta\right\}, \ \theta \in \{0, 1, 2\},$

and let $\mathcal{V}_\theta$ be the cardinality of $\mathbb{N}^{(j)}_{\theta_{\overline{OL}}}$, $\theta \in \{0, 1, 2\}$. Then the one step transition probability for going from state i to state j is given as

$$\mathbb{P}_{ij} = \begin{cases} 0 & (38) \text{ or } (39) \text{ holds} \\ \prod_{k \in \mathbb{N}^{(j)}_{1_{OL}}} \left(\psi^{(k)}_m\right) \prod_{k \in \mathbb{N}^{(j)}_{1_{\overline{OL}}}} \left(\psi^{(k)}_m\right) (p)^{\mathcal{V}_1} \times & \text{Otherwise} \\ \prod_{k \in \mathbb{N}^{(j)}_{0_{OL}}} \left(1 - \psi^{(k)}_m\right) \prod_{k \in \mathbb{N}^{(j)}_{0_{\overline{OL}}}} \left(1 - \psi^{(k)}_m\right) (p)^{\mathcal{V}_0} (1-p)^{\mathcal{V}_2} & \end{cases} \tag{44}$$

where $\psi^{(k)}_m$ is the probability of success of node k in level n and is given as

$$\psi^{(k)}_m = \sum_{m \in \mathbb{N}_{n-1}} C^{(k)}_m \exp\left(-\lambda^{(k)}_m \tau\right), \tag{45}$$

where $\mathbb{N}_{n-1} = \left\{m : \mathbb{I}^{(i)}_{m}(n-1) = 1\right\}$ was previously defined as the set of the slot indices of all those nodes that decoded the data perfectly in the previous level, $\lambda^{(k)}_m$

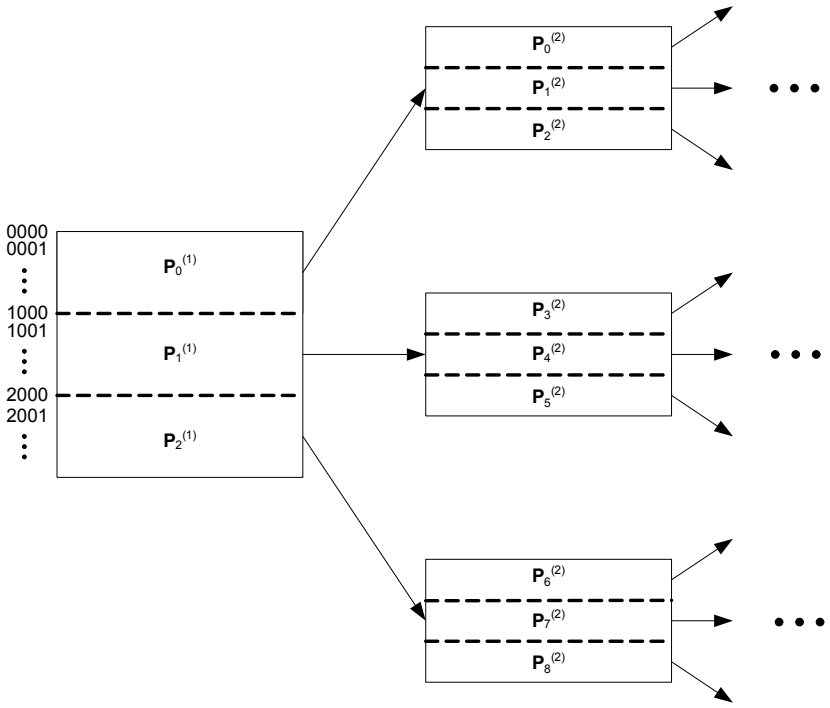

Figure 18: Ternary decomposition of the transition matrix

is given as

$$\lambda_m^{(k)} = \frac{d^\beta \left| h_d - m + k \right|^\beta \sigma^2}{P_t}, \tag{46}$$

and $C_m^{(k)}$ is defined as

$$C_m^{(k)} = \prod_{\zeta \neq m} \frac{\lambda_\zeta^{(k)}}{\lambda_\zeta^{(k)} - \lambda_m^{(k)}}. \tag{47}$$

4.2.2 Kronecker Representation of the Transition Matrix

Many transition probabilities, $\mathbb{P}_{ij}$, in (44), are zero and hence the transition probability matrix is sparse. Rather than computing each non-zero element separately, the Kronecker representation can enable obtaining the same matrix with fewer computations.

As the total number of states in the model is 3^M, where we may enumerate the state space as decimal equivalents of the ternary M-tuples, i.e., $\left\{0, 1, ..., 3^M - 1\right\}$, hence the transition matrix, $\mathbf{P}$, can be partitioned into three rectangular blocks as $\mathbf{P} = [\ \mathbf{P}_0^{(1)} \quad \mathbf{P}_1^{(1)} \quad \mathbf{P}_2^{(1)}\ ]^T$, where T denotes the block transpose, such that the most

significant symbol (MSS) in the ternary expansion of ith row of matrices $\mathbf{P}_0^{(1)}$, $\mathbf{P}_1^{(1)}$, and $\mathbf{P}_2^{(1)}$ is 0,1, and 2, respectively. In all the cases, the superscript (1) shows that we are dealing with the MSS. This procedure is shown in Figure 18, where the ternary expansion of some states are shown for $M = 4$.

Also note that the contribution to the received power at any node in the current level, n, is zero if the state of that MSS was either 0 or 2 in the previous level, $n-1$. This results in equal probability of transition to a given state, if the originating state's MSS is 0 or 2. Thus, the transition probabilities to all of the 3^M states from states with MSS= $\{0, 2\}$ are equal, since no power is originating from these MSS, and hence $\mathbf{P}_0^{(1)} \equiv \mathbf{P}_2^{(1)}$. If the dimension of $\mathbf{P}$, denoted as $dim(\mathbf{P}) = 3^M \times 3^M$, then $dim(\mathbf{P}_\alpha^{(1)}) = 3^{M-1} \times 3^M$, $\forall \alpha = \{0, 1, 2\}$. Hence, we can write

$$\mathbf{P} = \begin{bmatrix} 1 \\ 0 \\ 1 \end{bmatrix} \otimes \mathbf{P}_0^{(1)} + \begin{bmatrix} 0 \\ 1 \\ 0 \end{bmatrix} \otimes \mathbf{P}_1^{(1)} = \begin{bmatrix} \mathbf{P}_0^{(1)} \\ \mathbf{P}_1^{(1)} \\ \mathbf{P}_0^{(1)} \end{bmatrix}, \tag{48}$$

where $\otimes$ denotes the Kronecker or tensor product. Thus the explicit computation of $\mathbf{P}_2^{(1)}$ is not required. The representation in (48) is depicted for the case when the first slot in the previous level was either 0 or 2. Similarly, for the next location in previous level, each of the $\mathbf{P}_\alpha$'s are further divided into a set of three matrices, as shown in Figure 18, and this process of splitting matrices into a ternary tree goes on for all locations m in level $(n-1)$ such that $m = \{1, 2, ..., h_d\}$. If $V_0 := [\ 1 \quad 0 \quad 1\ ]^T$, and $V_1 := [\ 0 \quad 1 \quad 0\ ]^T$, then a compact representation of $\mathbf{P}$ is given as

$$\mathbf{P} = \sum_{\alpha=0}^{2^{h_d}-1} \left[\left(\otimes_{j=0}^{h_d-1} V_{\alpha_j} \right) \otimes \mathbf{P}_\alpha^{(h_d)} \right], \tag{49}$$

where $\alpha_j \in \{0, 1\}$ is the j^{th} digit in the binary expansion of α, such that $\alpha = \sum_{j=0}^{h_d-1} 2^j \alpha_j$. For each α, the $dim(\mathbf{P}_\alpha^{(h_d)}) = 3^{M-h_d} \times 3^M$, which is far less than that of $dim(\mathbf{P})$ itself for a large h_d. In other words, if 3^{2M} computations are required to find $\mathbf{P}$, then by using (49), $\left(\frac{2}{3}\right)^{h_d} 3^{2M}$ computations are required, which are fewer

computations by a factor of $\left(\frac{2}{3}\right)^{h_d}$. Since from Figure 17, we need more slots per hop for smaller granularity, the representation in (49) is helpful. For example, if hop distance is 6 and window size is 10, then by using above representation, we have to perform only 8.77% of the calculations as comparted to calcuating the full matrix $\mathbf{P}$. Also note that the total states are 3^M, however $|\mathcal{S}| = 3^M - 2^M$, where $|\mathcal{A}| = 2^M$ is the number of absorbing states. Hence the computations are further reduced. It has also been observed that the matrix is highly sparse due to conditions derived in (38) and (39). For example, for the aforementioned case, the resulting matrix is more than 98% sparse. Hence for the purpose of modeling, we can use these simplifications to reduce the computational complexity. The representation in (49) is used to derive the transition matrix with a large number of states and is called the stochastic automata network (SAN) descriptor [36]. If large window sizes and hop distances are needed to evaluate, then there exists methods like GMRES and Arnoldi iterations, that make use of this SAN representation to find the eigenvalues and the probability vector for the transition probability matrix. Interested readers can see, for instance, [37] (and the references therein), where the problem of state space explosion is studied and solved using the SAN repsentation and iterative methods.

4.3 Results and System Performance

Up to this point, we showed how the transition matrix is fully characterized by its Perron eigenvalue and the corresponding left eigenvector, which gives the quasi-stationary distribution of the chain. However, the Perron eigenvalue, which is the one-OLA-hop success probability in our case, depends upon many parameters like transmit power, path loss exponent, inter-slot distance etc. Hence we define Υ as in (26), which can be interpreted as the SNR margin at a receiver from a single transmitting node, a distance d away. However, Υ is not the only independent parameter, because β and h_d also separately impact the value of $\lambda_m^{(k)}\tau$ in (46), through the factor $|h_d - m + k|^{\beta}$

and $\mathbb{P}_{ij}$ also depends upon the granularity level p.

In the following, we will discuss the case depicted in Figure 17, i.e., a mean hop distance of 2 and its corresponding different network topologies with random placement and path loss exponent of 2. Similar results and analysis can be done for other topologies. Note that the window size, M, is one of the factors that affects the values of ρ and the model space dimension. M is an *artificial* constraint because there is no real physical need for it, however, it strongly impacts the size of the state space and therefore the computational complexity of finding the success probability. Therefore, we would like for M to be as small as possible without significantly impacting the system performance results. As in Section 3.4, we propose to find M by increasing the window size for a given hop distance, until the one-hop success probability (i.e., the Perron-Frobenius eigenvalue, ρ) ceases to change significantly. This implies that even if we add another slot at the trailing edge of the window, there is no or little effect on the success probability because the transmissions reaching that specific slot are attenuated owing to the large path loss. Figure 19 depicts the trend of eigenvalues as we increase the SNR margin for different window sizes and a mean hop distance of 2 with $p = 1/2$. The behavior is quite obvious that increasing SNR margin increases the probability of survival of the transmissions. It can be further noticed that for a given value of SNR margin, the curves start to converge as we increase the window size, thereby indicating that after a specific window size, even if we increase M, there is no change in the transmissions outcome. Thus we select the window size where this convergence is achieved.

In the following, we will discuss the case depicted in Fig. 17, i.e., a mean hop distance of 2 and its corresponding different network topologies with random placement and path loss exponent of 2. Similar results and analysis can be done for other topologies. The mean hop distance refers to the hop distance in the deterministic deployment. Note that the window size, M, is one of the factors that affects the values

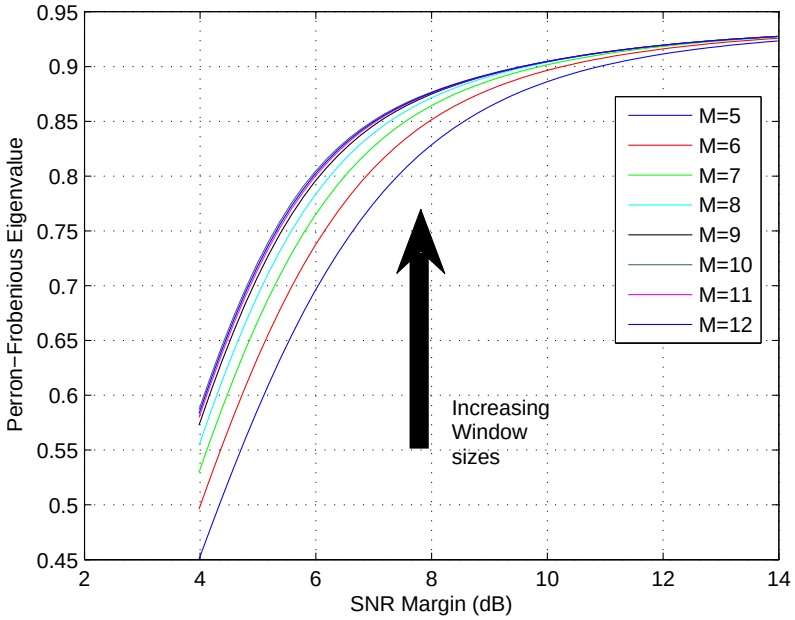

Figure 19: Behavior of success probabilities with the increase in window size for a mean hop distance of 2

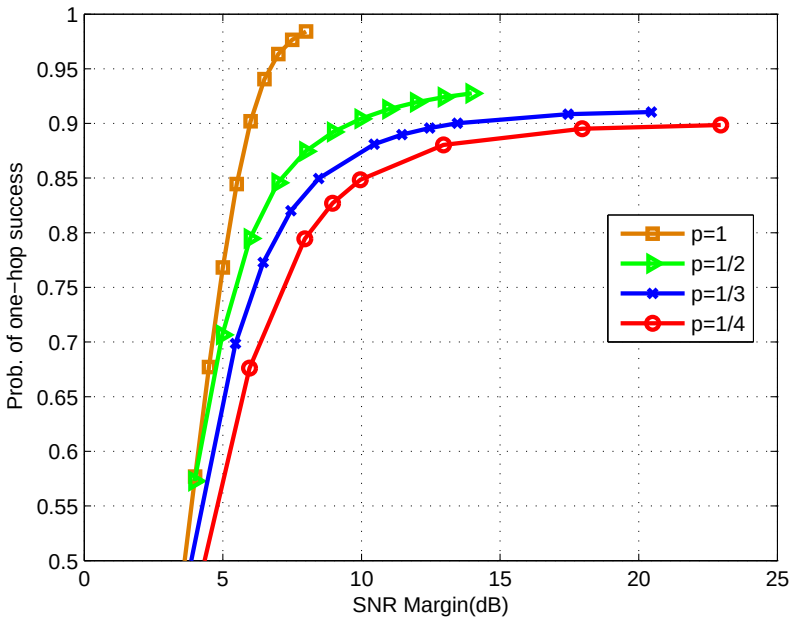

Figure 20: Success probabilities as a function of SNR Margin for a mean hop distance of 2 and various granularity levels

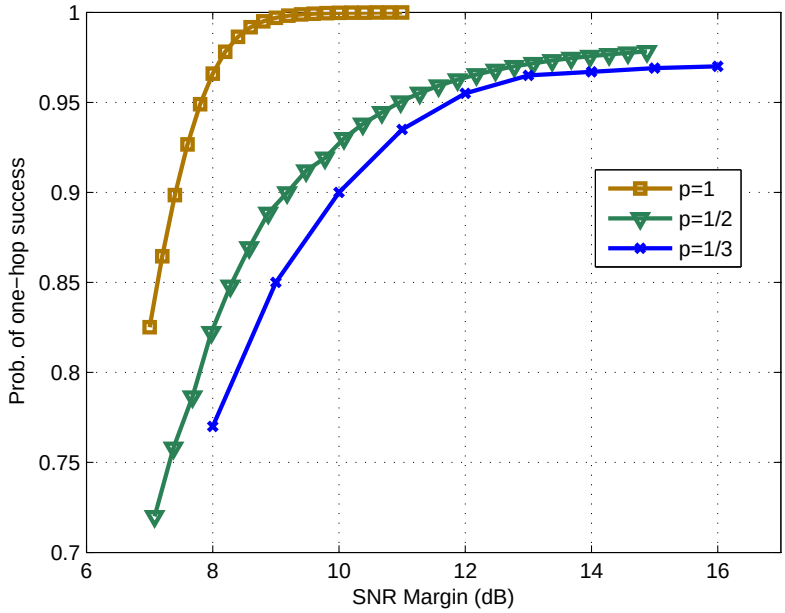

Figure 21: Success probabilities as a function of SNR Margin for a mean hop distance of 3 and various granularity levels

of ρ and the model space dimension. M is an *artificial* constraint because there is no real physical need for it, however, it strongly impacts the size of the state space and therefore the computational complexity of finding the success probability. Therefore, we would like for M to be as small as possible without significantly impacting the system performance results. We propose to find M by increasing the window size for a given hop distance, until the one-hop success probability (i.e., the Perron-Frobenius eigenvalue, ρ) ceases to change significantly. This implies that even if we add another slot at the forward edge of the window, there is no or little effect on the success probability because the transmissions reaching that specific slot are attenuated owing to the large path loss. Fig. 11 depicts the trend of eigenvalues as we increase the SNR margin for different window sizes and a mean hop distance of 2 with $p = 1/2$. The behavior is quite obvious that increasing SNR margin increases the probability of survival of the transmissions. It can be further noticed that for a given value of SNR margin, the curves start to converge as we increase the window size, thereby

indicating that after a specific window size, even if we increase M, there is no change in the transmissions outcome. Thus we select the window size where this convergence is achieved.

To compare the SNR margin required for a given quality of service, which can be the one-hop success probability in this case, the behavior of success probability is plotted versus SNR margin for different granularity levels in Fig. 20. In all cases, the mean hop distance is 2. Thus it can be seen that a smaller SNR margin is required to get the same success probability for deterministic deployment as compared to the random deployment. For example, for 85% success probability, the deterministic deployment requires 5.55dB of the SNR margin, whereas the SNR margins required are 7.1dB, 8.5dB, and 10dB for $p = 1/a$, $a = \{2, 3, 4\}$, respectively. A similar plot is also shown for a mean hop distance of 3 in Fig. 21, where we can observe that the behavior of curves is the same as for mean hop distance 2, however we can achieve higher values of success probabilities as the SNR margin increases, because larger hop distance corresponds to more transmitters per hop and therefore more diversity gain.

From the deployment perspective of the network, it is sometimes desirable to determine the values of certain parameters such as transmit power of relays to obtain a certain quality of service (QoS), η. In other words, we are interested in finding the probability of delivering the message at a certain distance without having entered the absorbing state, and we desire this probability to be at least η where $\eta \sim 1$ ideally. Thus (11) gives us a nice upper bound on the value of m (the number of hops) one can go with a given η, i.e. $\rho^m \geq \eta$, which gives

$$m \leq \frac{\ln \eta}{\ln \rho}. \tag{50}$$

Thus if the destination is far off, we require more hops, which will require a larger value of ρ. Fig. 22 shows the relationship between QoS, η, and the normalized distance for different values of granularity level. The normalized distance, which

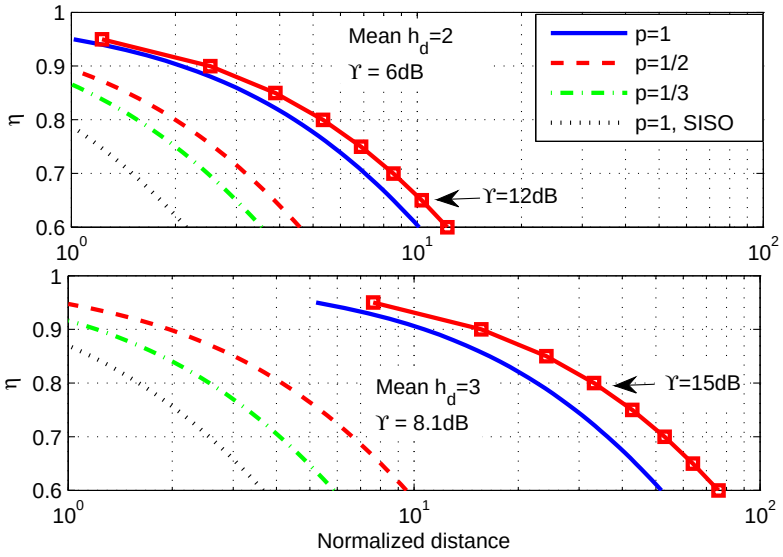

Figure 22: Normalized distance for given quality of service with different mean hop distances. The squared-marker curves show the $p = 1/2$ case at an indicated higher SNR margin

is the true distance divided by d, is defined as the product of h_d and the number of hops (made to reach the destination).We have taken three values of granularity level p, to show our result and the SNR margins for mean hop distances of 2 and 3 are 6dB and 8.1dB, respectively. We have also added the square-marker curves for $p = 1/2$ at the higher SNR margins of 12dB and 15dB, in the upper and lower graphs, respectively, as well as the SISO case in both graphs. We observe that for a fixed SNR margin (i.e., not including the square-marker curves) more random deployment or higher granularity implies a shorter distance can be covered for a given QoS. At low QoS, e.g., $\eta = 0.7$, the network is able to reach a particular distance with different granularity levels. Whereas, at high QoS, e.g., 0.9, the highest granularities are not possible. The $p = 1$ case always gives the best coverage for all values of the quality of service. The square-marker curves show that increasing the SNR margin can compensate the "random placement loss." We notice that the deterministic SISO

topology has very small coverage as compared to any cooperative topology with or without random deployment. We point out that retransmissions would increase the reliability of the SISO case, as well as the CT cases. However, retransmissions are quite challenging to implement in OLA-based networks, therefore we have assumed no retransmissions.

CHAPTER V

SNR ESTIMATION

In this chapter, we derive two types of estimators for SNR, a maximum likelihood estimator (MLE) and an estimator that uses data statistics, such that neither of them assume prior knowledge of the noise power. Our algorithm is also applicable for any value of M in an M-FSK receiver, where $M = 2^n$; n being a positive integer. We also consider two types of channels: one with fast Rayleigh fading and the other with slow block fading. However, we notice that the estimators derived for both cases are significantly different and lead to dramatically different analysis and results. [48] derives the average SNR estimate for pilot and data symbols separately. We provide ML versions of partially data-aided (PDA), non-data aided (NDA), joint PDA-NDA, and fully data-aided (FDA) estimators for average SNR. The PDA approach uses only the training sequence for estimation while the NDA approach does blind estimation using the entire sequence. The joint PDA-NDA uses all the information, operating blindly on the non-training part of the sequence. The FDA estimator uses the detected data as training sequence for SNR estimation and is reasonable in a multi-hop broadcast application, where every node must decode the entire message; the detected data are all assumed to be correct in the analysis regardless of the value of SNR.

The organization of this chapter is as follows. In the next section, we describe the system model and the notations used for the MFSK case. Section 5.2 treats the derivations of the SNR estimators, for a Rayleigh fading channel, including three sub-cases for MLE and also the estimator using data statistics. Section 5.3 considers the estimators for a block flat fading channel. Then we will derive the Cramer Rao Bound (CRB) for the Rayleigh fading case, and in Section 5.5, we will discuss the

simulation results for various estimators and overall estimator performance in terms of mean-squared error and CRB.

5.1 System Model for the Rayleigh fading case

Consider a Rayleigh fading communication system employing M-ARY FSK modulation, where each transmitted symbol is corrupted independently by fading and noise and the number of symbols in the constellation is $M = 2^n$, for a positive integer n. The received signal, after the matched filtering and passing the signal through the square law device, is given as

$$\mathbf{x}_i = |\mathbf{s}_i \alpha_i + \mathbf{n}_i|^2, \tag{51}$$

where $|.|$ is the magnitude operator applied on each element of the above equation and i is the time index. Each of $\mathbf{x}_i$, $\mathbf{s}_i$, and $\mathbf{n}_i$ are vectors with a dimension of $M \times 1$, and $\mathbf{s}_i = [0, ..., 0, 1, 0, ..., 0]^T$, where 1 is in the m_ith position ($1 \leq m_i \leq M$), where m_i indicates the symbol transmitted at time i, and the other positions have a zero. For the sake of simplicity, we assume that the average symbol energy is unity so that the expected energy of the ith received symbol is given as $E|\alpha_i|^2 = S$, where α_i is a zero mean fading coefficient drawn from a complex Gaussian distribution. Similarly, the elements of $\mathbf{n}_i$ are also independent complex Gaussian random variables with zero mean and variance $N/2$ per real dimension, thus the signal-to-noise ratio (SNR) is given by $\gamma = S/N$. $\mathbf{s}_i$, α_i, and $\mathbf{n}_i$ are assumed independent of each other. Our interest is to find the estimate of the average SNR using the observed data vector $\left[\mathbf{x}_1^T \ \mathbf{x}_2^T \ \cdots \ \mathbf{x}_k^T\right]^T$. For the estimation schemes considered, we assume that that there are g pilot symbols and l data symbols so that the total packet length is $k = g + l$. Throughout the analysis, we assume perfect timing recovery at the receiver.

5.2 Estimation Techniques for the Rayleigh Fading Environment

As mentioned previously, we will derive the ML estimators for three cases, namely PDA, NDA and *Joint* PDA-NDA. Another approach uses the statistics of observable data, which we call Estimation using Data Statistics (EDS).

5.2.1 Partially Data Aided MLE

Without the loss of generality, the g pilot symbols are each set to $[1 \;\; 0 \;\; ... \;\; 0]^T$. The received symbols from M branches are denoted as $x_{m,i}$, where first index m denotes the branch index where $m = 1, 2, ..., M$ and second index i is the time index such that $i = 1, 2, ..., g$. Since both the α_i and n_i in (51) are complex Gaussian, $x_{1,i}$ will have an exponential distribution with a mean of $E|\alpha_i|^2 + E|n_i|^2$. The probability density functions (PDFs) of the received pilot symbols $\mathbf{x}_i = [x_{1,i} \;\; x_{2,i} \;\; ... \;\; x_{M,i}]^T$, are given as

$$p_{x_{1,i}}(x_{1,i}) = \frac{1}{S+N} \exp\left(-\frac{x_{1,i}}{S+N}\right), \tag{52}$$

and

$$p_{x_{m,i}}(x_{m,i}) = \frac{1}{N} \exp\left(-\frac{x_{m,i}}{N}\right) \quad , m = 2, ..., M. \tag{53}$$

The joint PDF of $\mathbf{x}_i$ is given as

$$p_{\mathbf{x}_i}(\mathbf{x}) = \frac{1}{(S+N)N^{M-1}} \exp\left(-\frac{x_1}{(S+N)} - \frac{1}{N}\sum_{m=2}^{M} x_m\right). \tag{54}$$

Thus the log-likelihood distribution of g received symbols is given as

$$\begin{aligned} \Lambda_{\mathbf{x}_i}(\mathbf{x}; S, N) = &- g \ln(S+N) - g(M-1) \ln N \\ &- \frac{1}{S+N}\left(\sum_{i=1}^{g} x_{1,i}\right) - \frac{1}{N}\sum_{m=2}^{M}\sum_{i=1}^{g} x_{m,i}. \end{aligned} \tag{55}$$

To find the MLE of the SNR, $\hat{\gamma}$, we use the property that the ML estimate of the ratio of two parameters (S and N here), is the ratio of the individual ML estimates of the two parameters [49]. Thus

$$\hat{\gamma} = \frac{\hat{S}_{ML}}{\hat{N}_{ML}}. \tag{56}$$

Thus by differentiating (55) with respect to S and N, and setting the derivatives equal to zero results in

$$\hat{\gamma}_{DA} = \frac{(M-1)\sum_{i=1}^{g} x_{1,i} - \sum_{m=2}^{M}\sum_{i=1}^{g} x_{m,i}}{\sum_{m=2}^{M}\sum_{i=1}^{g} x_{m,i}}. \tag{57}$$

5.2.2 Non-Data Aided MLE

The PDF of the received symbol, given a 1 at the nth position is expressed as

$$p_{\mathbf{x}_i}(\mathbf{x}|s_n = 1) = \frac{1}{(S+N)N^{M-1}} \exp\left(-\frac{x_{n,i}}{S+N} - \sum_{m=1, m\neq n}^{M} \frac{x_{m,i}}{N}\right). \tag{58}$$

Assuming equal prior probabilities of transmitted symbols, the unconditional joint PDF of the received symbols for M-FSK is given as

$$\begin{aligned} p_{\mathbf{x}_i}(\mathbf{x}) = &\frac{1}{M(S+N)N^{M-1}} \Bigg[\underbrace{\exp\left(-\frac{x_{1,i}}{S+N} - \sum_{m=2}^{M} \frac{x_{m,i}}{N}\right)}_{a_1} + \\ &\underbrace{\exp\left(-\frac{x_{2,i}}{S+N} - \sum_{m=1, m\neq 2}^{M} \frac{x_{m,i}}{N}\right)}_{a_2} + \cdots + \underbrace{\exp\left(-\frac{x_{M,i}}{S+N} - \sum_{m=1}^{M-1} \frac{x_{m,i}}{N}\right)}_{a_M} \Bigg]. \end{aligned} \tag{59}$$

It can be seen from (59) that the PDF contains sum of M exponential terms, which are $a_1, a_2, ..., a_M$; taking the log-likelihood and then differentials with respect to S and N will make the expression very difficult to solve. The expression can be made simpler by factoring a common term, $\exp\left(-\frac{\sum_{m=1}^{M} x_{m,i}}{N}\right)$, from the exponents in (59) to get

$$p_{\mathbf{x}_i}(\mathbf{x}) = \frac{1}{M(S+N)N^{M-1}} \exp\left(-\frac{\sum_{m=1}^{M} x_{m,i}}{N}\right) \left[\sum_{m=1}^{M} \exp\left(-x_{m,i}\phi\right)\right], \tag{60}$$

where $\phi = \left[\frac{1}{S+N} - \frac{1}{N}\right]$. Thus the log-likelihood function for the k received symbols is given as

$$\begin{aligned}\Lambda_{\mathbf{x}_i}(\mathbf{x}; S, N) = &- k \ln M - k \ln (S+N) - k(M-1) \ln N \\ &- \sum_{m=1}^{M} \sum_{i=1}^{k} \frac{x_{m,i}}{N} + \sum_{i=1}^{k} \ln \left(\sum_{m=1}^{M} \exp \left(-x_{m,i} \phi \right) \right).\end{aligned} \tag{61}$$

Taking the partial derivative of (61) with respect to S and N results in

$$\frac{\partial \Lambda_{\mathbf{x}_i}(\mathbf{x}; S, N)}{\partial S} = - \frac{k}{(S+N)} + \frac{1}{(S+N)^2} \sum_{i=1}^{k} \frac{\sum_{m=1}^{M} x_{m,i} \exp \left(-x_{m,i} \phi \right)}{\sum_{m=1}^{M} \exp \left(-x_{m,i} \phi \right)}, \tag{62}$$

$$\begin{aligned}\frac{\partial \Lambda_{\mathbf{x}_i}(\mathbf{x}; S, N)}{\partial N} = &- \frac{k}{(S+N)} - \frac{(M-1)k}{N} + \sum_{m=1}^{M} \sum_{i=1}^{k} \frac{x_{m,i}}{N^2} \\ &+ \left[\frac{1}{(S+N)^2} - \frac{1}{N^2} \right] \sum_{i=1}^{k} \frac{\sum_{m=1}^{M} x_{m,i} \exp \left(-x_{m,i} \phi \right)}{\sum_{m=1}^{M} \exp \left(-x_{m,i} \phi \right)}.\end{aligned} \tag{63}$$

Putting the above equations equal to zero and solving them simultaneously gives us following result

$$\hat{S} + M \hat{N} = \frac{1}{k} \sum_{m=1}^{M} \sum_{i=1}^{k} x_{m,i}, \tag{64}$$

$$\frac{1}{k} \sum_{m=1}^{M} \sum_{i=1}^{k} x_{m,i} - (M-1) \hat{N} = \frac{1}{k} \sum_{i=1}^{k} \frac{\sum_{m=1}^{M} x_{m,i} \exp \left(-x_{m,i} \phi \right)}{\sum_{m=1}^{M} \exp \left(-x_{m,i} \phi \right)}. \tag{65}$$

The above forms of the equations seem to prohibit the closed form solutions for estimates of S and N. Thus using high-SNR approximations (see Appendix B), the summation term is approximated as

$$\sum_{i=1}^{k} \frac{\sum_{m=1}^{M} x_{m,i} \exp \left(-x_{m,i} \phi \right)}{\sum_{m=1}^{M} \exp \left(-x_{m,i} \phi \right)} \approx \sum_{i=1}^{k} \max \left(x_{1,i}, x_{2,i}, ..., x_{M,i} \right) = \sum_{i=1}^{k} \max_{m=1,...,M} \left(x_{m,i} \right). \tag{66}$$

Thus the estimate of noise power is given as

$$\hat{N} = \frac{1}{(M-1)k} \left[\sum_{m=1}^{M} \sum_{i=1}^{k} x_{m,i} - \sum_{i=1}^{k} \max_{m=1,...,M} \left(x_{m,i} \right) \right], \tag{67}$$

and the estimate of signal to noise ratio is given by

$$\hat{\gamma}_{NDA} = \frac{- \sum_{m=1}^{M} \sum_{i=1}^{k} x_{m,i} + M \sum_{i=1}^{k} \max_{m=1,...,M} \left(x_{m,i} \right)}{\sum_{m=1}^{M} \sum_{i=1}^{k} x_{m,i} - \sum_{i=1}^{k} \max_{m=1,...,M} \left(x_{m,i} \right)}. \tag{68}$$

5.2.3 Joint Estimation Using Pilot and Data Symbols

Consider g pilot symbols and l data symbols, so that the total packet is of length $k = g + l$. Assuming independent received symbols, the joint PDF is the product of PDFs resulting from pilot and data symbols. So we use (54) for $i = 1, 2, ..., g$ and (60) for $i = g + 1, ..., g + l = k$. Thus the log-likelihood function from the joint PDF is given as

$$\begin{aligned}\Lambda_{joint} = &- k \ln (S + N) - k(M - 1) \ln N \\ &- \frac{1}{S + N} \sum_{i=1}^{g} x_{1,i} - \frac{1}{N} \sum_{m=2}^{M} \sum_{i=1}^{g} x_{m,i} \\ &- \frac{1}{N} \sum_{m=1}^{M} \sum_{i=g+1}^{k} x_{m,i} + \sum_{i=g+1}^{k} \ln \left(\sum_{m=1}^{M} \exp (-x_{m,i}\phi) \right).\end{aligned} \tag{69}$$

Using similar approximations as in the previous section and taking partial derivatives with respect to S and N and setting them equal to zero result in the estimate of SNR as

$$\hat{\gamma} = \frac{\Psi + M \sum_{i=g+1}^{k} \max_m (x_{m,i}) + (M - 1) \sum_{i=1}^{g} x_{1,i}}{\Psi - \sum_{i=g+1}^{k} \max_m (x_{m,i})}. \tag{70}$$

where $\Psi = \sum_{m=2}^{M} \sum_{i=1}^{g} x_{m,i} + \sum_{m=1}^{M} \sum_{i=g+1}^{k} x_{m,i}$.

5.2.4 EDS Approach

In this subsection, we derive another type of NDA estimator that uses the statistics of the received signal for making an estimate of the SNR. We will show that this estimator performs better in the low SNR region and thus can be used as an alternative to ML-NDA estimator derived in the previous subsection, which suffers from approximation errors in the low SNR region.

In the EDS approach, we are interested in using the statistics of the received data so that we are able to get the estimates of our parameters of interest, namely the signal and the noise power. Owing to the i.i.d. (in time) nature of received data, we will drop the time index i from the rest of the section. It is known that the optimal

non-coherent FSK receiver requires a complex branch (i.e., I and Q channels) for each FSK frequency, because the phase is unknown [45]. Therefore, we can extend the scalar Equation (8) for BPSK in [51], to a vector formulation for MFSK, and define an $M \times M$ matrix $\mathbf{Z}$ given as

$$\mathbf{Z} = \left(\mathbb{E}\left\{\mathbf{x}_m\right\}\right)\left(\mathbb{E}\left\{\mathbf{x}_m\right\}\right)^T \left(\mathbb{E}\left\{\mathbf{x}_m \mathbf{x}_m^T\right\}\right)^{-1}, \tag{71}$$

where $\mathbb{E}\left\{\mathbf{x}_m\right\} = \left[\mathbb{E}\left\{x_1\right\} \quad \mathbb{E}\left\{x_2\right\} \quad \cdots \quad \mathbb{E}\left\{x_M\right\}\right]^T$. Assuming equally likely probable transmitted symbols, the ensemble average of the received data is given as

$$\mathbb{E}\left\{x_m\right\} = \frac{1}{M}\left[S + MN\right], \quad m = 1, ..., M. \tag{72}$$

Thus $\mathbb{E}\left\{\mathbf{x}_m\right\}\mathbb{E}\left\{\mathbf{x}_m\right\}^T$ is given as

$$\mathbb{E}\left\{\mathbf{x}_m\right\}\mathbb{E}\left\{\mathbf{x}_m\right\}^T = \frac{1}{M^2}\left[S + MN\right]^2 \mathbf{1}_M, \tag{73}$$

where $\mathbf{1}_M$ is an $M \times M$ matrix of all ones. The autocorrelation matrix of the received data, given by $\mathbb{E}\left\{\mathbf{x}_m \mathbf{x}_m^T\right\}$, contains $\mathbb{E}\left\{x_m^2\right\}$ on the main diagonal given as

$$\mathbb{E}\left\{x_m^2\right\} = \frac{2}{M}\left[S^2 + 2SN + MN^2\right], \quad m = 1, ..., M \tag{74}$$

while the rest of all elements will be $\left(\mathbb{E}\left\{x_m\right\}\right)^2$, where $\mathbb{E}\left\{x_m\right\}$ is given by (72). Thus we can write

$$\mathbb{E}\left\{\mathbf{x}_m \mathbf{x}_m^T\right\} = \frac{\left[S + MN\right]^2}{M^2} \underbrace{\begin{bmatrix} a & 1 & \cdots & 1 \\ 1 & a & \cdots & 1 \\ \vdots & \vdots & \ddots & \vdots \\ 1 & 1 & \cdots & a \end{bmatrix}}_{\mathbf{H}} \tag{75}$$

where the element a is given as

$$a = \frac{\mathbb{E}\left\{x_m^2\right\}}{\mathbb{E}\left\{x_m\right\}^2} = 2M\frac{\gamma^2 + 2\gamma + M}{(\gamma + M)^2}, \tag{76}$$

and $\gamma = S/N$ is the signal-to-noise ratio. It can be noticed that the matrix $\mathbf{H}$ in (75) is a special kind of Hankel matrix which is also circulant [52]. The inverse of such a

circulant matrix, of order M, is given as

$$\mathbf{H}^{-1} = \frac{1}{\zeta}\begin{bmatrix} a+M-2 & -1 & \cdots & -1 \\ -1 & a+M-2 & \cdots & -1 \\ \vdots & \vdots & \ddots & \vdots \\ -1 & -1 & \cdots & a+M-2 \end{bmatrix}, \tag{77}$$

where $\zeta = a^2 + (M-2)a - (M-1)$. Thus the matrix $\mathbf{Z}$ from (71) is given as

$$\mathbf{Z} = \mathbf{1}_M \mathbf{H}^{-1} = \frac{a-1}{a^2+(M-2)a-(M-1)}\mathbf{1}_M. \tag{78}$$

Since the resulting $\mathbf{Z}$ from above equation contains identical elements at each location of $M \times M$ matrix, we can now utilize any one of the element from $\mathbf{Z}$. Thus, using value of a from (76), any $z \in \mathbf{Z}$ is given by

$$z = \frac{(\gamma+M)^2}{M^3 + M^2(2\gamma+1) + M\gamma(3\gamma+2) - \gamma^2}. \tag{79}$$

We may solve for γ to get an estimate as

$$\begin{aligned} \hat{\gamma} = & \frac{1}{3Mz - z - 1}\left[M(1 - Mz - z)\right. \\ & \left. + \sqrt{}(2(M-1)M^2 z(1 - Mz - z))\right]. \end{aligned} \tag{80}$$

To make this approach practical, we replace the expectations in (71) with the corresponding block averages to compute the estimate of $\mathbf{Z}$ as

$$\hat{\mathbf{Z}} = (\overline{\mathbf{x}})\,(\overline{\mathbf{x}})^T \left(\overline{\mathbf{x}\mathbf{x}^T}\right)^{-1}, \tag{81}$$

where $\overline{\mathbf{x}}$ is a column vector of time averages of M branches; $\overline{\mathbf{x}} = [\bar{x}_1, \bar{x}_2, ..., \bar{x}_M]^T$, and each $\bar{x}_m$ is given as

$$\bar{x}_m = \frac{1}{k}\sum_{i=1}^{k} x_{m,i}, \quad m = \{1, 2, ..., M\}. \tag{82}$$

We have plotted the results from (80) for the computed statistic, z, against the SNR, γ, in Figure 23 for various values of M. Each curve in the figure exhibits smooth monotone behavior for low values of SNR, i.e., when SNR $\in$ [0,10]. Thus,

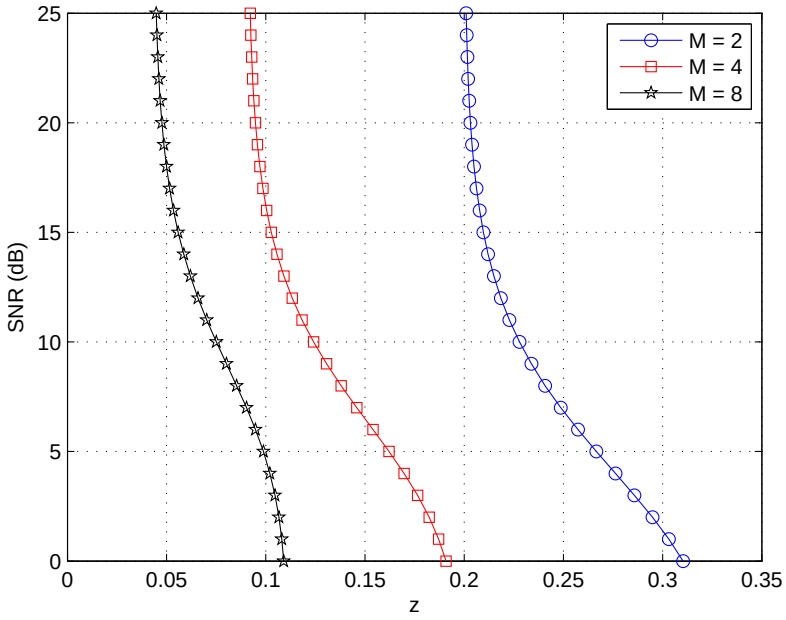

Figure 23: Relationship between the computed statistics, z, and γ for different modulation orders, M, for the Rayleigh fading channel.

the estimator performance is anticipated to be good in this SNR region. However, as the SNR increases, all the curves appear to approach a vertical asymptote . This implies that a very small change in the computed statistics of data would cause a huge variation in the estimated value of SNR. Hence this approach will suffer in the estimation of high SNR values. Therefore, this approach can be used as an NDA approach for SNR estimation for low SNR regions.

5.3 SNR Estimation for a block Fading channel

In this section, we will briefly describe the approach for estimating SNR in a block fading environment, which is the case when a block of data with k symbols undergoes a constant non-random fade. Using the complex data model, the received symbols are given as

$$\mathbf{v}_i = A\mathbf{s}_i + \mathbf{n}_i. \tag{83}$$

In the above equation A is the complex signal amplitude assumed constant over the entire frame and $\mathbf{n}_i$ is the noise vector whose elements are drawn from a zero mean complex Gaussian distribution with a variance of $N/2$ per real dimension. Thus the SNR for block fading environment is given as $\gamma = \frac{|A|^2}{N}$. As previously, in this section, we will assume that the SNR estimation is done after the square law. Thus, we will estimate the SNR using the observed data $\mathbf{x}_i = \left[(|\mathbf{v}_1|^2)^T \ \cdots \ (|\mathbf{v}_k|^2)^T \right]^T$.

5.3.1 Partially Data-Aided Estimation

Using the same notations and assumptions as done in Section 5.2, the first branch output, containing a 1, is given as

$$x_{1,i} = |A + n_i|^2, \tag{84}$$

where A and n are as defined in the previous section. Since the noise is complex Gaussian, thus the resulting PDF of $x_{1,i}$ will be non-central chi square distribution, where the non centrality parameter λ is given as

$$\lambda = (\Re\{A\})^2 + (\Im\{A\})^2 = |A|^2, \tag{85}$$

where $\Re\{A\}$ and $\Im\{A\}$ denote the real and imaginary parts of the complex signal amplitude A, respectively. Thus, the PDF of $x_{1,i}$ is given as

$$p_{x_{1,i}}(x) = \frac{1}{N} \exp\left(-\frac{x + |A|^2}{N} \right) I_0\left(\frac{2\sqrt{x}|A|}{N} \right), \tag{86}$$

where $I_0(.)$ is the modified Bessel function of zero order first kind. The PDF for each of the rest of the branches $m = 2, ..., M$, is exponential, and is given as

$$p_{x_{m,i}}(x_m) = \frac{1}{N} \exp\left(-\frac{x_m}{N} \right). \quad m = 2, ..., M. \tag{87}$$

Thus the joint PDF of the received symbols is given as

$$p_{\mathbf{x}_i}(\mathbf{x}) = \frac{1}{N^M} \exp\left(-\frac{x_1 + |A|^2}{N} - \frac{1}{N} \sum_{m=2}^{M} x_m \right) I_0\left(\frac{2\sqrt{x_1}|A|}{N} \right). \tag{88}$$

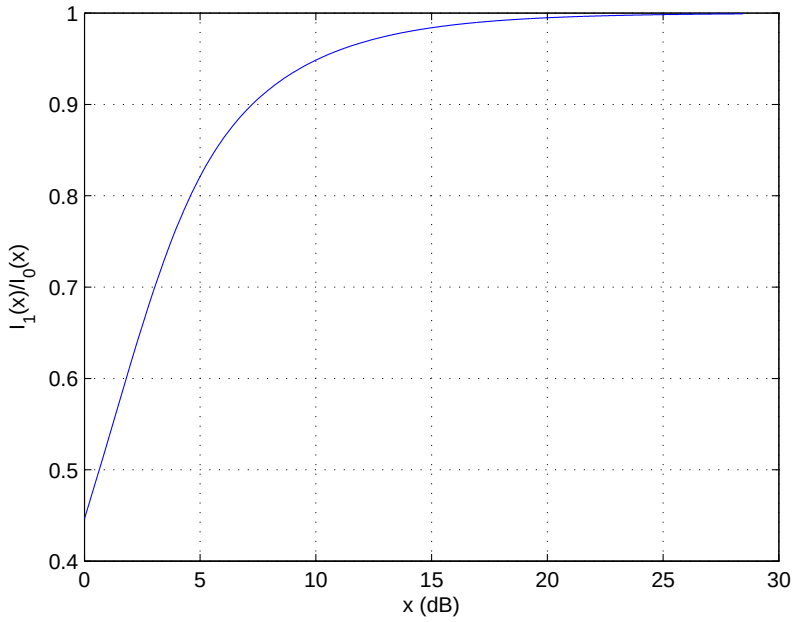

Figure 24: Behavior of the ratios of modified Bessel functions of the first kind.

The log-likelihood for the g received symbols is given as

$$\begin{aligned}\Lambda_{\mathbf{x}_i}(\mathbf{x}; A, N) = &- gM\ln(N) - \frac{1}{N}\left(\sum_{i=1}^{g} x_{1,i} + g|A|^2 + \sum_{m=2}^{M}\sum_{i=1}^{g} x_{m,i}\right) \\ &+ \sum_{i=1}^{g} \ln\left(I_0\left(\frac{2\sqrt{x_{1,i}}|A|}{N}\right)\right).\end{aligned} \tag{89}$$

Taking the derivative of (89) with respect to A and using the relations $\frac{d}{dx}I_n(x) = I_{n+1}(x)$, $\frac{\partial A}{\partial A} = 1$, $\frac{\partial A^*}{\partial A} = 0$, and $\frac{\partial A A^*}{\partial A} = A^*$ [53], [54], we get

$$\frac{\partial \Lambda_{\mathbf{x}_i}(\mathbf{x}; A, N)}{\partial A} = -\frac{gA^*}{N} + \sum_{i=1}^{g} \frac{I_1\left(\frac{2\sqrt{x_{1,i}}|A|}{N}\right)}{I_0\left(\frac{2\sqrt{x_{1,i}}|A|}{N}\right)} \frac{A^*\sqrt{x_{1,i}}}{N|A|}. \tag{90}$$

An exact solution to the above equation is difficult to obtain because of the non-linearity of modified Bessel function. However, it can be observed that for high values of the argument, the ratio of first order modified Bessel function to the zero order modified Bessel function, i.e. $\frac{I_1(.)}{I_0(.)}$, is approximately equal to 1. This phenomenon can be seen in the Figure 24. Thus using this approximation, the estimate of $|A|$ is

given as

$$|\hat{A}| = \frac{1}{g}\sum_{i=1}^{g}\sqrt{x_{1,i}}. \tag{91}$$

Differentiating (89) with respect to N and using similar approximations, the estimate of N is given as

$$\hat{N} = \frac{1}{Mg}\left[\sum_{i=1}^{g} x_{1,i} - g|\hat{A}|^2 + \sum_{m=2}^{M}\sum_{i=1}^{g} x_{m,i}\right]. \tag{92}$$

Using (91) and (92), we can find the estimate of SNR for the data-aided case as $\frac{|\hat{A}|^2}{\hat{N}}$.

5.3.2 Non-Data Aided Estimation

The PDF of the received symbol, given 1 at the nth position, is given as

$$p_{\mathbf{x}_i}(\mathbf{x}|s_n = 1) = \frac{1}{N^M}\exp\left(-\frac{1}{N}\left[x_n + |A|^2 + \sum_{m=1,m\neq n}^{M} x_m\right]\right) I_0\left(\frac{2\sqrt{x_n}|A|}{N}\right). \tag{93}$$

Assuming equal prior probabilities of transmitted symbols, the unconditional joint PDF of the received symbols for M-FSK block fading case is given as

$$p_{\mathbf{x}_i}(\mathbf{x}) = \frac{1}{MN^M}\exp\left(-\frac{1}{N}\left[\sum_{m=1}^{M} x_m + |A|^2\right]\right)\left[\sum_{m=1}^{M} I_0\left(\frac{2\sqrt{x_m}|A|}{N}\right)\right]. \tag{94}$$

For k received symbols, the log-likelihood function is given as

$$\begin{aligned}\Lambda_{\mathbf{x}_i}(\mathbf{x}; A, N) = &- k\ln(M) - kM\ln(N) - \frac{1}{N}\left(\sum_{m=1}^{M}\sum_{i=1}^{k} x_{m,i} + k|A|^2\right) \\ &+ \sum_{i=1}^{k}\ln\left[\sum_{m=1}^{M} I_0\left(\frac{2\sqrt{x_{m,i}}|A|}{N}\right)\right].\end{aligned} \tag{95}$$

The partial derivative with respect to A is given as

$$\frac{\partial\Lambda_{\mathbf{x}_i}(\mathbf{x}; A, N)}{\partial A} = -\frac{KA^*}{N} + \sum_{i=1}^{k}\frac{\sum_{m=1}^{M} I_1\left(\frac{2\sqrt{x_{m,i}}|A|}{N}\right)}{\sum_{m=1}^{M} I_0\left(\frac{2\sqrt{x_{m,i}}|A|}{N}\right)}\frac{A^*\sqrt{x_{m,i}}}{N|A|}. \tag{96}$$

Using some approximations of the modified Bessel functions (see Appendix C), the estimate of $|A|$ is given as

$$|\hat{A}| = \frac{1}{k}\sum_{i=1}^{k}\max_{m=1,\ldots,M}\sqrt{x_{m,i}}. \tag{97}$$

The noise power estimate is given in a similar manner as

$$\hat{N} = \frac{1}{Mk}\left[\sum_{m=1}^{M}\sum_{i=1}^{k} x_{m,i} - k|\hat{A}|^2\right]. \tag{98}$$

5.3.3 Joint Estimation Using Pilot and Data Symbols

Considering g pilot symbols and l data symbols the log-likelihood function from the joint PDF is given as

$$\begin{aligned}\Lambda_{joint} = &- kM\ln N - l\ln M + \sum_{i=1}^{g}\ln\left(I_0\left(\frac{2\sqrt{x_{1,i}}|A|}{N}\right)\right)\\ &+ \sum_{i=g+1}^{k}\ln\left[\sum_{m=1}^{M} I_0\left(\frac{2\sqrt{x_{m,i}}|A|}{N}\right)\right] - \frac{k|A|^2}{N}\\ &- \frac{1}{N}\left(\sum_{i=1}^{g} x_{1,i} + \sum_{m=2}^{M}\sum_{i=1}^{g} x_{m,i} + \sum_{m=1}^{M}\sum_{i=g+1}^{k} x_{m,i}\right).\end{aligned} \tag{99}$$

Using similar approximations as in the previous section and taking partial derivatives with respect to A and N and setting them equal to zero result in the estimates of signal and noise powers as

$$|\hat{A}| = \frac{1}{k}\left[\sum_{i=1}^{g}\sqrt{x_{1,i}} + \sum_{i=g+1}^{k}\max_{m=1,\ldots,M}\sqrt{x_{m,i}}\right], \tag{100}$$

$$\hat{N} = \frac{1}{kM}\left[\sum_{m=1}^{M}\sum_{i=1}^{g} x_{m,i} + \sum_{m=1}^{M}\sum_{i=g+1}^{k} x_{m,i} - k|\hat{A}|^2\right]. \tag{101}$$

5.3.4 EDS Approach

In order to get an estimate of SNR using the statistics of the received data, we define an $M \times M$ matrix $\mathbf{Z}$, similar to (71). Assuming equally likely probable transmitted symbols, the ensemble average of the received data is given as

$$\mathbb{E}\{x_m\} = \frac{1}{M}\left[|A|^2 + MN\right], \quad m = 1, ..., M \tag{102}$$

Thus $\mathbb{E}\{\mathbf{x}_m\}\mathbb{E}\{\mathbf{x}_m\}^T$ is given as

$$\mathbb{E}\{\mathbf{x}_m\}\mathbb{E}\{\mathbf{x}_m\}^T = \frac{1}{M^2}\left[|A|^2 + MN\right]^2\mathbf{1}_M, \tag{103}$$

where $\mathbf{1}_M$ is an $M \times M$ matrix of all ones. The autocorrelation matrix of the received data, given by $\mathbb{E}\left\{\mathbf{x}_m\mathbf{x}_m^T\right\}$, contains $\mathbb{E}\{x_m^2\}$ on the main diagonal given as

$$\mathbb{E}\left\{x_m^2\right\} = \frac{1}{M}\left[|A|^4 + 4N|A|^2 + 2MN^2\right], \quad m = 1, ..., M \tag{104}$$

while the rest of all elements will be $(\mathbb{E}\{x_m\})^2$, where $\mathbb{E}\{x_m\}$ is given by (102). Thus we can construct the matrix $\mathbf{H}$ as in Section 5.2.4, where the element a is given as

$$a = \frac{\mathbb{E}\{x_m^2\}}{\mathbb{E}\{x_m\}^2} = M\frac{\gamma^2 + 4\gamma + 2M}{\gamma^2 + M^2 + 2M\gamma}, \tag{105}$$

and $\gamma = |A|^2/N$ is the signal-to-noise ratio. Thus utilizing only one of the element from $\mathbf{Z}$, we get

$$z = \frac{\gamma^2 + 2M\gamma + M^2}{M^3 + 2M^2\gamma + M^2 + 2M\gamma^2 + 2M\gamma - \gamma^2}. \tag{106}$$

We may solve for γ to get an estimate as

$$\begin{aligned}\hat{\gamma} =& \frac{1}{2Mz - z - 1}\Big[M - Mz - Mz^2 \\ &+ \sqrt{(}\, - M^4z^2 + M^3z^2 + M^3z + 2M^2z^2 - 2M^2z)\Big].\end{aligned} \tag{107}$$

It can be seen from (106) that z has no solution at $z = 1/3$ for $M = 2$. Thus this method is not applicable for a BFSK system. This scheme follows the same behavior of curves as in Figure 23, except for $M = 2$ case which would be a vertical line. Otherwise we observe that in the higher SNR regime, the EDS approach will suffer due to the steepness of the curves. But it will be shown in the simulation section, that the EDS approach shows best performance for larger data set and in the low SNR region, compared to the MLE algorithms discussed in the previous subsection, because there are no approximation errors in this approach.

5.4 Cramer-Rao Lower Bound for Rayleigh Fading Channel

In this section, we will derive the CRB for the SNR estimator, for the Rayleigh fading channel. It can be noticed, that we can have different CRBs for the different cases discussed in the previous section. However, the FDA estimator serves as a benchmark on the variance of all estimators; FDA is same as PDA but uses all information in the packet as training sequence. We also show that the CRB for the NDA estimator is identical to the CRB of the FDA estimator if we use the high SNR approximation.

Since the unknown parameter is a vector i.e., $\theta = [S \quad N]^T$, thus the CRB for the SNR is given as [53]

$$CRB = \frac{\partial \mathbf{g}(\theta)}{\partial \theta} \mathbf{I}^{-1}(\theta) \frac{\partial \mathbf{g}(\theta)^T}{\partial \theta}, \tag{108}$$

where $\mathbf{g}(\theta) = \frac{S}{N}$ and the Jacobian of $\mathbf{g}(\theta)$ is given as

$$\mathbf{J}_{\mathbf{g}}(\theta) = \begin{bmatrix} \frac{1}{N} & \frac{-S}{N^2} \end{bmatrix}, \tag{109}$$

and $\mathbf{I}(\theta)$ is the Fisher information matrix (FIM) given as

$$[\mathbf{I}(\theta)]_{ij} = -\mathbb{E}\left[\frac{\partial^2 \Lambda}{\partial \theta_i \theta_j}\right]. \tag{110}$$

The FIM for the FDA estimator is given as

$$\mathbf{I}(\theta) = \begin{bmatrix} \frac{k}{(S+N)^2} & \frac{k}{(S+N)^2} \\ \frac{k}{(S+N)^2} & \frac{k}{(S+N)^2} + \frac{k(M-1)}{N^2} \end{bmatrix}, \tag{111}$$

which gives the CRB from (108) as

$$CRB_{FDA} = \frac{M}{k(M-1)} (1+\gamma)^2. \tag{112}$$

This bound has been plotted in Figures 26 and 27, and is further discussed in the next section. The CRB of NDA estimator is given in Appendix D.

5.5 Simulation Results

In this section, we compare the normalized mean squared error (NMSE) (normalized with respect to the square of the true value of the SNR) of the estimators using simulations for different values of M and for different packet lengths averaged over 10,000 trials. The NMSE is given as

$$NMSE(\hat{\gamma}) = \frac{\mathbb{E}\left\{(\gamma - \hat{\gamma})^2\right\}}{\gamma^2}, \tag{113}$$

where γ is the true value of SNR and $\hat{\gamma}$ is the estimated value. The results shown in Figures 25 - 30 are for the Rayleigh fading channel. Figure 25 shows the NMSE vs.

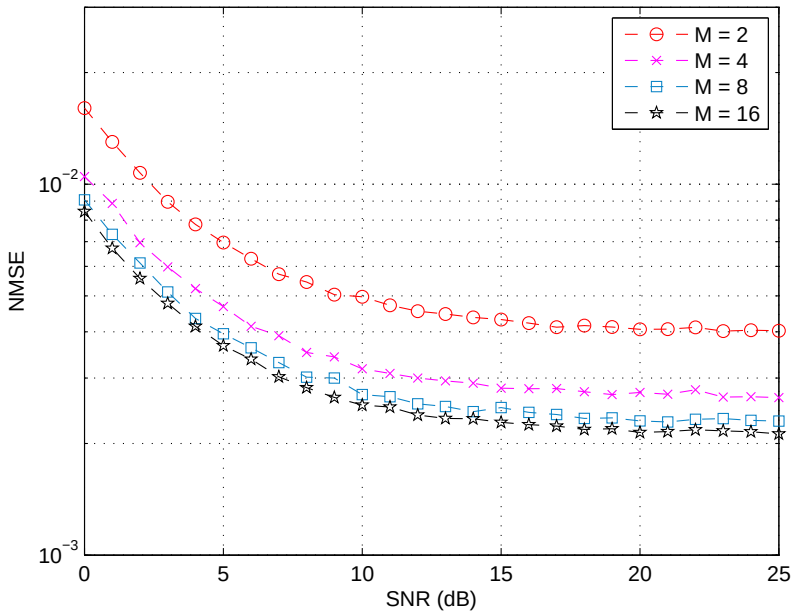

Figure 25: Effect of increasing M on NMSE for 1000 symbol-long packet for the PDA estimator for the Rayleigh fading channel.

true SNR for the PDA estimator, with 500 pilot symbols in the packet for increasing values of M. We observe that the estimates become more and more accurate as we have more and more branches with noise only. Thus increasing M indirectly increases the number of samples, which gives lower NMSE. Although not shown in the figures, this behavior is found in all techniques discussed in Sections 5.2 and 5.3.

Figures 26 and 27 treat the long packet, which is assumed to comprise 100 pilot symbols and 900 data symbols. We observe that the PDA NMSE is approximately constant over the entire SNR range. The NDA and *Joint* cases perform similarly because most of the packet is data and the NMSE is high in the low SNR region. The large error in low SNR range of NDA and joint estimators can be attributed to the approximation errors in the low SNR regime. To check the high SNR approximation (from Appendix B), we have plotted the NMSE between the true SNR (computed numerically using Equations (64) and (65)) and the estimated SNR using the approximation in Equation 66. Figure 29 shows this NMSE for different values of M

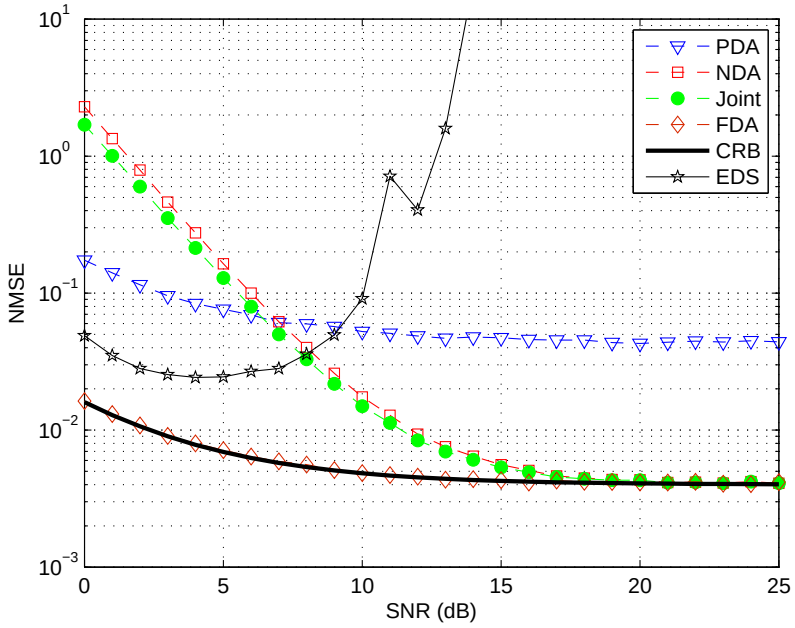

Figure 26: NMSE for different estimators for a Binary FSK receiver, (M=2), for the Rayleigh fading channel with 1000 symbols including 100 pilot symbols (g=100).

for a packet length of 100. It can be seen that the error decreases with the increase in SNR, which shows that the approximation in Appendix A is valid.

In Figures 26 and 27, we can observe the consequence of this approximation. We notice a small NMSE, for the NDA estimator, as the SNR increases from 8dB onwards. The EDS approach performs better for low SNR estimation as compared to the NDA scheme. However, the EDS method shows bad behavior at high SNR due to the steepness of curve from Figure 23, and therefore, we can see a rapid increase in the NMSE after 10dB. To do a fair comparison, we assume that both the pilot and the data symbols are available to the NDA and EDS approaches for the estimation. For high SNR, the *Joint* estimation scheme works the best, as expected. The crossing of the curves suggests that an adaptive mode of SNR estimation can also be derived consisting of estimation from the pilot only (PDA) or EDS during the low SNR while using the entire data packet for estimating high SNR values. In that case, the overall NMSE will remain minimum over a wide range of SNR values. In Figure 27, which

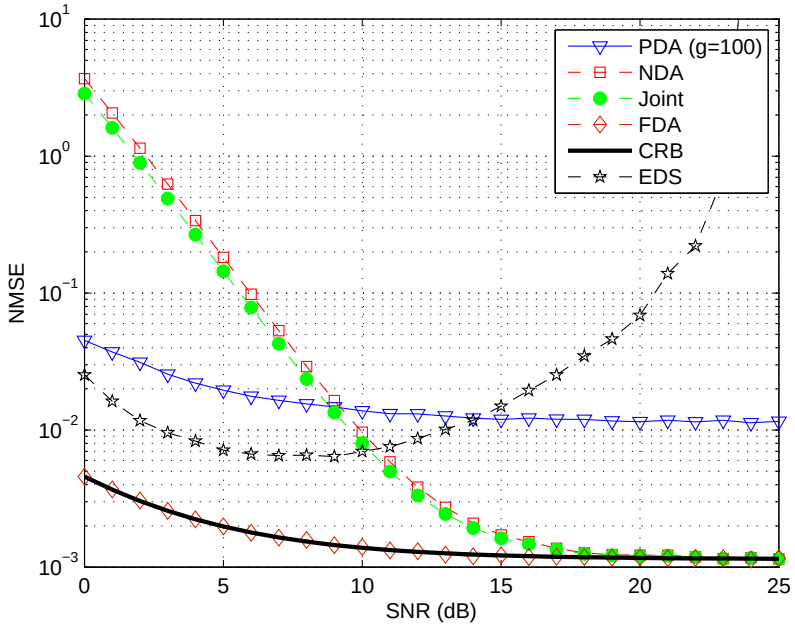

Figure 27: NMSE for different estimators for 8FSK receiver, (M=8), for the Rayleigh fading channel with 1000 symbols including 100 pilot symbols (g=100).

shows the results for $M = 8$, the curves have the same behavior as in the $M = 2$ case, but the NMSE for $M = 8$ is lower.

Figure 28 treats the short packet scenario, with 8 pilot symbols and 28 data symbols. We show this short packet case because the EDS approach does not perform well because of the limitations of the availability of data (approximation error of the ensemble averages with time averages for small data set is large). Thus for a short length packet and with the availability of pilot, the joint data estimation performs best. If the pilot is not available, then the NDA MLE also gives better performance.

Figures 26 to 28 include the results for the FDA approach (decision feedback), which utilizes the detected data, assuming no detection errors. It can be seen that the performance of the FDA estimator is enhanced significantly and it reaches the CRB. Using this approach, we gain two advantages: a larger data set and estimation using DA approach which has no approximation errors. The *no errors* assumption is good in the context of the decode and forward (DF) scenario, since passing the

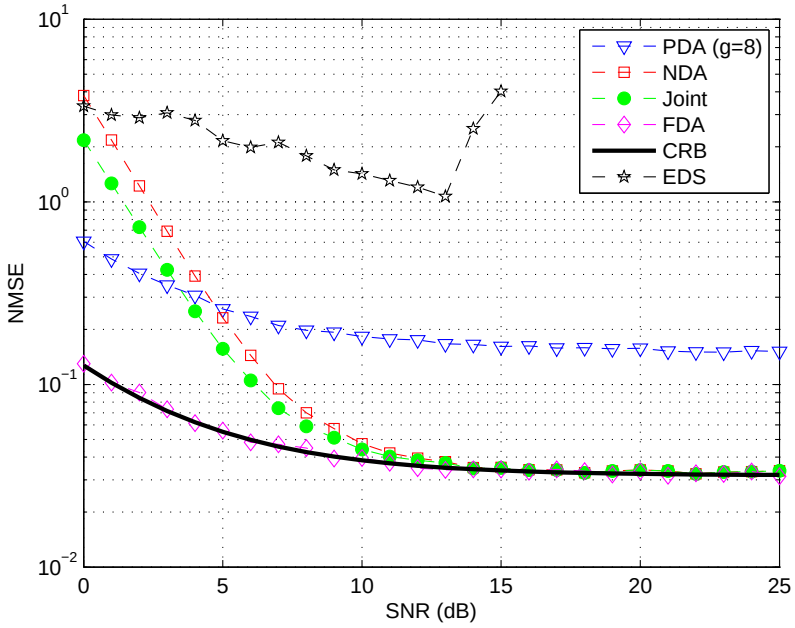

Figure 28: NMSE for different estimators for 8FSK receiver, for a Rayleigh fading channel with 36 symbols including 8 pilot symbols (g=8).

CRC check is a precondition for forwarding the packet [11]. Sometimes, it is desired to choose the packet length such that the NMSE should not exceed some specified value. A contour plot of NMSE for SNR versus the packet length for FDA case is shown in Figure 30 for $M = 8$. We observe that 5% error can be achieved with 50 symbols.

Figure 31 shows the estimation results for the block fading channel. It can be seen that the behavior of the curves is identical to those of Figures 26 to 28 but interestingly the EDS method outperforms the ML estimation with a considerable margin for low values of SNR because there are no approximation errors in the EDS scheme for a block fading channel. However, it shows bad behavior at high SNR due to the steepness of the curves from Figure 23. The CRB for this case is not derived due to tedious calculations involving modified Bessel function and hence is not plotted here.

In Sections 5.2 and 5.3, we have shown that the mathematical analysis for both the

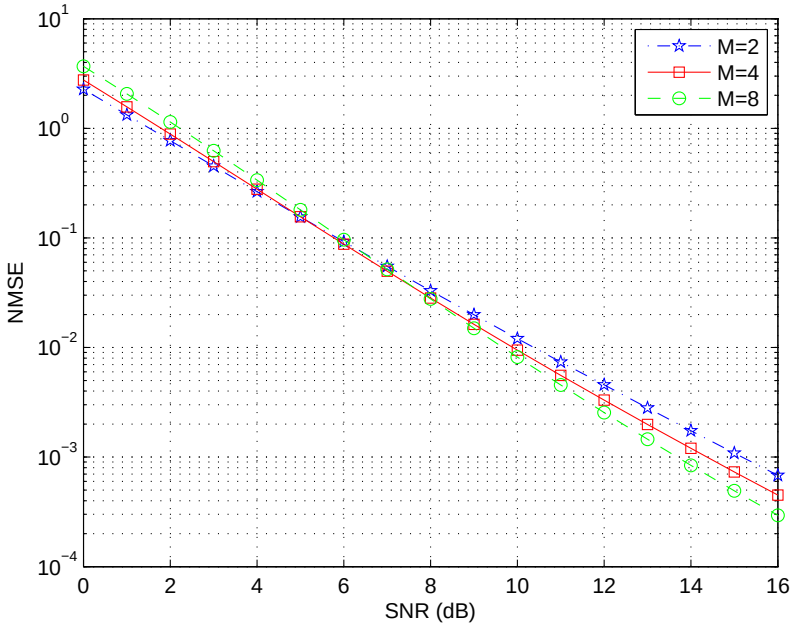

Figure 29: NMSE between actual and approximated SNR values for NDA estimator in Rayleigh fading for a packet length of 100

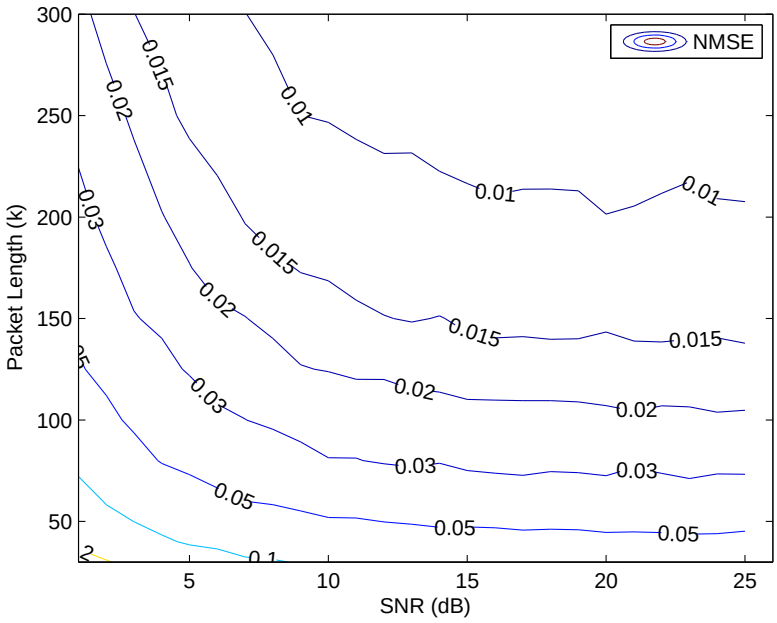

Figure 30: NMSE contours for various packet lengths for the FDA estimator for the Rayleigh fading channel.

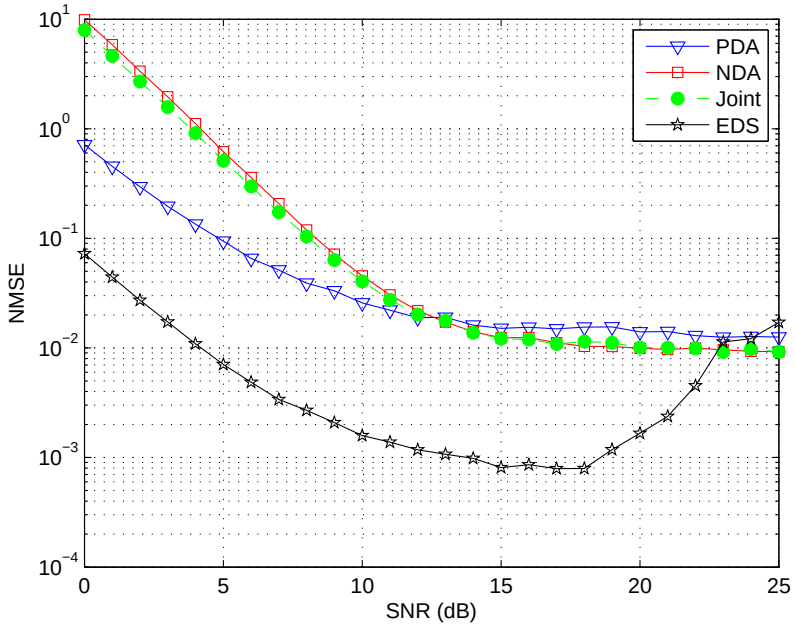

Figure 31: NMSE for different estimators for a block fading channel in 8FSK receiver, M=8, with 1000 symbols including 100 pilot symbols (g=100).

channel models are quite different from each other. However, an interesting scenario is to apply the SNR estimators designed for Rayleigh fading channels to the block fading case, and vice versa. We observe that the block fading estimator is better for the block fading channel (in terms of SNR gain) for all estimators except PDA at low SNR. The NMSE is higher at low-SNR region for the PDA approach, which can be attributed to the approximations of the modified Bessel function that we made in Section 5.3.1. We have simulated this effect for a short packet scenario for 8-FSK scheme such that the packet contains 8 pilot symbols and 28 data symbols. From Figure 32, it can be noticed that if we apply the reverse scenario, i.e., apply the block fading estimators on Rayleigh fading channel, the estimators fail to estimate the SNR. Intuitively, the block fading channel is a general case of Rayleigh fading channel so the cross-estimator works, but with lower efficiency. On the other hand, Rayleigh fading is not a general case of block fading channel, thus the cross-estimator fails to estimate the SNR of the received data. Thus both estimators give appropriate

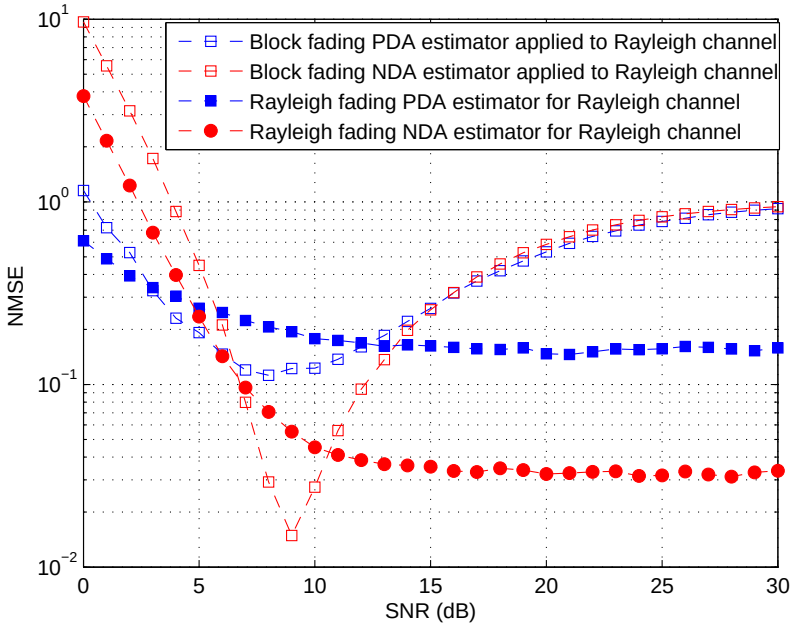

Figure 32: Effects of applying the estimators for a block fading channel on the data received through Rayleigh fading channel.

results for their respective channel models. From Figure 32, we observe that for a very short range of SNR, the cross-estimators work better. This could be due to the sub-optimality of PDA/NDA ML estimator cost functions in the mean-squared sense. For the rest of the SNR range, the actual estimators perform better.

CHAPTER VI

SNR ESTIMATION IN THE PRESENCE OF A CARRIER FREQUENCY OFFSET

An important application of estimating SNR is used in cooperative communications where the relay node decodes and forwards (DF) the received data only if the received SNR is higher than that of a specified threshold. Opportunistic Large Arrays with Threshold (OLA-T) [20] is one example, in which the authors assume perfect SNR estimation for the DF mode. In this chapter, we derive practical ways of estimating SNR for such applications. However, the carrier frequency offset (CFO) causes error in the estimation of SNR; this will degrade the performance of systems that depend upon the knowledge of SNR, e.g., amplify and forward (AF) cooperative algorithms [24]. Thus, in this chapter, we estimate the SNR of a non-coherent BFSK receiver in the presence of a carrier offset, treating the CFO as a nuisance parameter. The CFO estimation problem is quite tedious to solve because of its highly non-linear nature, hence analytical methods cannot be directly applied to solve the problem at hand. Therefore, we derive a maximum likelihood estimator for the SNR that uses a moment-based CFO estimator. We also derive the Cramer-Rao lower bound (CRB) for the SNR estimator. We provide two types of SNR estimators: a data-aided (DA) estimator that uses the pilot symbols and a non-data aided (NDA) estimator that does blind estimation on the received symbols.

The rest of the chapter is organized as follows. In the next section, we describe the system model and the notations used for the BFSK receiver operating in the presence of CFO. Section 6.2 treats the derivations of the SNR estimators for the data-aided scenario in the presence of a Rayleigh fading channel. Section 6.3 considers the

estimators for non data-aided case and in Section 6.4, we will discuss the simulation results for various estimators and overall estimator performance in terms of mean-squared error and the CRB.

6.1 System Model

Consider a Rayleigh fading communication system employing binary FSK modulation, where a block of data with k symbols undergoes symbol-rate fading. The received signal observed at the receiver end is given as

$$\begin{aligned} r(t) = \sqrt{E_s}\alpha(t)\exp\left(j2\pi(f_c + f_m + \Delta f)t + \theta\right) + n(t), \\ 0 \leq t \leq T, \quad m \in \{1, 2\}, \end{aligned} \tag{114}$$

where E_s is the signal power, T is the symbol time, f_c is the carrier frequency, and f_m is the BFSK frequency corresponding to the message signal. The shift in the carrier frequency at the receiver is denoted as Δf and θ is the unknown carrier phase. Without the loss of generality we will set $\theta = 0$, since we are dealing with the non-coherent receiver. The noise at the receiver is $n(t)$, which is additive white Gaussian noise (AWGN) and $\alpha(t)$ is the Rayleigh fading envelope. Thus, the integrator output, matched to the transmitted signal S_m is given as

$$v_m = \int_0^T r(t)\sqrt{E_s}\exp\left(-j2\pi(f_c + f_m)t\right)dt, \tag{115}$$

where we get the the signal part, after simplifying the above equation, as

$$v_{ms} = P\alpha\left[\frac{1 - \exp\left(-j2\pi\Delta fT\right)}{j2\pi(m-1) + j2\pi\Delta fT}\right], \quad m \in \{1, 2\}, \tag{116}$$

where $P = \frac{E_s T}{2}$. For the sake of simplicity, we assume that the average symbol energy is unity, i.e., $P = 1$, and thus the signal output after the square law detector for the BFSK receiver having a frequency carrier shift of Δf is given as

$$x_{m,i} = \left|\alpha_i\left[\frac{1 - \exp\left(-j2\pi\rho\right)}{j2\pi(m-1) + j2\pi\rho}\right] + n_{m,i}\right|^2, \quad m \in \{1, 2\}, \tag{117}$$

where $\rho = \Delta f T$ is the normalized frequency error, $|.|$ is the magnitude operator, and the CFO factors in both branches are given as

$$A_m = \left| \frac{1 - \exp\left(-j2\pi\rho\right)}{j2\pi(m-1) + j2\pi\rho} \right|^2, \quad m \in \{1, 2\}. \tag{118}$$

The received symbols from 2 branches are denoted by $x_{m,i}$, where the first index m denotes the branch index and the second index i is the time index such that $i = \{1, 2, ..., k\}$; k being the packet length. The channel gains, α_i, and the noise elements, n_i, are zero mean complex Gaussian random variables with variance of $S/2$ and $N/2$ per real dimension, respectively. We can express $\mathbf{x}_i = [x_{1,i} \;\; x_{2,i}]^T$ to be the received signal vector at time i. Since we assumed that the average symbol energy is unity, the expected energy of the ith received symbol is given as S. Thus, the signal-to-noise ratio is given by $\gamma = \frac{S}{N}$. Our interest is to find the estimate of the average SNR using the observed data, after the square law detector but it can be seen that the factor A_m in (118) will reduce the signal power if $\rho \neq 0$. Thus, in this section, we will try to estimate the CFO, ρ, and treat it as a nuisance parameter which is essential to estimate the actual parameter of interest namely, the signal to noise ratio. Throughout the analysis, we assume perfect timing recovery at the receiver.

6.2 Data Aided Estimation

In this section, we derive the SNR estimator for the BFSK receiver in the presence of CFO, while having full knowledge of the transmitted data. Therefore, without the loss of generality, we assume that all the transmitted symbols are identical, and correspond to frequency f_1. We drop the time index i for the ease of notation and use the received data in one symbol period, because the received symbols are independent at each time slot. From (117), it can be seen that the signal power is reduced by the CFO factor, A_1, in the upper branch (x_1) and there is also a signal spill which introduces some part of signal power in the lower branch, given by A_2, where these factors are given as $A_1 = \frac{\sin^2(\pi\rho)}{(\pi\rho)^2}$ and $A_2 = \frac{\sin^2(\pi\rho)}{(\pi(1+\rho))^2}$. Because of the signal leakage in

both of the branches, the two branches no longer remain orthogonal and hence there exists a correlation between the outputs x_1 and x_2, given by the cross-correlation coefficient as

$$\xi = \frac{2A_1A_2S^2 + SN(A_1 + A2) + N^2}{(A_1S + N)(A_2S + N)} - 1. \tag{119}$$

From (117), as α and n are zero-mean complex Gaussian, therefore, the probability density function (PDF) of both the branches become exponential after passing through the envelope detector. As shown in [48], the best performance of SNR estimator, in terms of CRB, can be obtained if the likelihood function for the received data is maximized after the envelope detector, i.e., the best estimator is obtained if the input data to the SNR estimator is the vector $\mathbf{x}$. However, there exists a correlation between the elements of $\mathbf{x}$, because of which the joint PDF of the received signal vector is given by Downton's bivariate exponential distribution [43], containing a modified Bessel function. The presence of modified Bessel function makes the problem at hand very tedious to solve analytically. However, a reasonable solution can be obtained if the input data to the estimator is the difference between x_1 and x_2, which is also available in the BFSK receiver. Thus we use the Laplace distribution [44], which is obtained by taking the difference of two exponential random variables as $y = x_1 - x_2$. In order to further simplify the PDF expression, we define the following: $\mu = A_1 + A_2$, $\nu = A_1 - A_2$, and $\phi = \sqrt{4N^2 + 4\mu SN + \nu^2S^2}$. Thus, the PDF of y is given as

$$p_y(y) = \frac{2}{4\sigma_1^2\sigma_2^2(1-\xi)\eta} \exp\left(-\frac{\alpha y}{4}\right), \quad y \geq 0, \tag{120}$$

where $2\sigma_m^2 = A_mS + N, \quad m \in \{1, 2\}$, $\eta = \frac{2\phi}{N^2+\mu SN}$, and $\alpha = \frac{8}{\nu S+\phi}$. It can be seen from (120), that a closed form solution will be prohibitive if we try to maximize the log-likelihood function of (120) with respect to three parameters namely S, N, and ρ. Specifically the CFO parameter is very difficult to solve analytically through this optimization problem. A solution can be obtained if we somehow know the CFO factor, ρ. In the following subsection, we estimate ρ using the moments based method,

which turns out to be a very accurate estimate, especially at high SNR. Then we will show how the estimate of CFO can help in estimating the SNR using the conventional ML method.

6.2.1 Method of Moments Approach

In the method of moments (MM) approach, we use the first order self and cross statistics of the received data to estimate the CFO, which will subsequently be used in the estimation of SNR. In this case, the first order statistics obtained from both the branches are as follows

$$\mathbb{E}\{x_m\} = A_m S + N, \quad m \in \{1, 2\}, \tag{121}$$

and the first cross-moment is given as

$$\mathbb{E}\{x_1 x_2\} = 2A_1 A_2 S^2 + SN(A_1 + A_2) + N^2. \tag{122}$$

In practice, we replace the ensemble averages in previous equations with those of time averages, i.e., $\mathbb{E}\{x\} \approx \frac{1}{k}\sum_{i=1}^{k} x_i$. Hence we denote the time averages as $\mathbb{E}\{x_1\} := X$, $\mathbb{E}\{x_2\} := Y$, and $\mathbb{E}\{x_1 x_2\} := Z$. We also let $\tilde{A}_1 = A_1 S$ and $\tilde{A}_2 = A_2 S$, then equations (121) and (122) can be solved simultaneously to get the estimate of the noise power, N, as

$$\hat{N} = \frac{1}{2}\left(X + Y - \sqrt{(X^2 - 6XY + Y^2 + 4Z)}\right), \tag{123}$$

and the estimates of $\tilde{A}_1$ and $\tilde{A}_2$ are given as $\hat{\tilde{A}}_1 = X - \hat{N}$ and $\hat{\tilde{A}}_2 = Y - \hat{N}$. Finally, we get the estimates of ρ and then the signal power, as given by following equations,

$$\hat{\rho} = \frac{\hat{\tilde{A}}_2 + \sqrt{\hat{\tilde{A}}_1 \hat{\tilde{A}}_2}}{\hat{\tilde{A}}_1 - \hat{\tilde{A}}_2}, \tag{124}$$

$$\hat{S} = \frac{\hat{\tilde{A}}_1}{\hat{A}_1} = \hat{\tilde{A}}_1 \left(\frac{\pi\hat{\rho}}{\sin(\pi\hat{\rho})}\right)^2. \tag{125}$$

If we define $\zeta(\theta) := \frac{1}{n}\sum_{i=1}^{n}(\hat{\theta}_i - \theta)^2$ as the sample variance of the error of estimator for parameter θ, where $\theta \in \left\{\tilde{A}_1, \tilde{A}_2, \rho\right\}$, then a plot of ζ is shown for various values

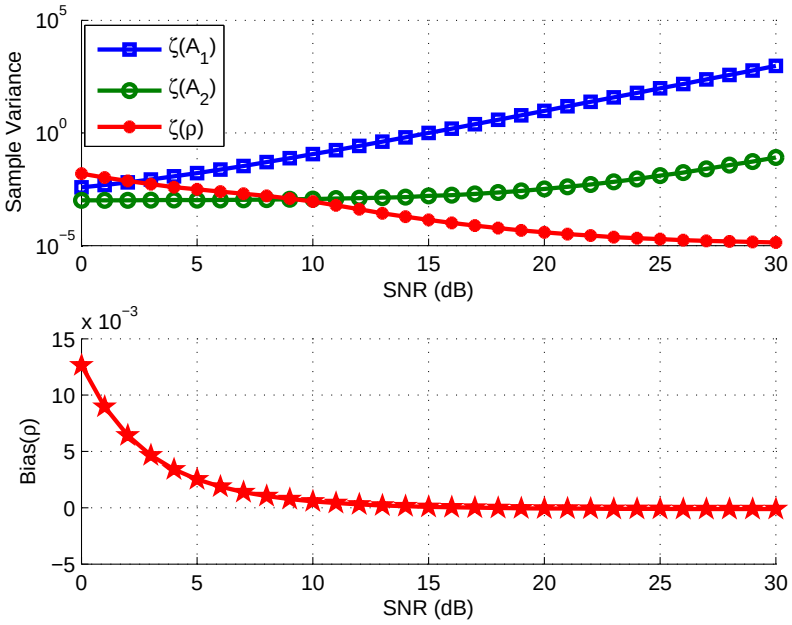

Figure 33: Sample variance of error for different parameters and bias of CFO estimator; g=1000

of SNR in top plot of Fig. 33. It can be seen that though $\zeta(\tilde{A}_1)$ and $\zeta(\tilde{A}_1)$ increases with increasing SNR, the variance of error for ρ decreases. Thus the estimator of ρ is anticipated to give better performance as SNR increases. However, since $\zeta(\tilde{A}_1)$ increases with increasing SNR, the SNR estimate resulting from (125) will show a high mean squared error in the high SNR region. We can write $\hat{\rho} = f(\mathbf{z})$, where $\mathbf{z} = [z_1\ z_2\ z_3]^T$, and the non-linear function f is given as

$$f(\mathbf{z}) = \frac{z_2 - z_1 + 2\sqrt{z_3 - z_1 z_2} + \sqrt{z_1^2 - 6z_1 z_2 + z_2^2 + 4z_3}}{2(z_1 - z_2)}. \tag{126}$$

Let $\boldsymbol{\mu} = [\mu_1\ \mu_2\ \mu_3]^T$ be the vector of true moments, then a second order Taylor series expansion of f about $\boldsymbol{\mu}$ yields $\hat{\rho} \approx \rho + \mathbf{v}^T(\mathbf{z} - \boldsymbol{\mu}) + 1/2(\mathbf{z} - \boldsymbol{\mu})^T\mathbf{H}(\mathbf{z} - \boldsymbol{\mu})$, where $\mathbf{v} = \bigtriangledown f|_{\mathbf{z}-\boldsymbol{\mu}}$ and $\mathbf{H}$ is the Hessian matrix of f. Taking expectation on both sides yields

$$Bias(\hat{\rho}) \approx \frac{1}{2g} tr(\mathbf{HC}). \tag{127}$$

In the above equation, tr represents the trace of a matrix and $\mathbf{C}$ is the symmetric

covariance matrix of $\boldsymbol{\mu}$, where $c_{ii} = \{\mu_1^2,\ \mu_2^2,\ 2\mu_3^2 + 4\mu_1\mu_2\,(\mu_3 - \mu_1\mu_2)\}$, $i \in \{1,2,3\}$, $c_{21} = \mu_3 - \mu_1\mu_2$, and $c_{3i} = \mu_i(c_{21} + \mu_3)$, $i \in \{1,2\}$. The final expression of bias from (127) can thus be obtained, which is given as

$$
\begin{aligned}
Bias(\hat{\rho}) \approx \frac{1}{2gP^3\sqrt{Q}R^{3/2}} \Big[& -2P^4\sqrt{Q}\,(2Q+R) + P^2\left\{-8Q^{3/2}\left(R + \mu_1^2 - 4\mu_1\mu_2 + \mu_2^2\right)\right. \\
& + R^{3/2}\,(-7Q + \mu_1\mu_2) + \sqrt{Q}\left(\mu_1^2\left(R - \mu_1^2 + 6\mu_1\mu_2 - 17\mu_2^2\right) - \right. \\
& \left.\left. 4\mu_3\left(R + \mu_1^2 - 6\mu_1\mu_2 + 2\mu_3\right)\right)\right\} + 2\sqrt{Q}\left\{-4\,(QR)^{3/2} + \left(2\sqrt{Q}R^{3/2} + R^2\right)\left(\mu_1^2 + \mu_2^2\right)\right. \\
& \left. +\ 2Q\left(\mu_1^4 + 44\mu_1\mu_2\mu_3 - 6\mu_1^2\left(3\mu_2^2 + \mu_3\right) + \left(\mu_2^2 - 8\mu_3\right)\left(\mu_2^2 + 2\mu_3\right)\right)\right\}\Big],
\end{aligned}
\tag{128}
$$

and where $P = \mu_1 - \mu_2$, $Q = c_{21}$, and $R = \mu_1^2 - 6\mu_1\mu_2 + \mu_2^2 + 4\mu_3$. The bottom plot of Fig. 33 shows this approximate theoretical bias of the CFO estimator and it can be seen that the estimator shows a very low bias and is asymptotically zero for $SNR \geq 7dB$.

6.2.2 Maximum Likelihood Approach

In the ML approach, we assume the knowledge of CFO, which we get from the MM estimator in the previous subsection. Based upon the known value of ρ, we can treat μ and ν in (120) as constant parameters. Thus, the log-likelihood of the k symbols, $y_i,\ \ i = \{1,2,...,k\}$, is given as

$$
\Lambda(\mathbf{y}; S, N|\rho) = -\frac{k}{2}\log\phi^2 - \frac{2}{(\nu S + \phi)}\sum_{i=1}^{k} y_i. \tag{129}
$$

Maximizing the above likelihood with respect to S and N again prohibits a closed form expression for the estimates of signal power and noise power. However, it will be shown in the results section that the estimate of the CFO and hence the noise power from the MM estimator is fairly accurate. Therefore, we can use the estimate of the noise power from the MM estimator to derive the ML estimator.

Based on the above discussions, the log-likelihood function can be further simplified by using SNR γ, i.e., S/N, and the noise, N, as the parameters of interest. Thus

we get,

$$\Lambda(\mathbf{y};\gamma|N) = -k\log N - k\log\tilde{\phi} - \frac{2}{N\left(\nu\gamma+\tilde{\phi}\right)}\sum_{i=1}^{k} y_i, \tag{130}$$

where $\tilde{\phi} = \sqrt{4+4\mu\gamma+\nu^2\gamma^2}$. Finding the maxima of the log-likelihood with respect to γ gives the following estimate of SNR

$$\hat{\gamma} = \frac{\left(\sum_{i=1}^{k} y_i\right)^2/(k\hat{N}) - k\hat{N}}{\nu\sum_{i=1}^{k} y_i + \mu k\hat{N}}. \tag{131}$$

6.2.3 Cramer-Rao Lower Bound

The Cramer-Rao bound (CRB), which is the benchmark on the variance of an estimator, is a function of the Fisher information, $F(\gamma)$, [53], and is given as $CRB = 1/F(\gamma)$, where $F(\gamma)$ is given as

$$F(\gamma) = -\mathbb{E}\left\{\frac{\partial^2\Lambda}{\partial\gamma^2}\right\}. \tag{132}$$

Thus twice differentiating (130) with respect to γ and taking the expectation gives the following Fisher information

$$F(\gamma) = \frac{1}{\tilde{\phi}^4}\left[k\left\{-\mu^2\tilde{\phi}^2 + 2(2\nu+\mu^2\gamma)^2 - \frac{\psi}{(\phi+\mu\gamma)^3}\right\}\right], \tag{133}$$

where $\psi = 2\mu\tilde{\phi}\gamma(\tilde{\phi}(\mu\tilde{\phi}+6\nu) + 2\mu\gamma(\mu\tilde{\phi}+\nu) + \mu^3\gamma^2)(2\nu+\mu(\tilde{\phi}+\mu\gamma))$.

6.3 Non Data-Aided Estimation

In this section, we derive the MM and ML estimators for the non-data aided scenario where we assume the equally likely probability of the transmission of the data symbols. We follow the same approach of finding $\hat{\rho}$ and $\hat{N}$ from the MM estimator and then use these estimates to find the ML SNR estimator.

6.3.1 Method of Moment Estimator

For the NDA case, we assume that $\mathbb{P}\{\text{signal} \in x_1\} = \mathbb{P}\{\text{signal} \in x_2\} = 1/2$. Hence the average value of both branches remains the same. Thus, we use the following

statistics of the data in order to estimate the CFO.

$$\mathbb{E}\{x_m\} = \frac{1}{2}\left[\tilde{A}_1 + \tilde{A}_2 + 2N\right], \quad m \in \{1, 2\}, \tag{134}$$

$$\mathbb{E}\{x_1 x_2\} = 2\tilde{A}_1\tilde{A}_2 + N(\tilde{A}_1 + \tilde{A}_2) + N^2. \tag{135}$$

Since we need three linearly independent equations in order to get the estimates of three parameters, we use the following vector formulation of the received data

$$\mathbf{Z} = (\mathbb{E}\{\mathbf{x}\})(\mathbb{E}\{\mathbf{x}\})^T \left(\mathbb{E}\left\{\mathbf{x}\mathbf{x}^T\right\}\right)^{-1}, \tag{136}$$

where $\mathbb{E}\{\mathbf{x}\} = [\mathbb{E}\{x_1\} \quad \mathbb{E}\{x_2\}]^T$. Thus $\mathbb{E}\{\mathbf{x}\}\mathbb{E}\{\mathbf{x}\}^T$ is given as

$$\mathbb{E}\{\mathbf{x}\}\mathbb{E}\{\mathbf{x}\}^T = \frac{1}{4}\left[\tilde{A}_1 + \tilde{A}_2 + 2N\right]^2 \mathbf{1}_2, \tag{137}$$

where $\mathbf{1}_2$ is an 2×2 matrix of all ones. The autocorrelation matrix of the received data, given by $E\left\{\mathbf{x}_m\mathbf{x}_m^T\right\}$, contains $E\{x_m^2\}$ on the main diagonal given as

$$\mathbb{E}\left\{x_m^2\right\} = (\tilde{A}_1^2 + \tilde{A}_2^2) + 2N(\tilde{A}_1 + \tilde{A}_2) + 2N^2, \quad m \in \{1, 2\}, \tag{138}$$

while the off-diagonal elements are given as $\mathbb{E}\{x_1 x_2\}$, which are given by (135). Thus, taking the inverse of this matrix and multiplying it with (137) gives us the following $\mathbf{Z}$

$$\mathbf{Z} = \frac{\left(\tilde{A}_1 + \tilde{A}_2 + 2N\right)^2}{4\left[\left(\tilde{A}_1 + \tilde{A}_2\right)^2 + 3N\left(\tilde{A}_1 + \tilde{A}_2\right) + 3N^2\right]}\mathbf{1}_2. \tag{139}$$

Since the resulting $\mathbf{Z}$ from the above equation contains identical elements at each location of 2×2 matrix, therefore, we can select only one of the elements from $\mathbf{Z}$. As in the previous case, we let $\mathbb{E}\{x_m\} := X$, then any $z \in Z$ can be written as

$$z = \frac{X^2}{(2X - 2N)^2 + 3N(2X - 2N) + 3N^2}, \tag{140}$$

which gives the estimate of the noise power, N, as

$$\hat{N} = X\left[1 - \sqrt{1/z - 3}\right]. \tag{141}$$

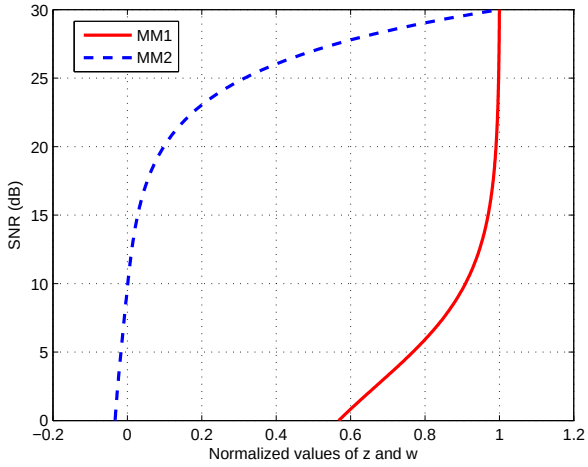

Figure 34: Behavior of MM1 and MM2 estimators for non data-aided case

Let us denote this estimator (resulting from the statistic z) as MM1. We have plotted the results from (140) for the computed statistic, z, against the SNR, γ , in Figure 34 for a CFO factor $\rho = 0.1$. The curve in the figure exhibits smooth monotone behavior for low values of SNR, i.e., when $SNR \in [0, 10]$. Thus, the estimator performance is anticipated to be good in this SNR region. However, as the SNR increases, the curve appears to approach a vertical asymptote. This implies that a very small change in the computed statistics of data would cause a huge variation in the estimated value of SNR. Hence this approach will suffer in the estimation of high SNR values. Therefore, this approach of MM1 can be used as an NDA approach for SNR estimation for low SNR values.

In order to design an estimator which performs better at high SNR values, we consider another statistic of the received data

$$\mathbb{E}\left\{x_1 x_2^2\right\} = N(3NX - 2X^2) - Y(2N - 3X), \tag{142}$$

where, as before, $Y := \mathbb{E}\left\{x_1 x_2\right\}$. Let $W := \frac{\mathbb{E}\left\{x_1 x_2^2\right\}}{\mathbb{E}\left\{x_1^2\right\}}$, then an estimate of the noise power in terms of statistic W is given as

$$\hat{N} = \frac{1}{W - 3X}\left[WX - X^2 - Y + \sqrt{f(W, X, Y)}\right]. \tag{143}$$

where $f = X^4 - 7X^2Y + Y^2 + W^2(Y - 3X^2) + 2W(5X^3 - XY)$. We denote this estimator as MM2. The estimator characteristics are also plotted in Figure 34. It can be seen that this estimator would not estimate accurately in the low SNR regime because of the vertical asymptote. However, the estimator performance is likely to be good in the high SNR region since the estimator characteristic exhibits almost linear behavior. Hence we can use MM2 for the NDA estimation of SNR in the high SNR region.

For the estimate of the CFO, we notice from the definitions of A_1 and A_2 that, $\frac{A_1A_2}{(A_1+A_2)^2} = \left(\frac{\rho(1+\rho)}{\rho^2+(1+\rho)^2}\right)^2$. If we denote this ratio of CFO factors as β, then ρ can be given as a function of β as follows

$$\rho = \frac{1 - 2\sqrt{\beta} - \sqrt{1-4\beta}}{2(2\sqrt{\beta} - 1)}. \tag{144}$$

We can calculate β from (134) and (135), which gives $\beta = \frac{Y - \hat{N}(2X - 2\hat{N}) - \hat{N}^2}{2(2X-2\hat{N})^2}$, where $\hat{N}$ can be found by either using MM1 or MM2. Finally the signal power is given as

$$\hat{S} = \frac{2X - 2\hat{N}}{\hat{A}_1 + \hat{A}_2}, \tag{145}$$

where $\hat{A}_1$ and $\hat{A}_2$ can be computed using the estimate of ρ from (144).

6.3.2 Maximum Likelihood Approach

Using the difference of random variables, $y = x_1 - x_2$, as done in the previous section and assuming equally likely probability of transmitted symbols, the PDF of the received symbols is given as

$$\begin{aligned} p_y(y) =& \frac{1}{4}\left[\frac{1}{\sqrt{\left(\hat{\sigma}_2^2 - \hat{\sigma}_1^2\right)^2 + 4\hat{\sigma}_1^2\hat{\sigma}_2^2(1-\xi)}} \exp\left(-\frac{1}{4}\alpha^+|y|\right)\right. \\ &\left. + \frac{1}{\sqrt{\left(\tilde{\sigma}_2^2 - \tilde{\sigma}_1^2\right)^2 + 4\tilde{\sigma}_1^2\tilde{\sigma}_2^2(1-\xi)}} \exp\left(-\frac{1}{4}\alpha^-|y|\right)\right] \end{aligned} \tag{146}$$

where $2\hat{\sigma}_1^2 = 2\tilde{\sigma}_2^2 = A_1S + N$, $2\hat{\sigma}_2^2 = 2\tilde{\sigma}_1^2 = A_2S + N$,

$$\alpha^+ = \frac{\sqrt{\left(\hat{\sigma}_2^2 - \hat{\sigma}_1^2\right)^2 + 4\hat{\sigma}_1^2\hat{\sigma}_2^2(1-\xi)} + \hat{\sigma}_2^2 - \hat{\sigma}_1^2}{\hat{\sigma}_1^2\hat{\sigma}_2^2(1-\xi)}, \tag{147}$$

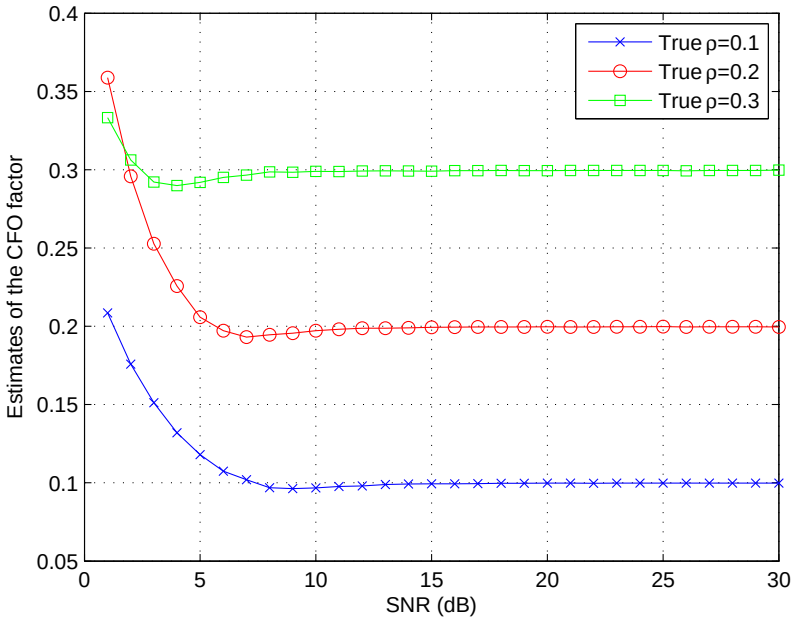

Figure 35: Estimation of ρ by MM estimator for $k = 1000$ in the data-aided scenario

and

$$\alpha^{-} = \frac{\sqrt{\left(\tilde{\sigma}_2^2 - \tilde{\sigma}_1^2\right)^2 + 4\tilde{\sigma}_1^2\tilde{\sigma}_2^2(1-\xi)} + \tilde{\sigma}_2^2 - \tilde{\sigma}_1^2}{\tilde{\sigma}_1^2\tilde{\sigma}_2^2(1-\xi)}. \tag{148}$$

However, $\alpha^{+} = \alpha^{-}$ and thus both terms are simply added up to give the PDF of the received symbols as

$$p_y(y) = \frac{1}{2\hat{\sigma}_1^2\hat{\sigma}_2^2(1-\xi)\eta} \exp\left(-\frac{\alpha|y|}{4}\right), \tag{149}$$

which is the same PDF as for the data-aided case in (120), with the only difference that the absolute of the data will be used now. Hence we use the same approach as in the Section 6.2. The likelihood and hence the resulting estimates of the SNR follow from (130) and (131), respectively. Even there is no change in the CRB, because the likelihood of both the schemes is the same and also $\mathbb{E}\{y\}$, $y \geq 0$ for the DA case is the same as $\mathbb{E}|y|$ for the NDA case. The Fisher Information and hence the CRB also remains equal.

6.4 Simulation Results

In this section, we compare the normalized mean squared error (NMSE) (normalized with respect to the square of the true value of the SNR) of the estimators using simulations for both the data-aided and non data-aided scenarios for a packet length, $k = 1000$, averaged over 20,000 trials. For the data-aided scenario, Figure 35 shows the estimates the CFO factor, ρ, using the MM approach for the DA case. It can be seen that the estimate of CFO is highly accurate for $SNR \geq 7dB$. Figure 36 shows the NMSE for the SNR estimation resulting from both the MM and the ML estimator. In the "No CFO estimation" case, the SNR is estimated without estimating the CFO from the algorithm derived in [34]. We observe that as the SNR increases, the leakage in the lower branch increases and consequently the error in the estimation increases. It can also be noticed that the MM estimator works well for the SNR estimation at low values of SNR. However, it suffers in the high SNR region due to a higher bias for high values of signal power in this range. The same cup shaped curve of MM estimator can also be seen in [47]. From the MM estimator, we know that the estimate of ρ is quite accurate and this estimate also depends on the noise estimate from Equations (123)–(124), hence we can use these estimates to derive the ML algorithm and the resulting curve in Figure 36 shows that the NMSE is quite small if we use the estimates from the MM estimator. The CRB is also plotted to compare the results. The high error in the low SNR region of ML estimator is due to two facts: 1) bad estimates of ρ in MM, 2) at low SNR, the condition of $y \geq 0$ is not always satisfied in the PDF from (120). However, the ML estimator shows good results at high SNR.

The above simulation results were for a packet length of $k = 1000$. However, it is interesting to note the performance of the estimate of ρ even at small packet lengths. The contour plot in Figure 37 shows the MSE of the estimation of CFO factor for various values of packet lengths. It can be seen that even if the packet length is small, we can get good estimates of ρ, which can be used in the ML estimator to accurately

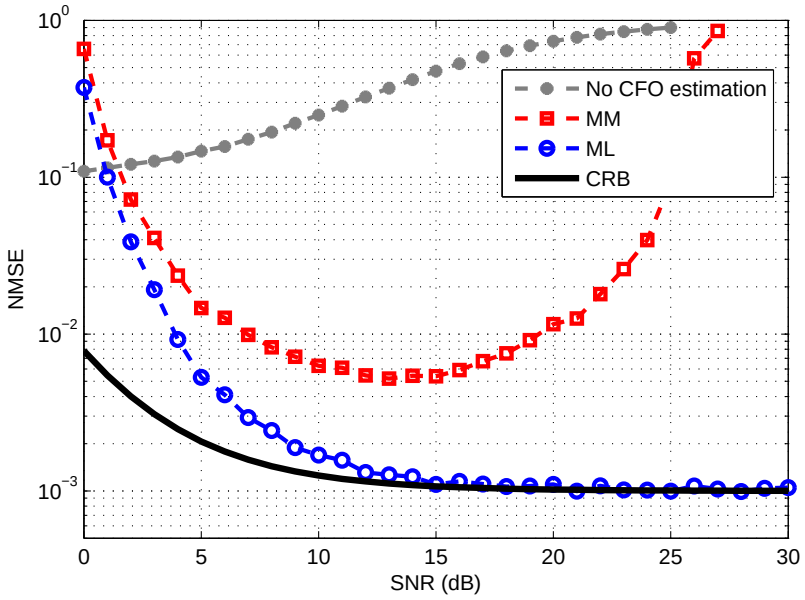

Figure 36: NMSE plot for SNR estimation for the data-aided scenario for $k = 1000$

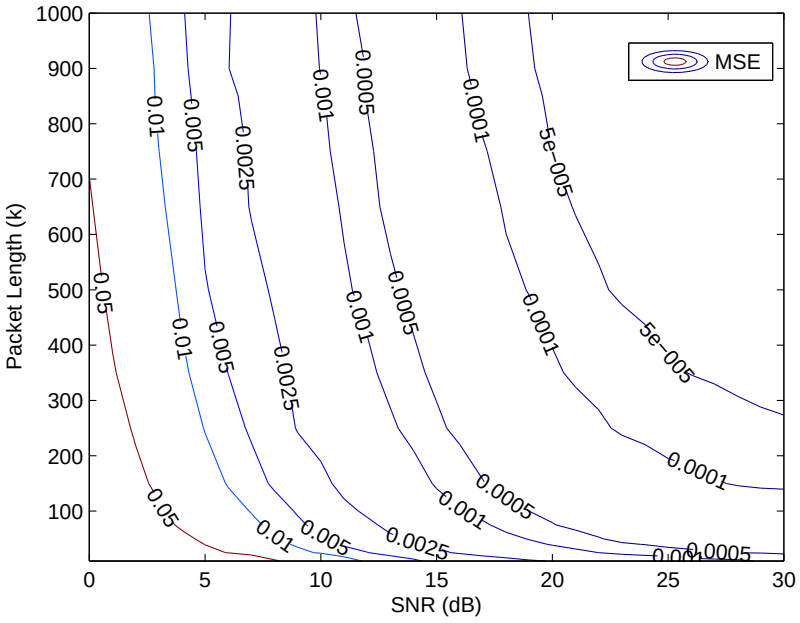

Figure 37: MSE contour plot for different packet lengths in the MM estimation of CFO for the data-aided case

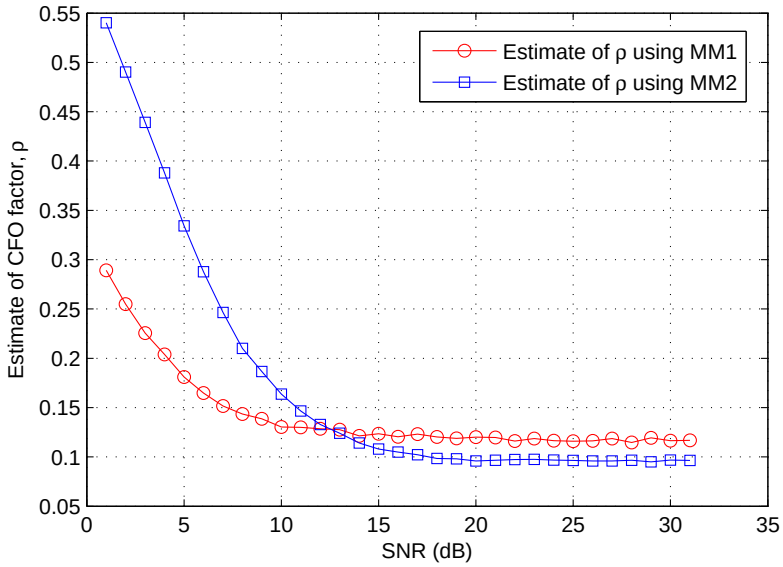

Figure 38: Estimation of ρ by NDA MM estimators; true value of $\rho = 0.1$

estimate the SNR.

Figure 38 shows the estimation of the CFO factor for the non data-aided case using both the MM1 and MM2 estimator for a packet length of 1000. It be seen that the MM1 estimator performs better at low SNR as compared to the MM2 estimator. However, in the high SNR region, the MM2 estimator gives a very accurate estimate of ρ, which is evident from the discussions in Section 6.3.1 and Figure 34. However, the NMSE at high SNR for both the estimators is very large (and is not plotted in Figure 39), hence both of them cannot be used for SNR estimation at high values of SNR. At low SNR, the MM1 estimator gives a fairly better performance as can be seen from Figure 39. We have plotted the NMSE for the NDA ML estimator using both the estimates from MM1 and MM2. It can be seen that using the estimates from MM1 results in a better performance in low SNR region as expected, while the NMSE is higher for the MM2 estimator in the same SNR range. However, an interesting result arises in the high SNR regime. We observe that the NMSE performance is little better for MM2-ML estimator, however the performance is almost the same for both the NDA-MM1 and NDA-MM2 estimators, and the performance reaches to that of

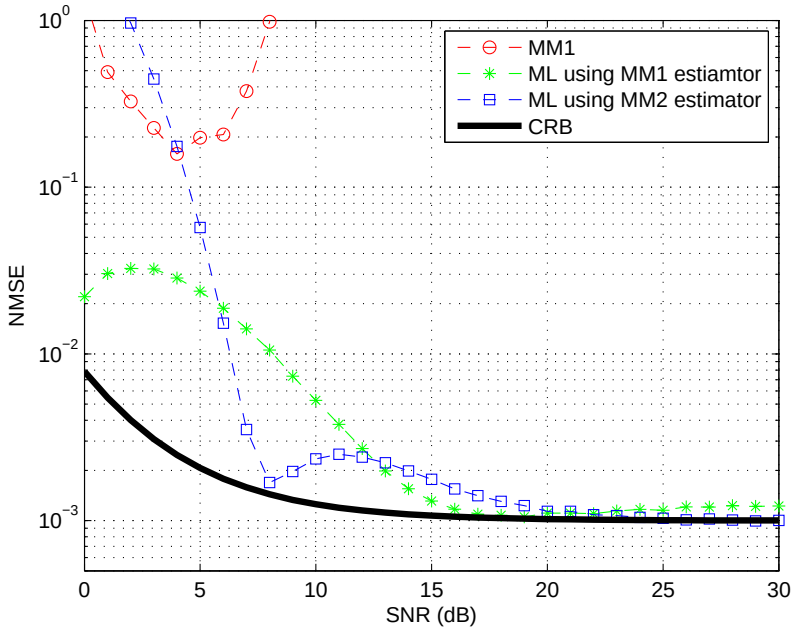

Figure 39: NMSE for SNR estimators for non data-aided case; $k = 1000$

the CRB at very high values of SNR.

CHAPTER VII

CONCLUSIONS AND SUGGESTED FUTURE WORKS

In this dissertation, we have created a framework for designing, modeling, and evaluating wireless network algorithms that take advantage of certain kinds of cooperation among terminals. Specifically, in these cooperative transmission (CT) schemes, we looked at a very simple and energy-efficient multi-hop scheme, known as the opportunistic large array (OLA), which can be used in many practical applications involving wireless sensor networks. To deploy a pragmatic wireless network using this CT scheme, there are many uncertainties that affect the performance of this network. These uncertainties include performance issues related to connectivity and coverage areas of the network, number of sensor nodes to deploy and their deployment geometry, and designing protocols and algorithms to attain maximum energy efficiency.

The prevailing theme of this doctoral research has been to advance this agenda with the modeling and analysis of novel cooperative protocols and to address the uncertainties that prevail in a communication system when these protocols are utilized. The dissertation consisted of two major parts. The first part addressed the modeling issues of these CT networks to optimize network parameters for obtaining maximum connectivity and coverage. The other part addressed the signal-to-noise ratio (SNR) estimation for the purpose of recruiting nodes and developing the geometry of the network to attain energy-efficient solutions, which are generally desired in most communication systems and particularly in sensor network applications.

The opportunistic large array (OLA) is a simple strategy that provides an SNR

advantage from the spatial diversity of distributed single-antenna radios. In this research, it is shown that a one-dimensional multi-hop network that does opportunistic large array transmission can be modeled as a Markov chain in discrete time. The steps that lead to the development of the sub-stochastic matrix of this chain are formulated in detail. The Perron-Frobenius eigenvalue and the corresponding eigenvector of this matrix helps in determining different parameters for achieving better performance in delivering the message to a destination. The research also considered two different topologies for deploying a one-dimensional sensor network where the nodes can be equi-distant from one another or they can be combined to form a co-located group. The stochastic models for the transmissions for both topologies are developed and it is shown that the co-located topology always outperforms the equi-distant topology, and the performance difference is larger for larger path loss exponents.

As a next step to this fixed node deployment topologies, it is shown that the quasi-stationary Markov chain model can also be applied to a one-dimensional ad hoc network, where the nodes can be randomly placed. The presence or absence of a node at a location is modeled using the Bernoulli process and the state space of this system is formulated using indicator random variables. A compact tensor representation of the transition probability matrix is also derived, which is based on the underlying hypoexpnential distribution of the received power at each sensor. The behavior of the Perron-Frobenious eigenvalue of the sub-stochastic matrix, referred as the success probability, indicated the level of quality of service that can be achieved for a certain transmission. It is shown that an additional SNR margin is required for the random placement of nodes as compared to deterministic placement for obtaining the same success probability.

Estimates of real-time SNR are required by many receivers to perform various functions. Typical applications include selection diversity and turbo decoding. Another useful application is that SNR is a way for a receiver to determine if it is in the

decoding range of its source and in a preferable position to take part in cooperative transmission. Many amplify and forward protocols rely on SNR. This research considered the problem of estimating the average SNR for a non-coherent MFSK receiver, taking into account both symbol-by-symbol Rayleigh fading and slow block fading channels. The corresponding Cramer Rao Bounds and the maximum likelihood estimators have been derived in addition to the EDS (estimation using data statistics) approach, which uses the data statistics to estimate the SNR. Different degrees of data knowledge in a packet is assumed and different versions of data-aided and non data-aided estimators are provided. From the theoretical perspective and simulation results, it is concluded that different scenarios lead to different results based on packet length, availability of pilot sequence, and the region of SNR considered (low/high).

The offsets in carrier synchronization (CFO) causes degradation of the estimates of SNR in the receiver. To combat this effect, the problem of estimating the SNR in the presence of a CFO is studied. Both the data aided and non data-aided estimators for the Rayleigh fading channel are derived and also derived are the method of moments estimator and the maximum likelihood estimator for each case. Concerning the difficulty of the CFO estimation problem (in terms of its non-linearity), it is shown that the estimates of CFO can be found using the method of moments estimators, which can then be used to derive the ML estimators, which give accurate estimates of the SNR at various high and low SNR scenarios.

The following is a list of possible directions for future research:

1. The stochastic modeling of the multi-hop cooperative wireless network has been achieved for a one-dimensional grid as well as randomly deployed line network. Though the one-dimensional modeling can be used in many wireless applications, a mathematical model for a general OLA broadcast scenario in strip shaped networks would broaden the scope of applications, for instance, to cooperate routes in ad hoc networks. This will require the modification of the

current model into a two-dimensional grid of particular width. The designed 2D model will mimic a general wireless sensor strip network for a given finite density of nodes.

2. Future research directions include extending the non-overlapped co-located groups of nodes study to the overlapping windows and to study the connectivity effects when more than one group is transmitting at the same time. A comparison with overlapping windows in equi-distant case will be interesting.

3. In all our modeling approaches, a computational barrier was present in terms of the length of window that corresponds to the number of candidate nodes that take part in CT at one time instant. Though this problem of window size, M, was alleviated using a compact Kronecker approach, however it would be better if we don't require this window size parameter at all. If an algorithm is designed that excludes this window size, the computational load would be minimized.

4. Though the SNR estimators are optimal corresponding to their working environments, there are still some errors in the estimation of the true value of SNR. These errors can cause a problem in selecting the most optimal node for transmission purposes and thus decrease the network performance. The possible solution to this problem is the design of a mathematical model and to incorporate this error model into the current network model. This will certainly reduce the probability of making erroneous decisions in the selection of nodes that will transmit for the next hop.

5. Another future direction would be to implement the OLA with transmission threshold [20] with the realistic SNR estimators that are designed in this research work. By using these real-time SNR estimators, the actual performance in terms of the energy efficiency of wireless networks can be obtained.

APPENDIX A

PROOF OF CLAIM 1

Let $N = 3^M$, where N is the possible number of states for a window size of M using ternary M-tuples. By construction, the window overlap size is $M - h_d$, thus we split a window such that

$$M = \underbrace{M - h_d}_{overlap} + \underbrace{h_d}_{shift}. \tag{150}$$

The *shift* part is always receiving transmissions from the previous window, thus the nodes contained in *shift* can either go to 0 or 1 but never 2. Thus the possible combinations in *shift* are those of 0 and 1 which make a total of 2^{h_d}. The *overlap* part can contain any combination and thus is 3^{M-h_d}. Using the multiplication rule of independent events, the effective states are given as

$$\hat{N} = 3^{M-h_d} \times 2^{h_d}. \tag{151}$$

If all the elements of the window form any combination of 0 and 2, the system will be in absorbing state. The effect of 2 in the *shift* has already been taken into account from above equation. Thus we want the additional combination of 0 and 2 to be excluded from the *overlap* part which makes a total of 2^{M-h_d}.

APPENDIX B

HIGH SNR APPROXIMATION FOR RAYLEIGH FADING ENVIRONMENT

For simplicity, lets discuss the case where $M = 2$. In that case, the summation term (denoted by A) is given by

$$A = \sum_{i=1}^{k} \frac{\sum_{m=1}^{2} x_{m,i} \exp\left(-x_{m,i}\phi\right)}{\sum_{m=1}^{M} \exp\left(-x_{m,i}\phi\right)} = \sum_{i=1}^{k} \frac{x_{1,i} \exp\left(-x_{1,i}\phi\right) + x_{2,i} \exp\left(-x_{2,i}\phi\right)}{\exp\left(-x_{1,i}\phi\right) + \exp\left(-x_{1,i}\phi\right)}. \quad (152)$$

From ϕ, it can be noticed that for high SNR where $S >> N$, ϕ can be approximated as $\phi = -\frac{1}{N}$, thus the A can be approximated as

$$A = \sum_{i=1}^{k} \frac{x_{1,i}}{1 + \frac{\exp(x_{2,i}/N)}{\exp(x_{1,i}/N)}} + \frac{x_{2,i}}{1 + \frac{\exp(x_{1,i}/N)}{\exp(x_{2,i}/N)}}. \quad (153)$$

Now one of the two branches, say x_1, contains the signal. For high SNR, since the noise power $N << S$, the denominator of first term approaches 1 because the ratio of exponentials results in a very small number. While the same phenomenon is reversed in the second term, where the denominator approaches a very large value since the ratio of exponentials results in a very large number. Thus overall the second term is negligible (since the numerator is also a small number), and we are just left with $x_{1,i}$. Thus A is approximated as

$$A \approx \sum_{i=1}^{k} \max_{m} x_{m,i}. \quad (154)$$

APPENDIX C

HIGH SNR APPROXIMATION FOR BLOCK FADING ENVIRONMENT

For simplicity, lets discuss the case where $M = 2$. In that case, the summation term (denoted by B) is given by

$$B = \sum_{i=1}^{k} \frac{\sum_{m=1}^{2} I_1\left(\frac{2\sqrt{x_{m,i}}|A|}{N}\right)}{\sum_{m=1}^{2} I_0\left(\frac{2\sqrt{x_{m,i}}|A|}{N}\right)} \sqrt{x_{1,i}} = \sum_{i=1}^{k} \frac{I_1\left(\frac{2\sqrt{x_{1,i}}|A|}{N}\right)\sqrt{x_{1,i}} + I_1\left(\frac{2\sqrt{x_{2,i}}|A|}{N}\right)\sqrt{x_{2,i}}}{I_0\left(\frac{2\sqrt{x_{1,i}}|A|}{N}\right) + I_0\left(\frac{2\sqrt{x_{2,i}}|A|}{N}\right)}. \tag{155}$$

Since $\frac{2|A|}{N}$ is constant throughout, thus denoting it as ψ and separating terms in the above equation, B can be written as

$$B = \sum_{i=1}^{k} \left[\frac{\sqrt{x_{1,i}}}{\frac{I_0\left(\psi\sqrt{x_{1,i}}\right)}{I_1\left(\psi\sqrt{x_{1,i}}\right)} + \frac{I_0\left(\psi\sqrt{x_{2,i}}\right)}{I_1\left(\psi\sqrt{x_{1,i}}\right)}} + \frac{\sqrt{x_{2,i}}}{\frac{I_0\left(\psi\sqrt{x_{1,i}}\right)}{I_1\left(\psi\sqrt{x_{2,i}}\right)} + \frac{I_0\left(\psi\sqrt{x_{2,i}}\right)}{I_1\left(\psi\sqrt{x_{2,i}}\right)}} \right]. \tag{156}$$

Using the approximation $\frac{I_0(x)}{I_1(x)} \approx 1$, one term in each denominator is always 1. For the other term, it can be observed that at high argument values, the modified Bessel function approaches a very high value. Thus if $\sqrt{x_{1,i}} > \sqrt{x_{2,i}}$, then $I_n(\sqrt{x_{1,i}}) >> I_n(\sqrt{x_{2,i}})$, where n is the order of modified Bessel function, which implies that $\frac{I_0(\sqrt{x_{2,i}})}{I_1(\sqrt{x_{1,i}})} \approx 0$. Thus the denominator of first term approaches a 1, while the same phenomenon is reversed for the other term where the denominator approaches extremely large value. Thus overall we are left with the maximum term, i.e. $\sqrt{x_{1,i}}$. Thus B can be approximated for any M as

$$B \approx \sum_{i=1}^{k} \max_{m=1,\ldots,M} \sqrt{x_{m,i}}. \tag{157}$$

APPENDIX D

CRB FOR THE NON-DATA AIDED ESTIMATOR

For finding the CRB of the NDA estimator, (110) needs be to be evaluated. However, the second derivatives of Equations (62) and (63), involved in this computation, are difficult to solve analytically. Even if we get a closed form solution, taking the expectation of those derivatives will be harder because of the correlation between the numerator and denominator in both equations. This problem has been considered in [55] and [56] for linear modulation schemes where the authors have used numerical techniques to find these expectations. However, an interesting case arises, if we use the approximation as done in Equation (66). The structure of the FIM remains the same as in (111), given as

$$I = \begin{bmatrix} a & a \\ a & b \end{bmatrix}, \tag{158}$$

where

$$a = \frac{k}{(S+N)^2}, \tag{159}$$

and

$$b = \frac{k}{(S+N)^2} + \frac{2k(S+NM)}{N^3} - \frac{(M-1)k}{N^2} - \frac{2k(S+N)}{N^3}. \tag{160}$$

Thus, the CRB from (108) is given as

$$CRB = \frac{1}{b-a}\left[\frac{S^2}{N^4} + 2\frac{S}{N^3} + \frac{1}{N^2}\frac{b}{a}\right], \tag{161}$$

where

$$b - a = \frac{2k(S+N)(M-1)}{N^3} - \frac{(M-1)k}{N^2}, \tag{162}$$

and

$$\frac{b}{a} = 1 + (M-1)(S+N)^2. \tag{163}$$

Thus

$$CRB_{NDA} = \frac{M(\gamma+1)^2}{k(M-1)}. \tag{164}$$

Thus by using this high SNR approximation, the CRB for the NDA case matches the CRB for the FDA case. This can also be seen from Figures 26-27, where the NDA approaches the CRB (derived for FDA) in the high SNR region.

REFERENCES

[1] A. Sendonaris, E. Erkip, and B. Aazhang, "User cooperation – part i: System description, part ii: Implementation aspects and performance analysis," *IEEE Trans. Commun.*, vol. 51, no. 11, pp. 1927–48, Nov. 2003.

[2] J. N. Laneman, D. Tse, and G. W. Wornell, "Cooperative diversity in wireless networks: Efficient protocols and outage behavior, "*IEEE Trans. Inf. Theory*, vol. 50, no. 12, pp. 3063–3080, Dec. 2004.

[3] K. Victor, Y.Wu, and Y. G. Li, "Error rate performance in OFDM-based cooperative networks," in *Proc. IEEE GLOBECOM*, pp. 3447-3451, Washington, USA, Nov. 2007.

[4] L. Sankaranarayanan and G. G. Kramer, "Cooperative diversity in wireless networks: A geometry-inclusive analysis," in *Proc. Annual ACCCC*, IL, USA, Sept. 2005.

[5] A. Bletsas, A. Khisti, D. P. Reed, and A. Lippman, "A simple cooperative diversity method based on network path selection," *IEEE J. Sel. Areas Commun.*, vol. 24, no. 3, pp. 659-672, Mar. 2006.

[6] A. Bletsas, H. Shin, and M. Z. Win, "Cooperative communications with outage-optimal opportunistic relaying," *IEEE Trans. Wireless Commun.*, vol. 6, no. 9, pp. 3450-3460, Sept. 2007.

[7] R. Tannious and A. Nosratinia, "Spectrally-efficient relay selection with limited feedback," *IEEE J. Sel. Areas Commun.*, vol. 26, no. 8, pp. 1419 – 1428, Oct. 2008.

[8] A. Scaglione and Y. W. Hong, "Opportunistic large arrays: Cooperative transmission in wireless multi-hop Ad hoc networks to reach far distances," *IEEE Trans. Signal Process.*, vol. 51, no. 8, pp. 2082–92, Aug. 2003.

[9] Y. W. Hong and A. Scaglione, "Energy-efficient broadcasting with cooperative transmissions in wireless sensor networks," *IEEE Trans. Wireless Commun.*, vol. 5, no. 10, pp. 2844–55, Oct. 2006.

[10] I. Maric and R. D. Yates, "Cooperative multi-hop broadcast for wireless networks," *IEEE J. Sel. Areas Commun.*, vol. 23, no. 1, pp. 1080–88, Aug. 2004.

[11] L. Thanayankizil, A. Kailas, and M.A. Ingram, "Routing for wireless sensor networks with an Opportunistic Large Array (OLA) physical layer," *Ad Hoc and Sensor Wireless Networks, Special Issue on Sensor Technologies and Applications*, Volume 8, Number 1-2, p. 79-117, 2009.

[12] B. Sirkeci-Mergen and A. Scaglione, "On the power efficiency of cooperative broadcast in dense wireless networks," *IEEE J. Sel. Areas Commun.*, vol. 25, no. 2, pp. 497–507, Feb. 2007.

[13] B. Sirkeci-Mergen and A. Scaglione, "A continuum approach to dense wireless networks with cooperation," *Proc. IEEE INFOCOM*, 2005, pp. 2755–63.

[14] B. Sirkeci-Mergen, A. Scaglione, G. Mergen, "Asymptotic analysis of multistage cooperative broadcast in wireless networks," *Joint special issue of the IEEE Trans. Inf. Theory and IEEE/ACM Trans, On Networking*, vol. 52, no. 6, pp. 2531–50, Jun. 2006.

[15] L. Thanayankizil, A. Kailas, and M. A. Ingram, "Two energy-saving schemes for cooperative transmission with Opportunistic Large Arrays," *Proc.* 50^{th} *Annual IEEE Global Telecommunications Conference (GLOBECOM)*, Washington, DC, Nov. 26–30, 2007, pp. 1038–1042.

[16] L. Thanayankizil, A. Kailas, and M. A. Ingram, "Energy-efficient strategies for cooperative communications in wireless sensor networks," *Proc.* 1^{st} *IEEE International Conference on Sensor Technologies and Applications (SENSORCOMM)*, Valencia, Spain, Oct. 14–20, 2007, pp. 541–546.

[17] A. Kailas, L. Thanayankizil, and M. A. Ingram, "Power allocation and self-scheduling for cooperative transmission using Opportunistic Large Arrays," *Proc.* 26^{th} *Annual IEEE Military Communications Conference (MILCOM)*, Orlando, FL, Oct. 29–31, 2007, pp. 1–7.

[18] A. Kailas, L. Thanayankizil, and M. A. Ingram, "A simple cooperative transmission protocol for energy-efficient broadcasting over multi-hop wireless networks," *Journal of Communications and Networks (Special Issue on Wireless Cooperative Transmission and Its Applications)*, Apr. 2008.

[19] A. Kailas and M. A. Ingram, "Alternating cooperative transmission for energy-efficient broadcasting," *Proc.* 51^{st} *Annual IEEE Global Telecommunications Conference (GLOBECOM)*, New Orleans, LA, Nov. 30–Dec. 4, 2008.

[20] A. Kailas and M. A. Ingram, "Energy efficient broadcasting in multi-hop networks using alternating Opportunistic Large Arrays," *IEEE Trans. Wireless Commun.*, Vol. 8, No. 6, pp. 2831-2835, June 2009.

[21] A. Kailas and M. A. Ingram, "Investigating multiple alternating cooperative broadcasts to enhance network longevity," *Proc. IEEE International Conference on Communications (ICC)*, Dresden, Germany, Jun. 14–18, 2009.

[22] Y.J. Chang and M.A. Ingram, "Cluster transmission time synchronization for cooperative transmission using software defined radio," in *IEEE (ICC) Workshop on Cooperative and Cognitive Mobile Networks (CoCoNet3)*, May 2010.

[23] T.R. Halfold and K.M. Chugg, "Barrage relay networks," in *Information theory and applications workshop (ITA)*, Feb. 2010.

[24] **S.A. Hassan**, Y.G. Li, P.S.S. Wang, and M. Green, "A full rate dual relay cooperative approach for wireless systems, " *KICS/IEEE Journal of Commun. and Networks*, 2010, to appear.

[25] **S.A. Hassan** and P. Wang, "Dual relay communication system: Channel capacity and power allocations," in *10th IEEE Int. Wireless and Microwave Technology Conference*, Clearwater, Fl, April 2009.

[26] **S.A. Hassan**, P. Wang, Y. G. Li, "Equalization for symmetrical cooperative relay scheme for wireless communications," *11th IEEE Radio and Wireless Symposium*, San Diego, CA, January 2009.

[27] P. Wang, **S.A. Hassan**, Y. G. Li, "A symmetrical cooperative diversity approach for wireless communications," *4th IEEE International Conference on Circuits and Systems for Communications ICCSC*, Beijing, China, May 2008.

[28] A. Kailas and M.A. Ingram, "Analysis of a simple recruiting method for cooperative routes and strip networks," *IEEE Trans. Wireless Commun.* Vol. 9, No. 8, pp. 2415-2419, Aug 2010.

[29] J.N. Darroch and E.Seneta, "On quasi-stationary distributions in absorbing discrete-time finite Markov chains," *Journal of Applied Probability*, vol. 2, No. 1, pp. 88-100, June 1965.

[30] E.A. van Doorn and P.K. Pollett, "Quasi-stationary distributions for reducible absorbing Markov chains in discrete time," *Journal of Markov Processes and Related Fields*, vol. 15, No. 2, pp. 191-204, 2009.

[31] S.M. Ross, *Introduction to Probability Models*, 9th Edition, Academic Press, 2007.

[32] C.D. Meyer, *Matrix Analysis and Applied Linear Algebra*, SIAM publishers, 2001.

[33] P. Chanchana, "An algorithm for computing the Perron root of a nonnegative irreducible matrix," Ph.D. Dissertation, North Carolina State University, Raleigh, 2007

[34] S.A. Hassan and M.A. Ingram, "SNR estimation for a non-coherent M-FSK Receiver in Rayleigh fading environment," in *Proc. IEEE Intl. Conf. Communications (ICC)*, South Africa, May 2010.

[35] E. Senta, *Non-Negative Matrices and Markov Chains*, 2nd edition, Springer New York, 2006.

[36] A.N. Langville and W.J. Stewart, "The Kronecker product and stochastic automata networks," *Elsevier Journal of Computational and Applied Mathematics*, vol. 167, no.2, pp.429-447, 2004.

[37] W.J. Stewart, K. Atif, B. Plateau, "The numerical solution of stochastic automata networks," *European Journal of Operations Research*, vol. 86, no.3, pp.503-525, 1995.

[38] D.R. Pauluzzi and N.C. Beaulieu, "A comparison of SNR estimation techniques for the AWGN channel," *IEEE Trans. Commun.*, vol. 48, No. 10, October 2000.

[39] Y. Chen and N.C. Beaulieu, "An approximate maximum likelihood estimator for SNR jointly using pilot and data symbols," *IEEE Letters Commun.*, vol. 9, No. 6, June 2005.

[40] A. Ramesh, A. Chockalingam and L.B. Milstein, "SNR estimation in generalized fading channels and its applications to turbo decoding," in *Proc. IEEE ICC*, Helsinki, Finland, June 2001.

[41] A. Ramesh, A. Chockalingam and L.B. Milstein, "SNR estimation in Nakagami-m fading with diversity combining and its applications to turbo decoding," *IEEE Trans. Commun.*, vol. 50, No. 11, November 2002.

[42] T. Ertas and E. Dilaveroglu, "Low SNR asymptote of CRB on SNR estimates for BPSK in Nakagami-m fading channels with diversity combining," *IEEE Elect. Letters*, vol. 39, No. 23, November 2003.

[43] F. Downton, "Bivariate exponential distributions in reliability theory," *J. Royal Statistical Soc.: Series B*, vol. 32, pp. 408417, 1970.

[44] M.K. Simon, *Probability distributions involving Gaussian random variables: A handbook for engineers and scientists*, New York: Springer, 2002.

[45] J.G. Proakis, *Digital Communications*, 4th Edition. McGraw-Hill Publishers.

[46] M.K. Simon and M.S. Alouini, *Digital communications over fading channels: A unified approach to performance analysis*, Wiley and Sons. New York, 2000.

[47] S.A. Hassan and M.A. Ingram, "SNR Estimation for a Non-Coherent Binary Frequency Shift Keying Receiver," in *Proc. IEEE Global Commum. Conf. (GLOBECOM)*, Honolulu, Hawaii, Dec. 2009.

[48] E. Dilaveroglu and T. Ertas, "CRBs and MLEs for SNR estimation on non coherent BFSK signals in Rayleigh fading," *IEEE Elect. Letters*, vol. 41, No. 2, January 2005.

[49] R.M. Gagliardi and C.M. Thomas, "PCM data reliability monitoring through estimation of signal-to-noise ratio," *IEEE Trans. Commun.*, vol. COM-16, pp. 479-468, June 1968.

[50] G. Strang, *Introduction to Linear Algebra*, 3rd edition, Wellesley-Cambridge Press, Wellesley, 2005.

[51] S. Im, and E.J. Powers, "An algorithm for estimating signal-to-noise ratio of UWB signals," *IEEE Trans. Veh. Tech.*, vol. 54, pp. 1905-1908, Sept. 2005.

[52] G.L. Stuber, *Principles of Mobile Communication*. 2nd edition, Kluwer Academic Publishers, Boston, 2001.

[53] S.M. Kay, *Fundamentals of statistical signal processing: estimation theory*. Prentice Hall. New Jersey, 1993.

[54] The Modified Bessel's Differential Equation. [Online]. Available: http://www.efunda.com/math/bessel/modifiedbessel.cfm

[55] A. Das, "NDA SNR estimation: CRLBs and EM based estimators," *in TENCON 2008 - 2008, TENCON 2008. IEEE Region 10 Conference*, pp. 1-6, 2008.

[56] W. Gappamair, "Cramer-Rao lower bound for Non-Data-Aided SNR estimation of linear modulation schemes," *IEEE Trans. Commun.*, vol. 56, no. 5, pp. 689-693, May 2008.

VITA

Syed Ali Hassan's doctoral work (as Graduate Research Assistant at Georgia Institute of Technology) addresses the modeling issues in wireless multi-hop networks. He received his MS in Mathematics from Georgia Tech in 2011 and MS in Electrical Engineering from University of Stuttgart, Germany, in 2007. He was awarded BE in Electrical Engineering from National University of Sciences and Technology (NUST), Pakistan, in 2004. His broader area of research is signal processing for communications with a focus on stochastic modeling and cooperative communications for wireless networks. He also held industry position, as a design engineer, in Center for Advanced Research in Engineering, Islamabad, Pakistan and research intern at Cisco System Inc., CA.